aspen aerogels

NANOTECHNOLOGY AT WORK

ASPEN AEROGELS, INC.
30 FORBES ROAD, BUILDING B
NORTHBOROUGH, MA 01532
PHONE: 508.691.1111
FAX: 508.691.1200
WEB SITE: WWW.AEROGEL.COM

MEMORANDUM

To: Distribution

From: Redouane Begag

Date: March 30, 2017

Re: Final Technical Report
Award No. DE-FE0013127
AAI Job No. R-13010

Enclosed please find the above referenced Final Report. If you have any questions, please feel free to contact me at 508-466-3124.

Redouane Begag, Scientist

Distribution:

Technical Monitor
E-mail: Isaac.Aurelio@NETL.DOE.GOV

NETL:
E-mail: FITS@NETL.DOE.GOV

AAI Distribution:

Begag
White

Bench Scale Development and Testing of Aerogel Sorbents for CO_2 Capture

Final Technical Report
February 7, 2017

Award No. DE-FE0013127
DOE Agency: Office of Fossil Energy
Reporting Period Start: October 1, 2013 End: December 31, 2016

Contractor Name: Aspen Aerogels, Inc.
Contract address: 30 Forbes Rd., Bldg. B, Northborough, MA 01532

PI Name: Redouane Begag
PI email: rbegag@aerogel.com

Submitting Official: Dr. George Gould
Title: VP, Research & Development
Email address: ggould@aerogel.com

George Gould

_____ _____ 3/30/17_____

Dr. George Gould **Date**
VP, Research & Development

DISCLAIMER

ABSTRACT:
The primary objective of this project was scaling up and evaluating a novel Amine Functionalized Aerogel (AFA) sorbent in a bench scale fluidized bed reactor. The project team (Aspen Aerogels, University of Akron, ADA-ES, and Longtail Consulting) has carried out numerous tests and optimization studies to demonstrate the CO_2 capture performance of the AFA sorbent in all its forms: powder, pellet, and bead. The CO_2 capture target performance of the AFA sorbent (all forms) were set at > 12 wt.% and > 6 wt.% for total and working CO_2 capacity, respectively (@ 40 °C adsorption / 100 – 120 °C desorption). The optimized AFA powders outperformed the performance targets by more than 30%, for the total CO_2 capacity (14 - 20 wt.%), and an average of 10 % more for working CO_2 capacity (6.6 – 7.0 wt.%, and could be as high as 9.6 wt. % when desorbed at 120 °C). The University of Akron developed binder formulations, pellet production methods, and post treatment technology for increased resistance to attrition and flue gas contaminants. In pellet form the AFA total CO_2 capacity was ~ 12 wt.% (over 85% capacity retention of that of the powder), and there was less than 13% degradation in CO_2 capture capacity after 20 cycles in the presence of 40 ppm SO_2. ADA-ES assessed the performance of the AFA powder, pellet, and bead by analyzing sorption isotherms, water uptake analysis, cycling stability, jet cup attrition and crush tests. At bench scale, the hydrodynamic and heat transfer properties of the AFA sorbent pellet in fluidized bed conditions were evaluated at Particulate Solid Research, Inc. (PSRI). After the process design requirements were completed, by Longtail Consulting LLC, a techno-economic analysis was achieved using guidance from The National Energy Technology Laboratory (NETL) report. This report provides the necessary framework to estimate costs for a temperature swing post combustion CO_2 capture process using a bituminous coal fired, super-critical steam cycle power plant producing 550 MWe net generation with 90% CO_2 capture using a methylethylamine (MEA) solvent. Using the NETL report as guidance, the designed CO_2 capture system was analyzed on a cost basis to determine relative cost estimates between the benchmark MEA system and the AFA sorbent system.

Key words: AFA, aerogel, CO_2 capture, pellet, CO_2 capacity, bench-scale, sol-gel, attrition, bead

TABLE OF CONTENTS

LIST OF FIGURES

LIST OF TABLES

Bench Scale Development and Testing of Aerogel Sorbents for CO_2 Capture
Award No. DE-FE0013127
Final Report
October 1, 2013 - December 31, 2016

1 EXECUTIVE SUMMARY

Techniques to capture and store the CO_2 generated by burning fossil fuels could help stabilize greenhouse gas concentrations in the atmosphere. Fossil Fuels are expected to remain a major energy source until at least the middle of this century. Since CO_2-free energy sources cannot be deployed quickly enough, near term new technologies for the capture and sequestration of CO_2 are needed. The most advanced post-combustion carbon dioxide capture option for coal-fired power plants is recirculating aqueous amine based solvents in flue gas that adsorbs and desorbs carbon dioxide through a temperature-swing adsorption (TSA) process. The amine solution is typically 30% monoethanolamine (MEA) by weight. Recent studies have shown that aqueous MEA for 90% CO_2 capture from a retrofit coal-fired power plant can reduce the thermal efficiency from ~35% (higher heating value basis) to 24% and cost $80 per ton CO_2 removed[1]. Most of this cost is associated with the energy penalty incurred when releasing purified CO_2 in the regeneration step. One promising option to reduce the energy penalty and cost associated with the material regeneration is to use solid sorbents, which require less energy to heat due to a lower specific heat.

Solid sorbents have shown great promise for reducing the overall cost associated with post-combustion CO_2 capture in coal-fired power plants, due to a significant reduction in the regeneration energy versus that of aqueous amines. However, these sorbents must be integrated into a viable capture process, and appropriate equipment must be developed and thoroughly demonstrated before the potential advantages of solid sorbents can be realized. On a previous SBIR funded project (DOE SBIR DE-SC0004289), Aspen demonstrated the feasibility of producing a novel solid sorbent based on Amine Functionalized Aerogels (AFA) that showed very promising CO_2 adsorption capacity and excellent stability over thousands of adsorption-desorption cycles. The aerogels have high surface area and porosity, unique and tailored pore size distribution, highly-stable functionality, and excellent hydrophobicity for resisting degradation from flue gas and its contaminants over long-term use.

Under this project, Aspen Aerogels teamed with CO_2 capture experts at ADA-ES, Longtail Consulting, and the University of Akron (UA) to develop and test, at bench scale, the AFA sorbent for coal-fired power plants. Aspen focused on optimizing the CO_2 capture performance of promising sol-gel/aerogel formulations developed in Aspen's previous program. The CO_2 capture targets for the AFA sorbent (all forms) were set at > 12 wt.% and > 6 wt.% for total and working CO_2 capacity, respectively (@ 40 °C adsorption / 100 – 120 °C desorption). The optimized AFA powders outperformed the performance targets by more than 30%, for the total CO_2 capacity (14 - 20 wt.%), and an average of 10 % more for working CO_2 capacity (6.6 – 7.0 wt.%, and could be as high as 9.6 wt. % when desorbed at 120 °C). The University of Akron developed binder formulations, pellet production methods, and post treatment technology for increased resistance to attrition and flue gas contaminants. In pellet form the AFA total CO_2 capacity was ~ 12 wt.% (over 85% capacity retention of that of the powders), and there was less than 13% degradation in CO_2 capture capacity after 20 cycles in the presence of 40 ppm SO_2.

Aspen also developed AFA sorbent in bead form, using the optimum AFA sol-gel formulations. The goal of preparing AFA in monolithic aerogel bead form rather than powder form, was to determine if the post processing pelletization step, performed by UA, can be eliminated while maintaining adequate sorbent performance with low attrition. The AFA bead and pellet fabrication process was optimized at lab scale producing sorbents that meet or exceed the CO_2 capture, moisture uptake, and attrition targets.

Later, the group selected the AFA sorbent pellet form to be further analyzed and tested at bench scale. The selection was made after performing a series of comparison tests between the two sorbent forms, including isobar testing, water uptake analysis, cycling stability (500 cycles), jet cup attrition and crush test. The test results showed that both sorbent forms of AFA demonstrated comparable CO_2 capture performance, including promising total and working CO_2 capacities (11 – 14 wt. %, 6 - 6.5 wt. %, respectively), low water uptake (< 3 wt. %), and cycling stability over 500 cycles (on a fixed bed and cycling between 40°C (adsorption), and 100 °C (desorption). The selection of pellets over beads was primarily made based on the scale-up production capabilities of the AFA at Aspen, and the pelletization capabilities at Akron, for future large scale production. During the last budget period, over 30 kg of AFA sorbent pellets were produced and tested in a bench scale fluidized bed reactor at Particulate Solid Research, Inc. (PSRI). The hydrodynamic and heat transfer properties of the sorbent in fluidized bed conditions were evaluated. This task was completed by Longtail Consulting, who joined this project at the beginning of budget period 3, after ADA-ES withdrew from the project. After the process design requirements were determined, a techno-economic analysis (TEA) was completed using guidance from The National Energy Technology Laboratory (NETL) report[2]. For TEA, adsorber and desorber modeling consisted of analysis of experimentally measured pellet isotherm kinetics, heat of reaction, particle size and density, fluidizing gas velocities, and fluidized bed heat transfer coefficients. Using these sorbent characteristics, process models of the turbulent fluidized adsorber bed were developed to assess flue gas CO_2 breakthrough and capture rates. The model output determined adsorber and desorber vessel number and size, heat exchanger size, and parasitic heating, cooling, and electric loads, all in order to achieve 90% flue gas CO_2 capture. These process models were then integrated to plant process models, and cost accounting was applied in accordance with NETL's report[2]. The total cost of electricity for the solid sorbent system was calculated to be $173.6/MWhr, while the MEA baseline case was listed as $142.8/MWhr. The difference in costs for the AFA solid sorbent system are driven primarily by the variable operating costs associated with sorbent attrition during fluidization. However, this is also a very significant unknown as the sorbent may last a greater or lesser number of cycles in a practical environment, highlighting the need for bench scale testing under practical CO_2 capture conditions, using real-world power plant flue gas stream, and for over 10,000 cycles. Additionally, the cost of the fuel increased because a substantial parasitic load was imposed on the plant as a result of the high particle density and corresponding large pressure drop across the adsorber.

As part of the Environmental Health and Safety (EH&S) Evaluation study, regulatory requirements and implications across multiple medias (air, waste, water, safety) of the manufacturing of AFA sorbent at full scale has been performed. Appropriate measures to mitigate (or minimize) any EH&S risk during pilot scale production has also been investigated.

2 EXPERIMENTAL METHODS

2.1 Amine Functionalized Aerogel Synthesis and Sol-Gel Process

Amine Functionalized Aerogel (AFA) sorbents derive from gels made through sol-gel chemistry, which refers to a process in which amino nanoparticles dispersed in a liquid (sol) react, by acid or base catalysis, to form a continuous three-dimensional network extending throughout the liquid to forma gel. This transition from sol to gel is also called gelation. An aerogel is obtained when the liquid is removed from the gel and replaced with air under supercritical conditions of the fluid filling the pores, thus preventing collapse of the porous gel structure. At Aspen, two high pressure vessels (1 gallon and 60 liter systems) were used for AFA sorbent fabrication.

Supercritical fluid is used to avoid the problem of large capillary forces created during solvent evaporation by, first exchanging the solvent for liquid CO_2, and then heating the CO_2 liquid-filled gels under pressure until the liquid converts to a supercritical fluid. In its supercritical fluid state there is just one phase so there is no gas–liquid interface causing surface tension, thus eliminating the capillary pressure, and the fluid can be removed from the gel without shrinking or cracking of the gel.

2.1.1 AFA powder sorbent development at Aspen Aerogels

Aspen focused on improving the total CO_2 capacity of its AFA sorbents while maintaining lifetime/cycling stability. A series of gel sorbents from the following formulations were synthesized and dried under supercritical conditions of CO_2 to produce the corresponding AFA sorbents:

2.1.1.1 Mono-amine alkoxysilane functionalized aerogel

A number of sorbent samples were synthesized and fabricated using a mono-amine alkoxysilane functionalized aerogel formulation (two different amine precursors were used, amine alkoxysilane 1 and amine alkoxysilane 2). Initially, sol-gels were made based on the "GE" formulation (the best performing sorbent from the previous SBIR Phase II effort[3]), but the solid content of the sols limited the target density of the resulting aerogel to 0.22 g/cc. Higher target densities were sought in order to increase amine loading and enhance mechanical stability. In order to make higher density aerogels, the water content of the sols was decreased and the solid content was increased to the maximum possible amount. Aerogels with densities as high as 0.35 g/cc and 0.4 g/cc have been achieved.

2.1.1.2 Polyimine loaded hydrophobic aerogel

This new family of sorbents was synthesized by the sol-gel process using two steps for the amine loading: 1) amine grafting by amino-alkoxysilane functionalization, and 2) amine loading (coating) by polyethylenimine (PEI) impregnation in a wet solution. The sorbents vary by their PEI content, water content in the sol-gel process, and their density.

2.1.1.3 Aerogel sorbents functionalized with bridging amino-siloxane precursors

This type of AFAs were formulated with a dipodal alkoxysilane that has a bridging portion containing a secondary amine. The precursor investigated was referred to as bridging amino siloxane, or BAS-1. BAS-based aerogel powders showed high CO_2 working capacities relative to their total CO_2 capacities. An additional dipodal bridging alkoxysilane co-gel precursor, was used

in some cases to provide rigid ethylene bis-siliconate bridges that strengthen the aerogel structure and prevent pore collapse.

2.1.2 AFA bead sorbent development at Aspen Aerogels

The chemistries tested for bead fabrication previously at Aspen used silica based chemistry with a gel time on the order of seconds. This rapid gelation allows the beads to become rigid enough to sustain any collisions between beads and prevents them from merging with each other during the process. For this project, the AFA formulations possess a gel time that varies between minutes for the mono-amine alkoxysilane and bridging amino-siloxane functionalized aerogels and hours for polyimine loaded and polyamine alkoxysilane terminated functionalized aerogels. Therefore, an optimization of the gel time and bead formation processing was required for AFA formulations. Numerous trials were performed on a small scale using silicon oil as a medium for bead dispersion and formation.

2.2 Physical and Structural Characterization of AFA (at Aspen).

The most promising AFA sorbents (in all forms, i.e., powder, pellets and beads) were subjected to physical and structural characterization knowing that that the CO_2 capture capacity performance is largely determined by the materials microstructure, including porosity, particle size, pore size/pore size distribution, surface area, and active amine site density. Given these performance drivers, AFA with high adsorption CO_2 capacity were characterized by the following methods:

N_2 adsorption-desorption for porosity, pore size, and surface area determination

Particle size measurement using particles size analyzer or laser diffraction technique

DSC/TGA for thermal stability evaluation

FT-IR for Chemical Structure Analysis

2.3 AFA sorbent Evaluation at ADA-Environmental Systems (ADA-ES)

ADA-ES, Inc. developed post-combustion CO_2 capture processes based on solid sorbents in a temperature-swing adsorption, fluidized-bed process. ADA-ES screened potential AFA for CO_2 working capacity, kinetics, moisture uptake, cyclic stability, sorbent selectivity, sorbent isotherms, jet cup attrition, crush strength, and sorbent heat of reaction. Initial screening was performed to rapidly down select the most promising AFA samples. The following are the experimental procedures used at ADA-ES.

2.3.1 Thermogravimetric analysis

A Perkin-Elmer Pyris 1 TGA was employed to conduct CO_2 capacity measurements at ADA-ES's laboratory in Highlands Ranch, CO under a range of temperatures and CO_2 partial pressures. The CO_2 partial pressure within the TGA assembly was controlled using CO_2/N_2 gas blends. A Hiden Analytical mass spectrometer (MS) was used to measure the gas concentration immediately above the sample of sorbent. Moisture was introduced into the gas stream by passing a portion of the gas through a heated bubbler. The moisture concentration was controlled by changing the bubbler temperature. The CO_2 capacity experiments contained a small amount of moisture because previous studies indicated completely dry conditions may lead to loss of amine reactivity.[4] For CO_2 capacity tests, moisture levels were calculated at *ca.* 1.5% by volume, minimizing its effect on the weight change of the sorbent due to CO_2 uptake. Note: TGA experiments conducted at ADA-ES in Highlands Ranch, CO, (elevation 1643 m) were operated at less than standard

atmospheric pressure; therefore with 100% CO_2, the atmospheric pressure was calculated to be 0.81 bar. The test setup is pictured in Figure 1.

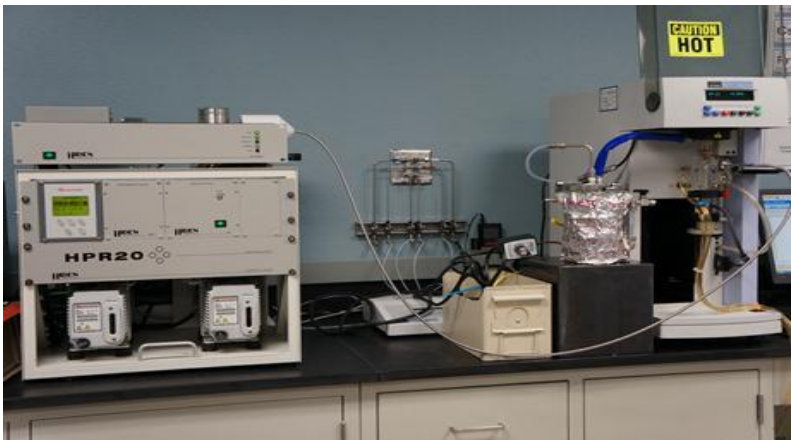

Figure 1. ADA-ES, Inc. TGA (right) and MS (left) setup with bubbler.

2.3.2 CO_2 working capacity

The TGA method to measure CO_2 working capacity at three different regeneration temperatures was used to screen potential sorbents, followed by a TGA CO_2 loading method. Approximately 3 to 5 mg of the AFA material undergoing analysis was loaded into the TGA sample pan. The gas flow rate was 50 sccm for all TGA experiments. The sample was purged under N_2 gas at 100 °C for 120 minutes until weight loss was stable. Then the TGA was cycled three times between adsorption conditions (40 °C and P_{CO2} = 0.15 bar) and regeneration conditions (100 °C, 110 °C and 120 °C and P_{CO2} = 0.81 bar). A room temperature bubbler was added to the TGA setup to introduce *ca.* 1 vol % H_2O into the gas stream to the TGA. The difference between the CO_2 loading at the adsorption conditions and regeneration conditions is the CO_2 working capacity. In addition to the CO_2 working capacity, kinetics at adsorption and regeneration conditions can be qualitatively measured.

2.3.3 Kinetics

One important reason that a sorbent may not achieve equilibrium CO_2 capacity in an actual operating system could be slow kinetics. Unfortunately, quantitatively measuring kinetics is not always straightforward. The rate of CO_2 uptake can be highly dependent on temperature, CO_2 partial pressure, sorbent particle size, gas/solids contacting, etc. If assessed properly, the kinetics can be used to determine many important process factors, such as required contact time, equipment size, contact scheme, etc. For each sorbent tested under this project, the kinetics were considered qualitatively. The time required for each sorbent to achieve 80% of its equilibrium capacity at adsorption conditions and P_{CO2} = 0.15 bar was calculated. A sorbent was considered to be at equilibrium when the weight of the sorbent stopped changing due to CO_2 uptake. The assumption was made that the sorbents were at equilibrium at the end of the 120 minute step. The weight gain during this step was identified as the equilibrium capacity. Then, by scanning the TGA data, the time required for the sorbent to achieve 80% of this weight gain was determined. If a sorbent's time to achieve 80% of equilibrium capacity was greater than 40 minutes, then the sorbent was classified as having slow kinetics. If the time to achieve 80% of equilibrium capacity was between 40 and 15 minutes then the sorbent was classified to have medium kinetics. If the time to achieve

80% of equilibrium capacity was less than 15 minutes, then the sorbent was classified as having fast kinetics. Figure 2 below shows fast kinetics on the left and slow kinetics on the right. The rate of CO_2 uptake was determined for all sorbents at the conditions of 40 °C and P_{CO2} = 0.15 bar. These conditions were selected for the kinetic analysis because 1) this is likely the optimal adsorption temperature and CO_2 partial pressure, and 2) because kinetics have been observed to be slowest at lower temperatures. Note that the time to 80% capacity is only a qualitative comparison because the temperature change in the TGA is not instantaneous. Therefore, it should not be used to calculate industrial scale contact times.

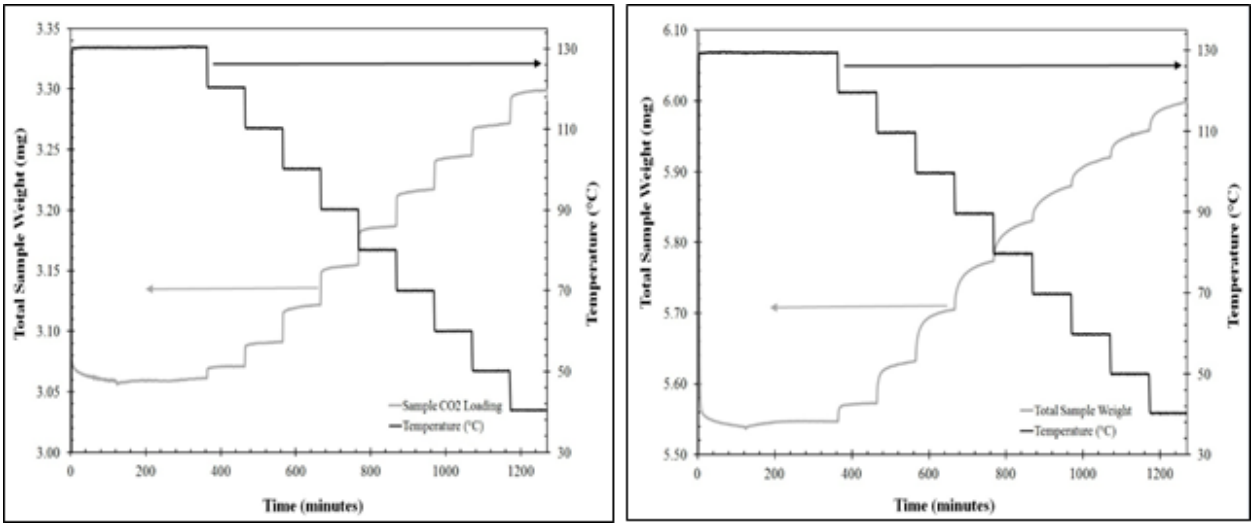

Figure 2. TGA Results for sorbent with fast (left) and slow (right) kinetics.

2.3.4 CO_2 Loading – Isobars

For the CO_2 loading evaluation, approximately 3 to 5 mg of the AFA sorbent was loaded into the TGA sample pan. The gas flow rate was 50 sccm for all TGA experiments. The sample was purged at 100 °C in the TGA under a N_2 atmosphere with approximately 1.0 vol% H_2O; this condition was held for 120 minutes until weight loss was stable. After 120 minutes the sample weight was recorded and considered the initial weight (i.e. no CO_2 adsorbed). After the initial weight was recorded, the N_2 purge gas was switched to either a N_2/CO_2 blend or pure CO_2, depending on the desired CO_2 partial pressure, still at 100 °C and 1.0 vol% H_2O. Then, after 120 minutes, the temperature was decreased by 10 °C. The temperature was decreased in 10°C increments until the final temperature of 40°C was reached. The incremental increase in weight at the end of each 120 minute step was recorded as the CO_2 loading at the test temperature and CO_2 partial pressure.

To develop isobars the CO_2 loading method was measured at CO_2 partial pressures of 0.08, 0.15, 0.30, and 0.81 bar. Sorbent characteristics that can be assessed from the TGA method are CO_2 loading at different temperatures, potential delta temperature of sorbent, and qualitative measurements of kinetics at each temperature. This method can be time consuming as each step needs to reach equilibrium to develop an accurate isobar curve. The kinetics can slow at lower temperatures as the sorbent reaches its CO_2 loading capacity.

2.3.5 Moisture Uptake

In addition to CO_2 working capacity, moisture uptake was used to evaluate and select a final sorbent. Moisture uptake is used to calculate the potential thermal energy required to regenerate a sorbent and can be measured using the TGA.

During the split gas moisture uptake procedure, the material was purged under N_2 gas at 100 °C for 120 minutes with the heated bubbler at room temperature until weight loss was stable. The estimated moisture introduced into the gas stream was about 1.5% by volume. The temperature was then lowered to adsorption conditions, 40°C, and measured for 90 minutes.

Under the 100% wet gas moisture uptake procedure, the material was purged under dry N_2 gas, 50 sccm, at 100 °C for 120 minutes with the room temperature bubbler until weight loss was stable. The gas stream flow rate was lowered to 15 sccm and passed through the room temperature bubbler, introducing about 1.57% H_2O by volume. The sample was then lowered to adsorption conditions, 40°C, and measured for 90 minutes. After 90 minutes, the sample was purged again under 100% dry N2 for 30 minutes. The volume of water was increased by changing the flow rate of the gas through the bubbler by increasing the flow rate to 30 sccm and then 50 sccm, to add 3.67% and then 4% H_2O by volume, respectively. Each condition was held for 90 minutes and sample weight was measured after the sample was purged under dry N_2 at 100 ^{0}C. The weight gain at the end of each 90 minute period was calculated to be the moisture loading for the sorbent at each condition, 0.008, 0.014, and 0.027 bar H_2O.

2.3.6 Automated Fixed Bed

In this phase of the carbon capture project, the ADA-ES lab-scale fixed bed sorbent screening device was used to evaluate sorbents that had been identified as potential sorbents. A Programmable Logic Controller (PLC) completely automates the testing process. With an automated system, a series of adsorption/regeneration cycles can be completed with little to no supervision. The flow rate of the flue gas is approximately 250 or 300 mL/min, and the amount of sorbent in the reactor is *ca.* 1 g. The sorbent and flue gas are contacted in a fixed bed through a sequence of temperature-controlled lines and electrically controlled valves. The adsorption and regeneration breakthrough curves are measured. Figure 3 is a schematic of the sorbent screening testing unit when configured for laboratory testing. The CO_2 analyzer is a continuous non-dispersive infrared (NDIR) sensor.

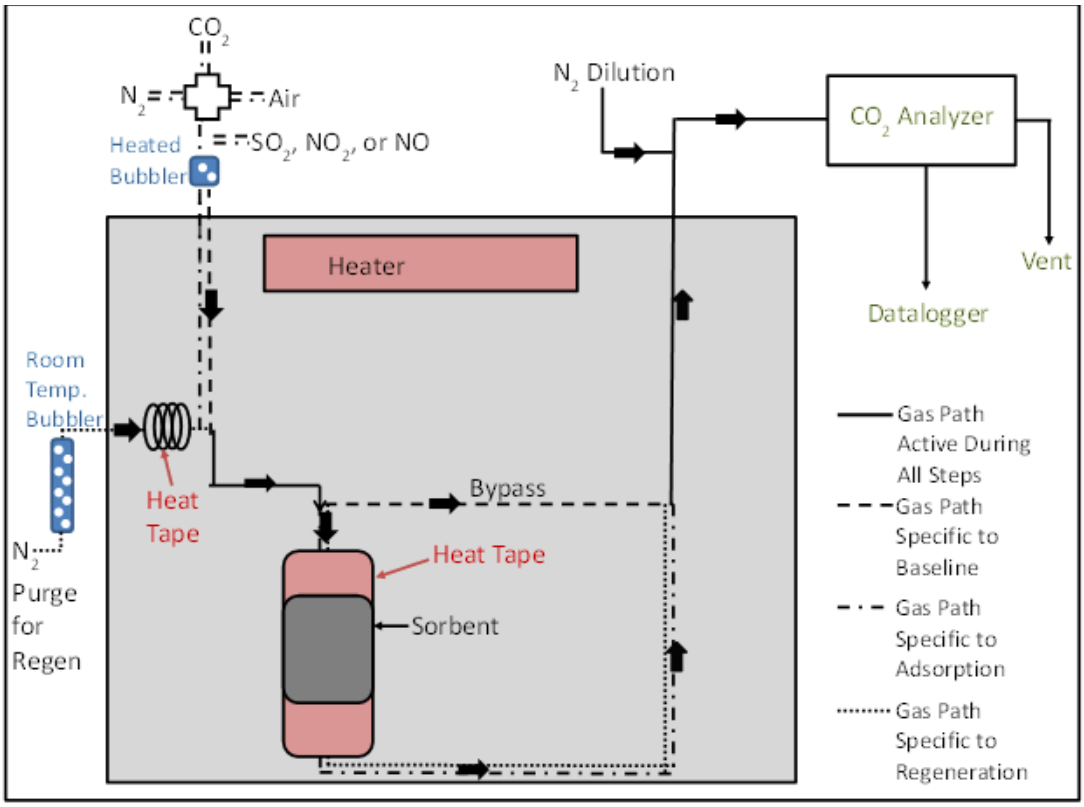

Figure 3. Schematic of the Sorbent Screening Test Unit, Automated Fixed Bed, Configured for the Laboratory.

After the sorbent is placed into the fixed bed, it is heated to an initial flushing temperature. The initial flushing temperature is based on the regeneration temperature. A thermocouple on the outside of the glass fixed bed is used to determine when the bed reaches the desired temperature. When the bed temperature matches the desired adsorption temperature, the sorbent is flushed with dry N_2 for 10 minutes or until no CO_2 is measured in the purge gas stream, whichever is longer. Then the simulated flue gas is sent through the bypass line circumventing the sorbent. The composition of the laboratory sample gas, by volume, was approximately 10% CO_2, with a balance of N_2. Approximately 4% moisture by volume was added directing the simulated flue gas through a bubbler at a temperature of 23°C. Note that if the gas were fully saturated at 40°C, the moisture concentration would be approximately 9% (by volume). However, ADA-ES selected the moisture level of 4% based on the design for ADA-ES's sorbent-based CO_2 capture 1 MW pilot; the increase in pressure required to overcome the adsorber pressure drop reduces the gas moisture concentration to ~4% (by volume). When the CO_2 reading is stabilized at the known CO_2 concentration (i.e. baseline reading), the gas flow is directed through the sorbent. The CO_2 concentration drops as the sorbent removes the CO_2 and then, as removal rate decreases, the CO_2 concentration increases. The end of the adsorption step occurs when the CO_2 levels return to their original levels i.e., the sorbent is saturated with CO_2. Figure 4 shows an example of an adsorption breakthrough profile.

A temperature swing with a N_2 purge gas is used to regenerate the sorbents and desorb the CO_2. The regeneration purge gas flow rate is the same as that of the flue gas, approximately 250 mL/min. The regeneration step begins with the system stopping flue gas flow in order to switch to heated N_2 gas only. While the heated purge gas flows through the sorbent, heat tape on the outside of the

fixed bed ensures that the sorbent is fully heated to the selected regeneration temperature. Upstream of the reactor, the N_2 purge gas is directed through a bubbler separate from the one used for adsorption. A breakthrough profile of desorption curve is shown in Figure 4.

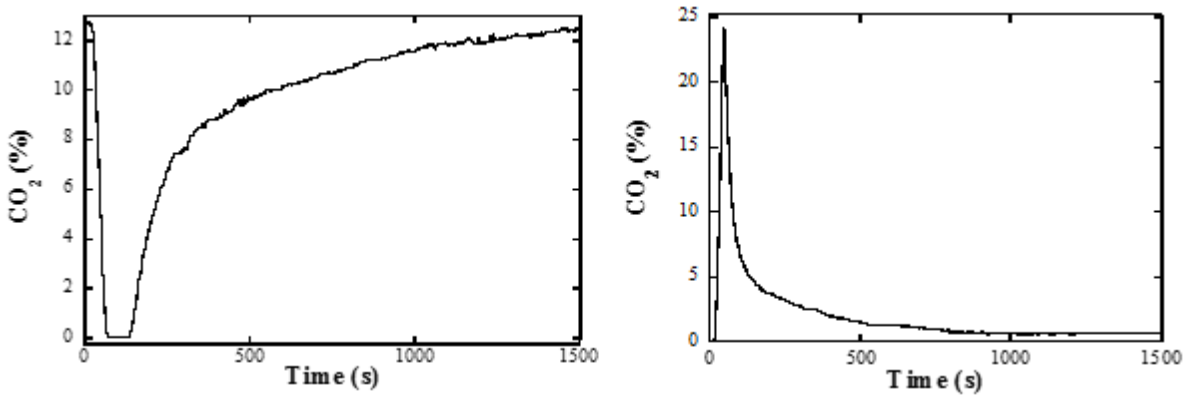

Figure 4. Example of an Adsorption (left) and Desorption (right) Breakthrough Profile on the Automated Fixed Bed

2.3.7 Cyclic Stability

For some supported amines, volatilization and degradation of the amine can occur due to a temperature swing. Because this is considered unacceptable for a commercial-process, potential CO_2 sorbents must be able to withstand thousands or tens of thousands of adsorption/regeneration cycles. In general, extensive cyclic testing is not discussed in the public literature, which is possibly due to the extensive time requirements. However, ADA-ES can complete long-term cyclic testing using an automated fixed bed with minimal work once the test has been started. Selected sorbents from the TGA screening were evaluated for cyclic stability using the fixed – bed described above with an adsorption temperature of 40°C and regeneration temperature of 100°C.

2.3.8 Mass Spectrometer Fixed Bed

Mass Spectrometer Fixed Bed temperature-controlled fixed-bed device coupled with a mass spectrometer (MS) was used to measure the selectivity of sorbents to a range of expected flue gas constituents and, through analysis of the results, estimate the flue-gas clean-up requirements upstream of the CO_2 capture process. A mixture of laboratory gases was introduced to the inlet of the fixed bed and the MS measures the effluent from the bed, tracking breakthrough for CO_2, water, and other species. Figure 5 shows the fixed-bed device coupled with the MS.

2.3.9 Breakthrough Curves

The breakthrough curves were needed to assess the sorbent selectivity, and were determined as follows:

A sorbent bed with about 100 mg of the sorbent was placed into the MS fixed bed. The sorbent was purged under 100% dry N_2, flow rate 100 sccm, at the regeneration temperature of 100 °C for 20 minutes. A thermocouple was placed on the outside of the glass fixed bed to determine when the bed reaches the desired temperature. The gas flow is switched to the bypass section of the MS fixed bed then the gas was changed to flue gas concentration and was baselined on the MS. During this time the bed was cooled to 40 °C. The flue gas flow was switched to the bed and adsorption curves were measured with the MS until the gas concentration is recovered to baseline levels. Then

gas flow is switched to 100% N_2 to flush the flue gas from the bed. The gas flow was moved back to bypass of the instrument and the sorbent bed was then heated to 100 °C for 20 minutes. After the 20 minutes, the bed was flushed with the 100% N_2 while the mass spectrometer measured the off gas of the purge.

Figure 5. Mass spectrometer-fixed bed (right); detail of heated fixed bed enclosure (left).

2.3.10 Heat of reaction of sorbent by DSC

The DSC signal is based on heat flow measurements between a reference and the sample of interest. It can be used to determine solid (or liquid) specific heat capacity, or in the case of CO_2 sorbents, can provide information on the heat of reaction in different environments. Both values are critical to assess a sorbent for the CO_2 capture process and make the comparison easier among many different types of sorbents for further process development.

A DSC/TGA combination instrument can be utilized to simultaneously measure heat flow and also weight change signal as the sample goes through the thermal program in a desired atmosphere. The samples of interest were exposed to three atmospheres in the instrument chamber to characterize the samples sorption behavior under different atmospheres. The method described below was programmed in the instrument software. For this project, a third party, Hazen Research, was employed to do the simultaneous DSC /TGA testing.

The method contains the steps below:

1- Isothermal hold at room temperature for 30 min, under dry N_2, Gas flow 100 ml/min
2- Conditioning step from room temperature to 120 °C in dry N_2 and hold at 120 °C for 100 min.
3- Cool down the sample from 120 °C to 40 °C under dry N_2 and hold at 40 °C for 30 min.
4- Once stabilized at 40 °C, switch gas to reacting gas at 40°C, hold for 60 min. (exothermic)
5- Switch gas to dry N_2 and hold for 30 min at 40 °C and then heat the sample up from 40 to 120 °C in dry N_2, hold for 15 minutes (endothermic)
6- Cool down the sample from 120 °C to 40 °C under dry N_2, hold for 15 minutes (exothermic)

The reacting gas in step 4 dictates the only difference among the methods in different environments. The three reacting gases include 15% CO_2 balanced in N_2, wet N_2 and wet 15 % balanced CO_2 in N_2. The wet condition refers to the moist gas blown to the bubbler to contain a

saturated gas containing ~ 3% volume of water. Specific heat capacity for the samples was also measured using DSC in different temperatures (in the range of 20-120 °C) in a dry N_2 environment.

2.3.11 Jet Cup Attrition Testing

Jet cup attrition testing was used to determine the tendency of sorbent particle to fragment when colliding with other particles and reactor walls in a fluidized bed process. For these tests, sorbents were sent to Particulate Solid Research Incorporated (PSRI) where the samples were tested in PSRI's jet cup attrition apparatus. The test involves cycling the particles through a cyclone at 300 ft/s for 2 hours under a nitrogen atmosphere. Particle size distributions are assessed before and after testing to determine the attrition of the particles.

2.3.12 Crush Strength Testing

Crush strength testing was performed by Southwest Research Institute (SwRI) using the ASTM D6175 method whereby the samples are dried and then crushed to determine the amount of compressive force required to fracture the particles. Combined with the jet cup attrition testing, crush strength testing can be useful in determine which sorbent particles may be most resistant to attrition.

2.4 AFA Pelletization and CO_2 Capture Performance Evaluation at University of Akron.

2.4.1 Aerogel sorbent screening test

The team at the University of Akron evaluated a number of sorbents produced by Aspen Aerogels. The first step for screening the sorbents was to measure the total CO_2 capacity at temperature and pressure approximately representative of adsorption and desorption conditions (i.e., T adsorp. = 40 °C, T desorp. = 100 °C). UA has the capability to measure the CO_2 capture capacity of up to 36 independent sorbents in a simultaneous run. In these measurements the sorbents are exposed to a common CO_2/air stream for adsorption and are heated in a common oven for desorption. The adsorption and desorption conditions (temperature, concentration, time) can be adjusted accordingly, and are the same for all the sorbents. By this quick test screening, Aspen and UA efficiently compared the different sorbents to select the optimum one for pelletization and further testing.

2.4.2 Strategy to address the SO_2 poisoning issue and pelletization of AFA powder

Amine-based sorbents suffer from SO_2 poisoning. There is currently not a sorbent which only adsorbs CO_2 without adsorbing SO_2 because the acidity of SO_2 is stronger than CO_2 and its binding strength to amines is stronger than CO_2 as well. What is worth pointing out is that existence of SO_2 not only poisons the sorbents but also decreases the purity of desorbed CO_2. The purity of CO_2 produced from the CO_2 capture process is very critical for practical applications. For example, the EOR (enhanced oil recovery) requires a CO_2 purity of > 99.9 mol% with no SO_2[5]. Protecting sorbents from SO_2 poisoning and generating high-purity CO_2 from the process are two unavoidable tasks in this project. The economic feasibility considerations are also important to the scale-up and commercialization of the CO_2 capture process. The University of Akron has previously developed polymeric binder formulations that promote agglomeration of sorbent particles, and provides linkage points that allow spacing for diffusion of CO_2. The binder includes epoxy functional groups, and helps make the pellets resistant to (i) attrition under fluidization

conditions, (ii) contact with water and steam, and (iii) the accelerated degradation of the sorbent upon long term cycling, in the presence of poisoning gas (SO_2).

Selected samples were pelletized by mixing the sorbent with binder solutions made at UA, extruding the resulting "wet paste" into 0.5 to 1 mm cylindrical pellets, and heating in a convection oven to dry the pellet and harden the structure. The ratio of binder to sorbent was adjusted to incorporate between 10 and 25 wt.% of solid binder in the final pellet, expressed by the ratio of binder solution to sorbent (binder/sorbent). The density of the pellets produced was estimated around 1.2 – 1.3 g/cc. Depending on the chemistry of the AFA powder, UA has developed two families of binder solutions/coatings: the standard binder solution and the SRE coating/binder. The compatibility matrix is shown in Table 1.

Table 1. Compatibility matrix of UA binder with Aspen's sorbents.

AFA type	Std. Binder	SRE
PEI loaded and PEI functionalized Aerogel	Yes	Yes
Mono-amine alkoxysilane and bridging amino-siloxane functionalized Aerogels	No	Yes

2.4.3 In-situ IR testing on AFA sorbent

The CO_2 adsorption on AFA sorbent was studied by in-situ FT-IR and mass spectrometer. Figure 6 shows the experimental setup consisting of (i) a gas manifold with mass flow controllers, a 4-port valve for switching the inlet gases between Ar and a 15% CO_2/air mixture, a six-port valve for CO_2 pulse calibration, and a DI water saturator, (ii) a DRIFTS (diffuse reflectance infrared Fourier transform spectroscopy) cell loaded with 45 mg of CQA12 sorbent placed inside a Nicolet 6700 FTIR bench (IR), (iii) a Pfeiffer QMS 200 quadruple mass spectrometer (MS), and (iv) a Labview module to control and monitor DRIFTS cell temperature and heating rate. The setup has the option to introduce the water vapor into the gas streams by flowing the gases via saturator prior to entering into the DRIFTS reactor. When conducting the experiment of dry runs, the gas streams bypass the saturator. Effluents of the DRIFTS reactor are monitored continuously by mass spectrometer. In case of humid run, which has 10% water vapor content in the gas streams, a condenser was placed in between DRIFTS outlet and inlet of mass spectrometer to avoid clogging of capillary of mass spectrometer by water present in the reactor effluents.

Dry runs: Prior to CO_2 adsorption, the sorbent was pretreated by heating to 100 °C for 5 min. in the presence of Ar flowing at 150 cm^3/min. CO_2 pulse and batch calibrations were subsequently performed. CO_2 pulse calibration was performed by pulsing 1 and 3 cm^3 of CO_2 via the 6-port valve. The DRIFTS cell was set into batch mode by closing inlet and outlet valves. CO_2 batch calibration was performed by injecting 2 cm^3 of pure CO_2 with increments of 0.5 cm^3 into the DRIFTS cell. The sorbent was cooled to 40 °C after calibration. A typical CO_2 capture cycle was performed by, (1) adsorbing CO_2 at 40 °C for 10 min by switching 4-port valve from Ar to 15% CO_2/Air mixture, (2) purging the gas phase CO_2 and weakly adsorbed CO_2 species by switching back 4-port valve from 15% CO_2/Air mixture to Ar, (3) regenerating the sorbent by heating it to 100 °C for 5 min. Three CO_2 capture cycles were performed for each case (dry, 4% water vapor, 10% water vapor). The first cycle was performed by normal temperature programmed desorption

(TPD), where the sorbent was regenerated by heating to 100 °C in the presence of Ar flowing at 150 cm^3/min. Second and third cycles were performed by batch TPD, where the sorbent was regenerated by heating to 100 °C in batch mode (both inlet and outlet valves closed).

Humid runs: To maintain 4% water vapor content in the inlet gas streams, the saturator is maintained at room temperature. The saturator was heated to 50 °C to maintain 10 % water vapor content in the inlet gas streams*. In case of the humid run with 10% water vapor, (i) all the lines between the saturator and the DRIFTS cell were heated to at least 60 °C to avoid condensation of water in the gas lines and, (ii) hot air at 60 °C from an inline heater was blown outside the dome of the DRIFTS reactor to avoid any condensation of water vapor on the ZnSe windows which may cause blockage of the IR signal. The specific humidity in this experiment was not measured.

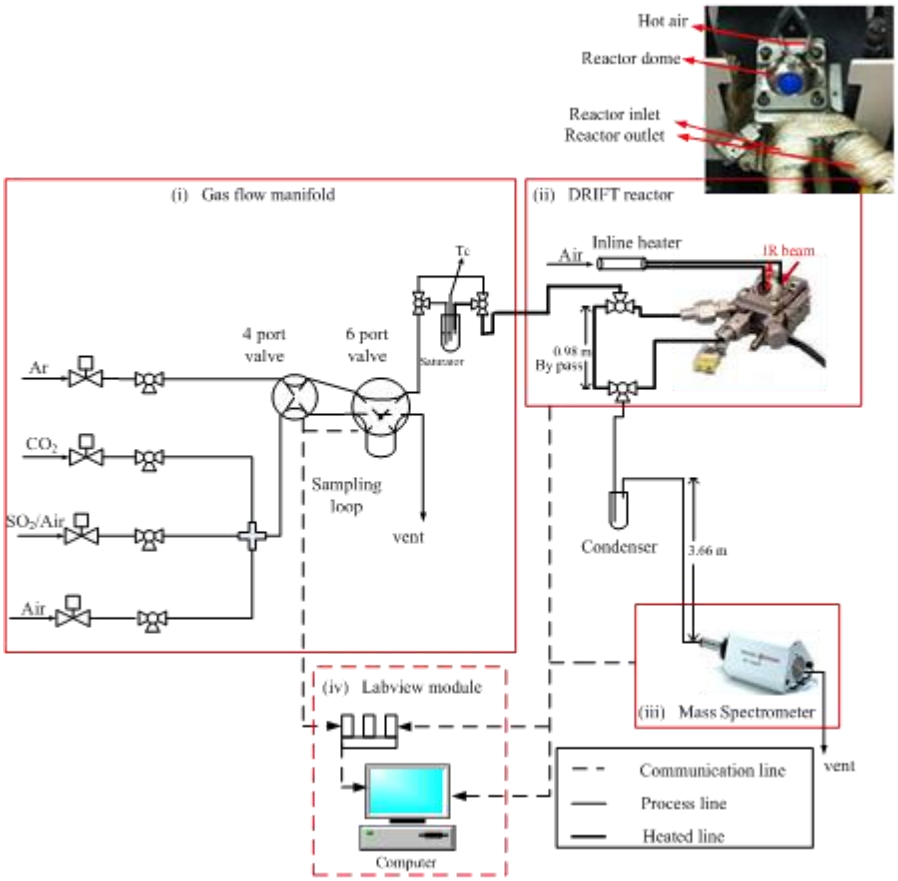

Figure 6. Schematic of the experimental set-up for the IR study on the effect of humidity on CO_2 adsorption.

2.4.4 Bench scale up AFA production and the pelletization process

A large amount (30 kg) of optimum AFA sorbent powder was prepared at Aspen during budget period 3, to be formed into pellets at UA for bench-scale fluidized bed testing. Prior to pelletization, the AFA aerogel was converted into a fine powder (particle size ~ 70 micron) using a large mill (a miller, ~ 60 l/hr) (see Figure 7).

Figure 7. The large mill used to pulverize the AFA sorbent to micron size particles.

A scaled-up pelletization process has been developed to convert the 30 kg AFA powder into pellets. The process included four steps: mixing, extrusion, spheronization, and drying:

2.4.4.1 Mixing

The mixing step is to achieve a uniform paste of the sorbent and binder ingredients for the extrusion step. 500 grams of sorbent is consumed in each batch. Mixing is completed with the help of a blender. Due to the unexpected performance of the sorbent, the SRE coating/binder could not be applied. Instead, a modified UA Standard Binder was used.

2.4.4.2 Extrusion

A commercial basket extruder (LCI BR-150) was used to extrude the prepared paste into cylindrical shapes which have a diameter of ~1.0 mm. The extruder has a pressure blade to feed the raw paste to the extrusion area. The extrusion blade pushes the paste against the extrusion die which has a whole diameter of 1.0 mm. The rotary speed of the extrusion blade was set to 30 rpm. The extruder and the extrudate are shown in Figure 8.

Figure 8. Commercial basket extruder and the extrudate (AFA sorbent + binder).

2.4.4.3 Spheronization

A homemade spheronizer (illustrated in Figure 9(a)) is utilized to spheronize the extrudate. The cylindrical extrudate is broken into shorter cylinders and further spheronized during the fast orbital movement. Photos of the spheronized pellets are shown in Figure 9 (b).

(a) (b)

Figure 9. (a) Illustration of the homemade spheronizer, (b) Spheronized AFA sorbent pellets in the spheronizer.

2.4.4.4 Drying

The spheronized pellets were dried in a convection oven at 100 °C for 12 hours. The pelletization process can be applied to other sorbents and binders as well. The pelletization process requires optimization of the process parameters and fine recipe adjustment. The process parameters include the rotary speed of the extruder, the rotary speed of the spheronizer, the batch size of the extrudate fed into the spheronizer, and the drying conditions. Recipe adjustment is required to achieve an optimal paste which has the best wetness for extrusion.

2.4.5 1 kW-Scale Pilot Unit Testing

UA owns a 1 kW system testing that can operate under different conditions (gas velocity, temperatures, gas composition, (Figure 10)) to collect useful data on CO_2 capture performance of solid sorbent. The 1 kW system has seen several changes and improvements. Numerous issues including CO_2 leak, temperature control, and issues in constructing and maintaining the moving bed fluidized system were resolved during the second budget period. UA has performed several blank tests prior to testing the pelletized AFA sorbent.

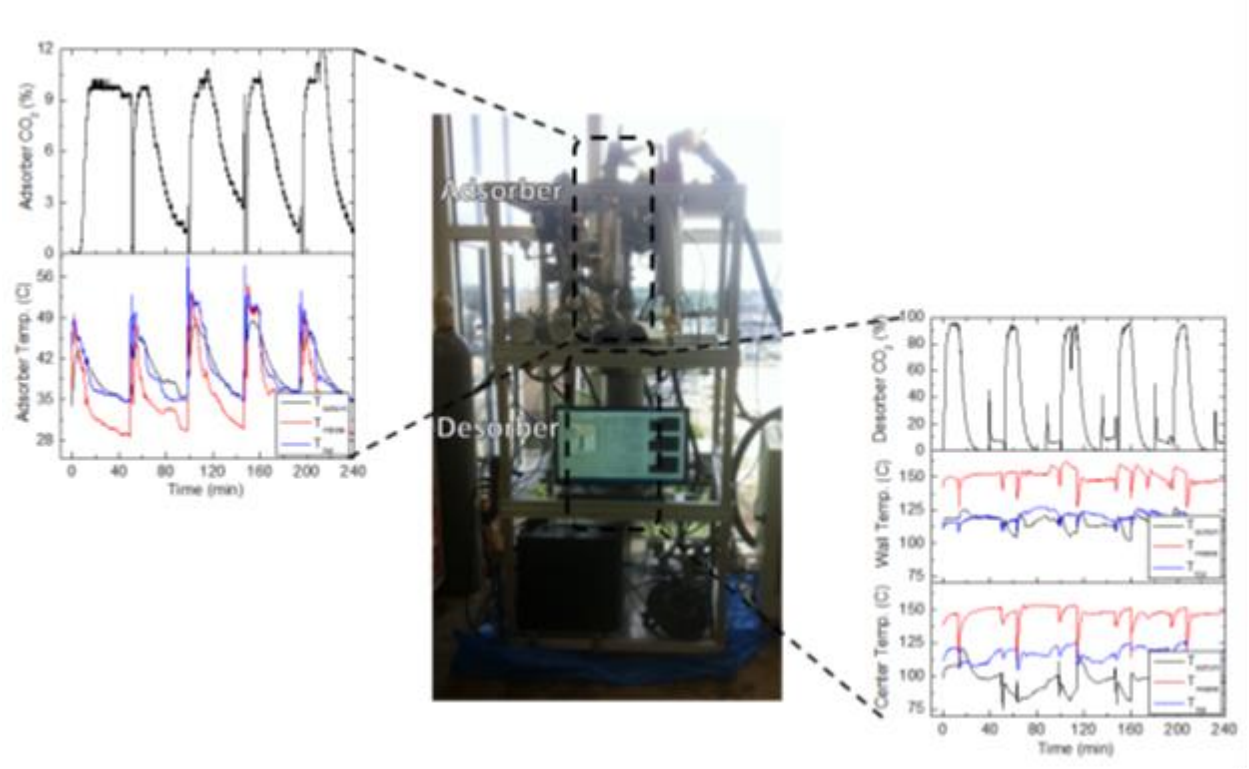

Figure 10. Overview of the pilot-scale CO_2 capture system.

The adsorber holds up to 3 L of sorbent, however, only half the maximum capacity for sorbent was used for testing (1.5 L, 0.5 kg of pelletized sorbent at 355-500 μm diameter). Initial trials were chosen to test the adsorption in the bed through varying flow rates of 15% CO_2/air mixture at 5/10/20 LPM (Liters Per Minute) at 40 ˚C and under desorption at 100 ˚C. A high temperature desorption trial at 120 ˚C was included to test for enhanced degradation under elevated desorption temperatures. A water saturator was put in-line with the CO_2/air mixture to the adsorber. It is also important to note that the high-pressure pellet blower uses humid outside air to cool the pellets and return them to the adsorber.

Two sets of trials, each approximately 30 cycles, were performed for each of the different flow rate conditions. The first set of trials suffered from an internal steam leak due to over tightening of a fitting in the steam line during checks for CO_2 leaks to the atmosphere. The set of trials were then repeated after drying the pellets. CO_2 flow rate from the desorber was a new capability added to the system for these trials, however, the power supply on the gas flow sensor failed during the 5 LPM trial and could not be replaced until the 10 and 20 LPM trials. Additional power supplies have been obtained for rapid replacement in the future. The testing protocol is listed below in Table 2.

Table 2. A basic outline of each step of the automated CO_2 capture process.

Step	Action…	End After/When…
0 – Warm up (this step is not repeated)	Run the steam system and recirculation pump until the desorber reaches	Set-point is reached
1 – Adsorption	Flow CO_2/air mix to the adsorber; recirculate and purge the desorber	After 10 min.; the desorber has been purged to >99% CO_2 (optional to set a control for %CO_2 in adsorber)
2 – Pellet Drop	Stop desorber recirculation; open valve at bottom of adsorber to drop pellets into desorber	After 8 sec.
3 – Fluidization/Desorption	Recirculate desorber	After 20 min. (usually set to 17 min. to include the 3 min. of Step 4 as part of the "20 min. desorption")
4 – CO_2 Extraction	Recirculate desorber and run CO_2 outlet vacuum pump to remove CO_2 from desorber and send to flow/% sensors	%CO_2 at outlet is <95% purity (optional to set a minimum time for this step; default to 3 min.) (optional to set a minimum flow rate from the vacuum)
5 – Pellet Return	Operate the pellet blower to move pellets from desorber to reserve	After 25 sec.
6 – Loop Seal	Operate the loop seal to move pellets from reserve to adsorber	After 5 sec. (usually disabled with the pellets moving directly from desorber to adsorber in Step 5; necessary for cycling multiple pellet beds)
7 – Wait for Adsorber to Equilibrate	Recirculate desorber while the pellet bed and adsorber thermocouples stabilize; then *go to Step 1*	After 2 min.

2.5 AFA Bench- Scale Testing

2.5.1 Sorbent pellet physical characterization and fluidizing regime

Sorbent pellet density, size distribution, fluidizing gas velocities, and void fraction, were measured by Particulate Solids Research Inc. (PSRI; Chicago, IL). Pellet apparent density was measured using mercury porosimetry in order to determine the volume of the pellets, excluding outward-connecting pore spaces but including closed voids. Particle size distributions were measured using a laser diffraction particle size analyzer (Sympatec HELOS III; Beckman Coulter, Brea, CA) binning particles into 17 equally-logarithmically spaced increments of 0.76 power, from 150 microns up to 1,750 microns.

Minimum fluidizing velocity, bed height, and bed pressure drop was tested in an 8-inch diameter (0.349 ft^2 cross sectional area) fluidizing bed vessel with sorbent pellet loose density height of 21.5 inches (in the absence of gas flow), with a distributor plate consisting of 19 holes with 9/32-inch diameter each. Twenty three gas velocities, measured as volumetric flow divided by vessel cross section, incrementing from 0.143 to 1.59 ft/s were delivered in an ascending-then-descending sequence to determine the minimum fluidizing velocity and onset of bubbling and slugging. The onset of vigorous bubbles and slugs is considered a turbulent fluidized bed.

Apparent bed density and standard deviation of pressure fluctuations were measured at gas velocities zero ft/s, 1.5, and up to 6 ft/s in 0.5 ft/s increments from which the void fraction could be calculated.

The heat transfer coefficient K_f was measured in the same 8-inch diameter vessel and distributor plate as above in previous experiments, but with a 17-inch height bed height at three velocities 2, 4.5, and 6 ft/s. This coefficient is of critical design importance because it determines how fast heat can be removed from the adsorber during the sorbent's exothermic reaction with CO_2.

3 RESULTS AND DISCUSSION

3.1 AFA Sorbent CO_2 Capture Performance

Aspen has principally focused on optimizing the CO_2 capture performance of its promising sol-gel/aerogel formulations developed in a previous program. ADA-ES and UA assisted Aspen by performing physical and CO_2 performance testing of its sorbents. Figure 11 shows the CO_2 capacity measured for several AFA sorbents as screened at UA. The most promising sorbents were further tested by ADA-ES for total and working CO_2 capacity, using TGA. Two types of AFA sorbents (i.e. two sol-gel formulations) were produced, characterized and tested for CO_2 capture:

- **AFA Sorbent Type #1**-(type 90414-4 or KD-240-24 sorbents):
  - Direct amine grafting process, using amino-alkoxysilane and dipodal bridging alkoxysilane precursors and sol-gel process.

- **AFA Sorbent Type #2** (type CQA-12 and CQC-XX):
  - "Double functionalization" process used by incorporating amino groups by grafting and impregnation methods.

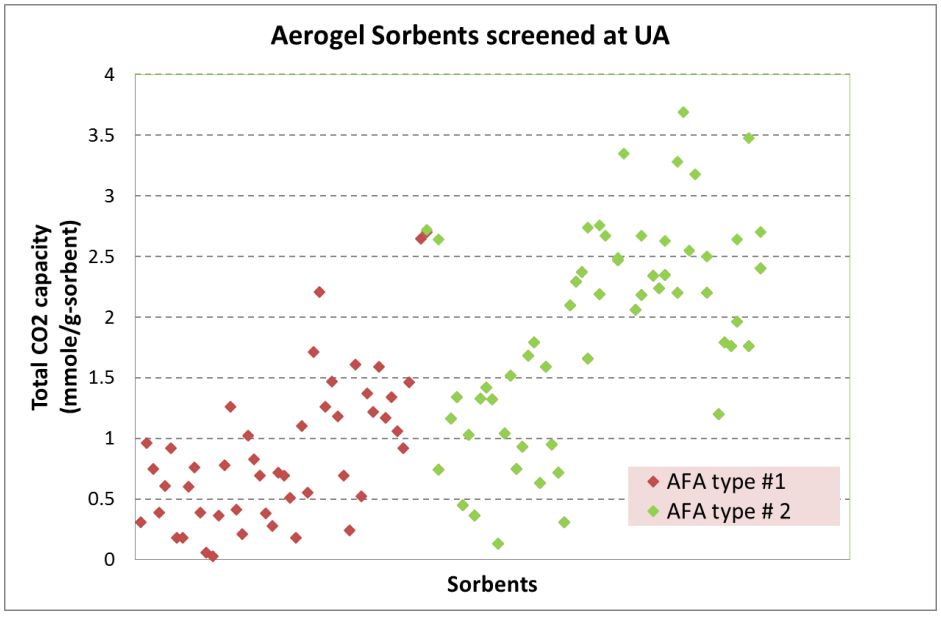

Figure 11. Aerogel sorbents screened by UA (target: > 2.72 mmole/g-sorbent (12 wt. %) for total CO_2 capture).

3.1.1 AFA type # 1 sorbent using amino-alkoxysilane precursors.

Chemistry optimization of the AFA sorbent type #1 relied heavily on the experimental approaches used to make the best performing sorbent, GE, from the previous SBIR Phase II effort[3], which demonstrated 6.3 wt.% working capacity with stability over 2,000 cycles (adsorption 40 °C and desorption 10 °C), and had fast kinetics. However, the corresponding pellets showed more than a 30% decrease in CO_2 working capacity and the kinetics decreased significantly. The aim of this optimization is to maximize CO_2 adsorption capacity and kinetics with a temperature swing (adsorption at 40 °C and desorption 100 – 120 °C), while maintaining hydrophobicity and stability over many cycles.

Initially, sol-gels were made based on the GE formulation, using two different amine-alkoxide precursors (amino-alkoxysilane 1, and amino-alkoxysilane 2), but the solid content of the sols limited the target density of the resulting aerogel to 0.22 g/cc. Higher target densities were sought in order to increase amine loading and enhance mechanical stability. In order to make higher density aerogels, the water content of the sols was decreased and the solid content was increased to the maximum possible amount. Aerogels with densities as high as 0.35 g/cc and 0.4 g/cc have been achieved.

IR spectroscopy on a few samples confirmed the incorporation of amine in the final aerogel (Figure 12). The spectra were normalized so that the Si-O-Si peak at 1120 cm^{-1} had the same intensity. Peaks corresponding to $–NH_3$ appear at 1570 and 1480 cm^{-1}, and after subtracting background signal, the intensity of the $–NH_3$ peaks correlate well with the amount of amino-alkoxysilane 1 used in each sol, confirming amine retention in the final aerogel.

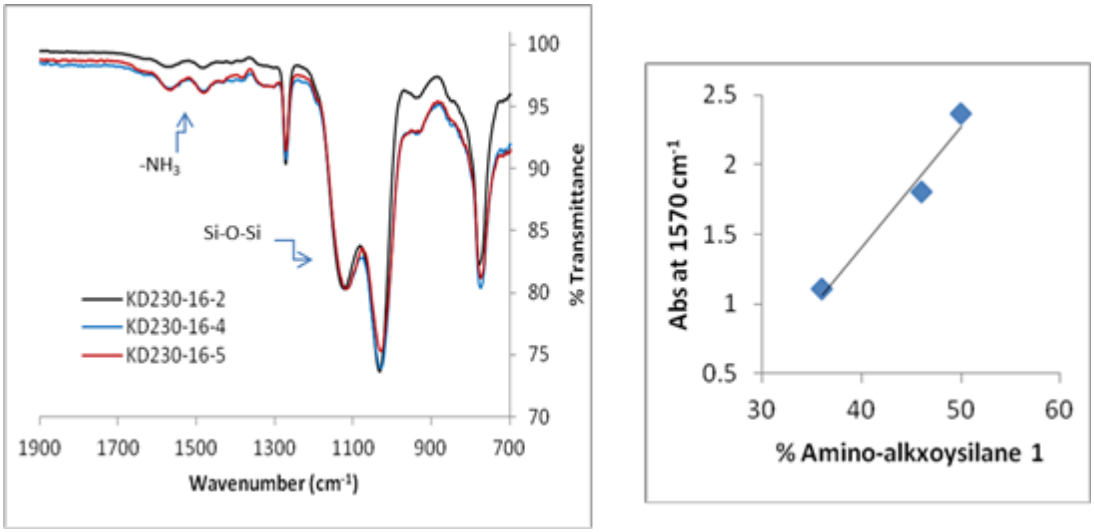

Figure 12. IR spectra of AFA sorbents, normalized to the Si-O-Si peak at 1120 cm^{-1}.

BET measurements and TGA/DSC were done on selected samples. The highest surface area was 394 m^2/g for the lowest density (0.1 g/cc) sample. Increasing the % amino-alkoxysilane led to lower surface area, this is likely due to weakening of the gel. Pore volume followed a similar trend as surface area, with the highest pore volume being 1.0 cm^3/g for the lowest density sample. Average pore width was higher for the samples with low surface area and pore volume. Structural properties of the selected AFA sorbent are reported in Table 3 and shown in Figure 13.

Table 3. BET measurements of selected AFA sorbents.

Sorbent #ID	Density (g/cc)	BET surface area (m^2/g)	BJH pore volume (cm^3/g)	BET average pore width (nm)
KD230-16-2	0.1	394	1.0	9.7
KD230-16-7	0.35	39	0.2	21.7
KD230-16-8	0.35	171	0.4	9.9
KD230-18-4	0.3	8	0.1	21.0

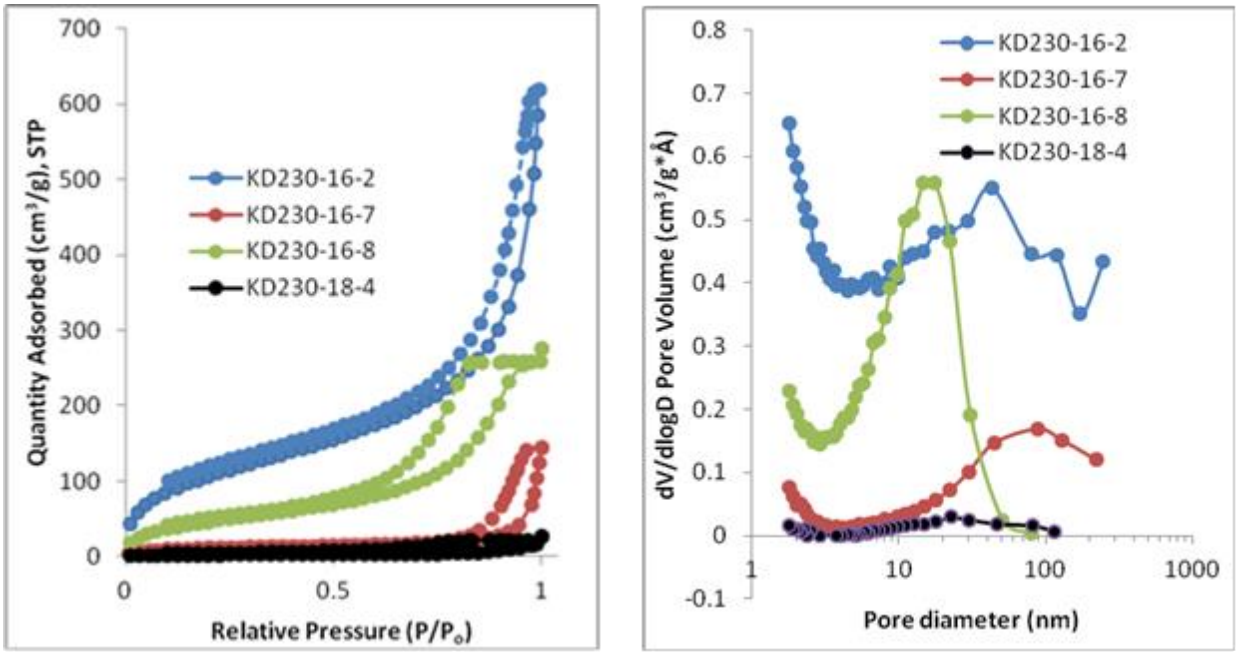

Figure 13. BET (liquid N_2 adsorption/desorption) and pore size distribution of selected AFA sorbents.

CO_2 uptake was measured at 40 °C after pre-treatment at 100 °C, at the University of Akron (UA). Gels of varying strengths were made with amino-alkoxysilane 1 at 0.1 and 0.35 g/cc densities by varying the wt.% amine precursor to just below the threshold value for gelation. Much higher wt.% CO_2 uptake was achieved for the higher density samples (Figure 14a). At both densities, the CO_2 uptake decreases as the amine content increases, presumably due to the corresponding weakening of the gel. Strong gels were also made at intermediate densities of 0.22 and 0.3 g/cc. As the wt.% amino-alkoxysilane 1 that can be incorporated into a strong gel increases with increasing density, the CO_2 uptake increases from 4.7 wt.% at 0.1 g/cc to 9.7 wt.% at 0.35 g/cc (Figure 14b). High-density samples made with amino-alkoxysilane 2 achieved somewhat lower CO_2 uptakes than those made with amino-alkoxysilane 1 at similar wt.% amine levels.

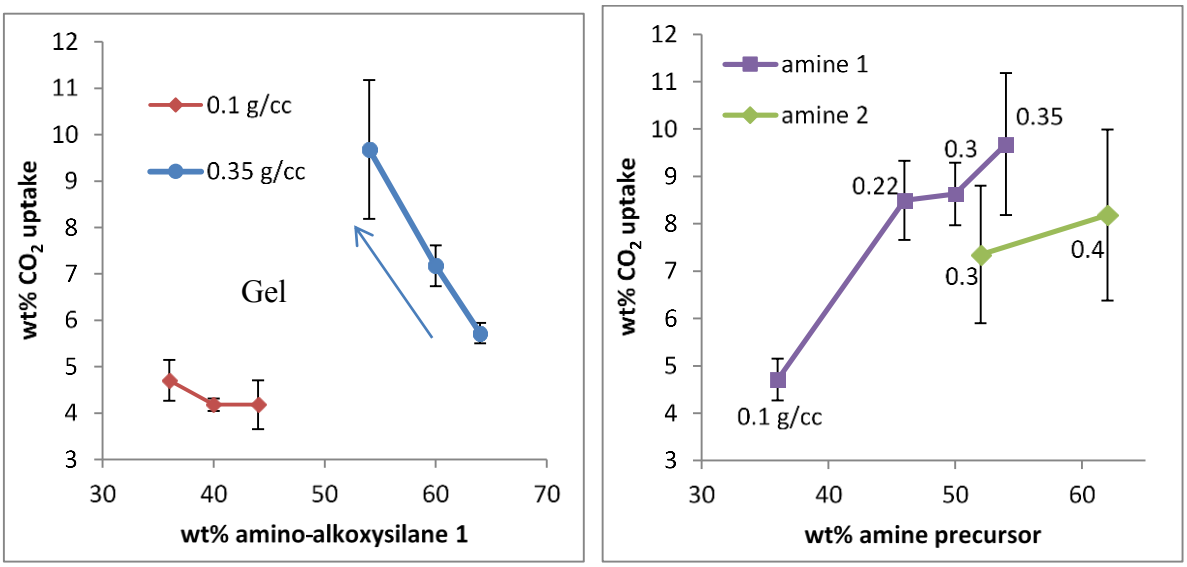

a) b)

Figure 14. CO_2 uptake as a function of a) wt.% amino-alkoxysilane 1 at 0.1 and 0.35 g/cc, and b) wt.% amino-alkoxysilane 1 and 2 for strong gels only at densities ranging from 0.1-0.4 g/cc.

The CO_2 uptake of high-density (0.3 - 0.35 g/cc) aerogels made with amino-alkoxysilane 1 was compared over an amine content range from 32 - 64 wt.% Figure 15. Lower amine content results in higher CO_2 uptake until 54 wt.% amine is reached, after which the CO_2 uptake declines. The fraction of active amine sites, as estimated by the calculated mol ratio of CO_2:NH_2, follows a similar trend over the higher end of the range, but the value plateaus at 32 - 52 wt.% amine. Assuming a 1:1 CO_2:NH_2 adsorption mode, at the optimized amino-alkoxysilane 1 content of 54 wt.% with 9.7 wt.% CO_2 uptake, 45% of the amine sites are active toward CO_2 adsorption.

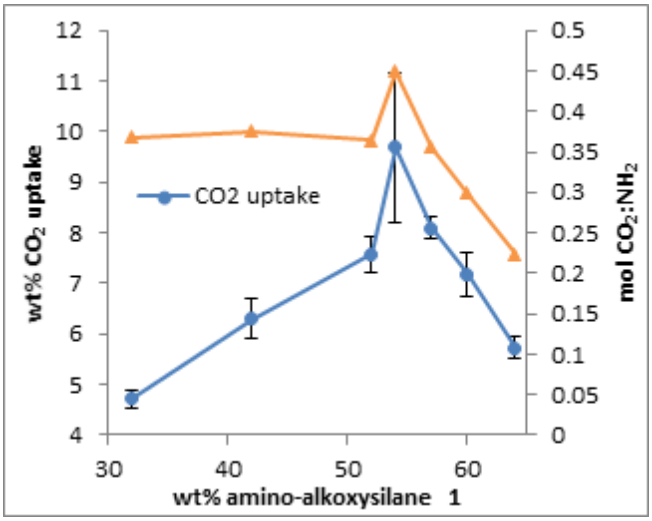

Figure 15. CO_2 uptake for high-density (0.3-0.35 g/cc) aerogels over a wide range of wt.% amino-alkoxysilane 1 levels.

Overall, the first AFA sorbents made with either amino-alkoxysilane 1 or amino-alkoxysilane 2, showed a maximum total CO_2 capture capacity of 9.68 wt.% (sorbent KD230-16-8) at low desorption temperature (100 °C). Increasing the amount of amino-alkoxysilane into a high-density (≤ 0.3 g/cc) aerogel, with the goal to increase the percentage of active amine sites, was accomplished by adjusting the amount of water in the sol-gel synthesis. The percentage of active amine sites has shown to be low due to leaching of the amine during solvent exchange.

3.1.2 AFA type # 1 sorbent using bridging amino-siloxane precursors

The other AFA type #1 sorbent focused on AFA powders formulated with a combination of BAS-1 and AS-1. BAS-1 is a bridging amino siloxane that contains a secondary amine, while AS-1 is an amino siloxane that contains a primary amine. AFA formulated with these precursors showed high working CO_2 capacities and high thermal stability.

Formulations with lower and higher percentages of AS-1 were made. Increasing the AS-1 content from 25% to 35% increased the total CO_2 uptake at 40 °C from 9.1 to 10.3 wt% (Figure 16a). The addition of PEI increases the total CO_2 uptake from 9.1 to 14.1 wt% for the highest PEI content tested (Figure 16b). While PEI was added to the sol at weight ratios of 0.1, 0.5, and 0.9, the masses of the resulting materials indicate that only a portion of the PEI is retained in the final aerogel at weight ratios of about 0.08, 0.19, and 0.30, respectively.

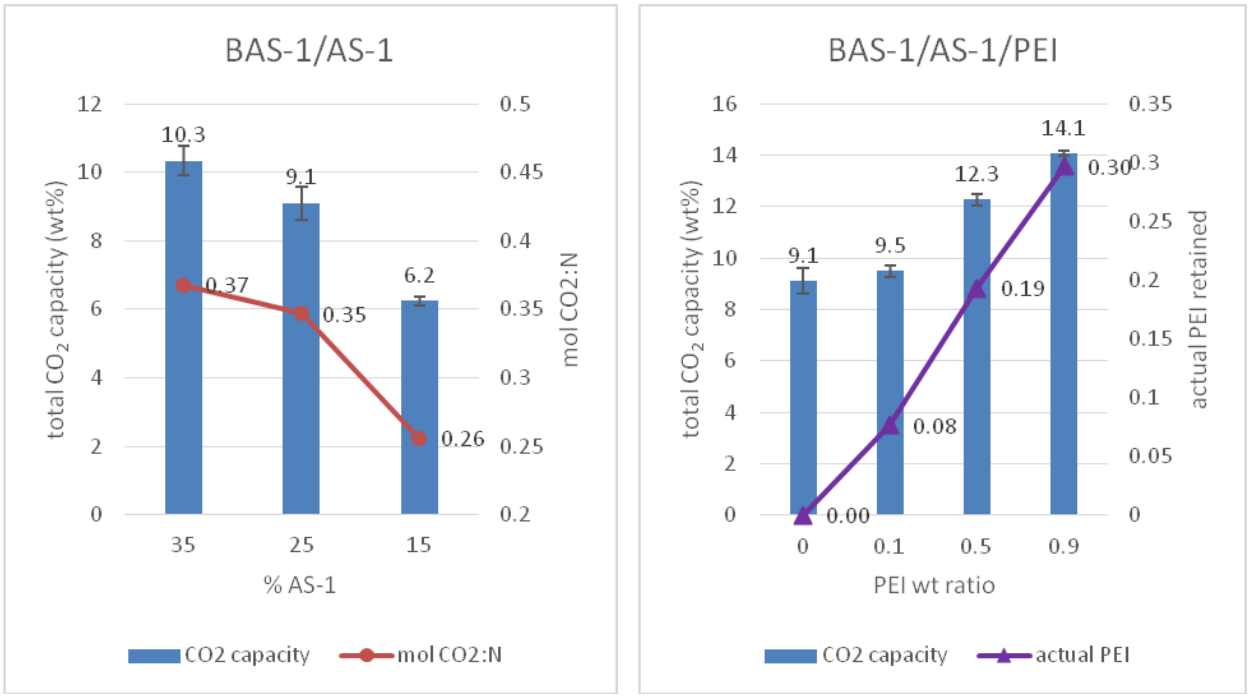

a) b)

Figure 16. Total CO_2 capacity of BAS-1/AS-1 AFA powders (adsorption 40 °C) with (a) varying AS-1 content, and (b) varying PEI content.

Because an increase in total capacity does not necessarily correspond to an increase in working capacity, thermogravimetric analysis (TGA) was used to determine the working capacity of select

samples. Samples were held at 40 °C under CO_2 for 1 h for adsorption, then the temperature was raised to 100 °C, still under CO_2, and held for 30 min. desorption to determine the working capacity. The gas was then switched to N_2 for 30 min. to further desorb the CO_2 and determine the total capacity. The standard 75% BAS-1/25% AS-1 formulation showed 6.73 wt% working capacity and 8.91 wt% total capacity (Figure 17).

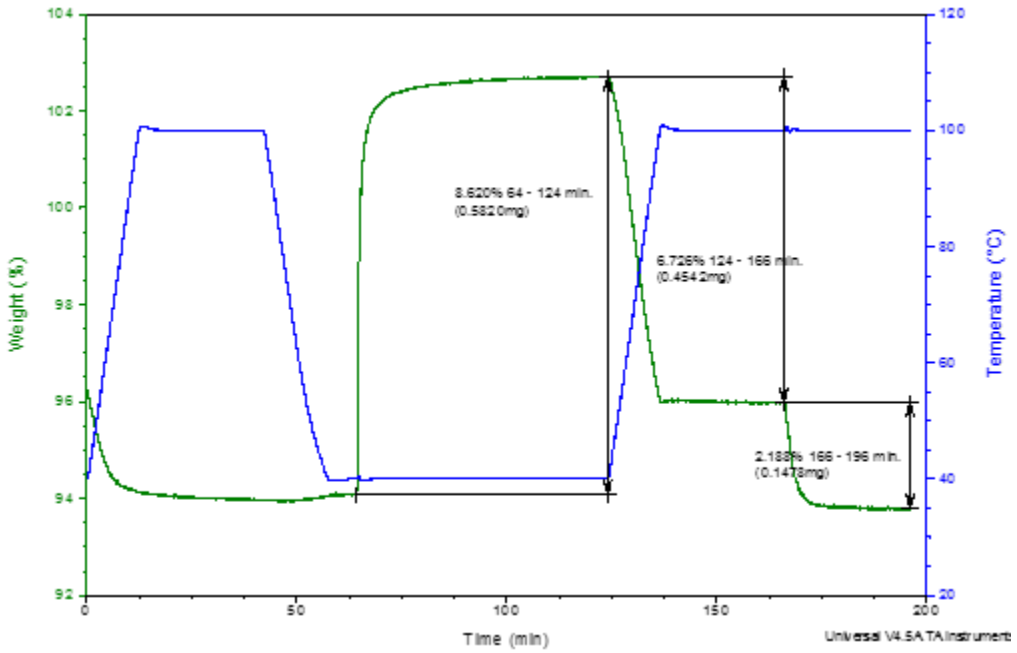

Figure 17. TGA of standard 75% BAS-1/25% AS-1 formulation showing working CO_2 capacity and total CO_2 capacity with 40 °C adsorption and 100 °C desorption.

The formulation with increased AS-1 (65% BAS-1/35% AS-1) had a significantly higher total capacity of 10.54 wt%, but only a slightly increased working capacity of 7.15 wt% (Figure 18). The working capacity for this formulation is only 68% of the total capacity, compared to 76% for the standard formulation, because CO_2 is not as easily desorbed from AS-1 as it is from BAS-1.

The formulation with 0.9:1 PEI added to 75% BAS-1/25% AS-1 had a much higher total capacity of 13.70 wt%, but a slightly lower working capacity of 6.62 wt% (Figure 19). Evidently, most of the CO_2 that is adsorbed by PEI at 40 °C is not desorbed at 100 °C, resulting in a working capacity that is only 48% of the total capacity. The CO_2 capacity results from TGA are summarized in Table 4.

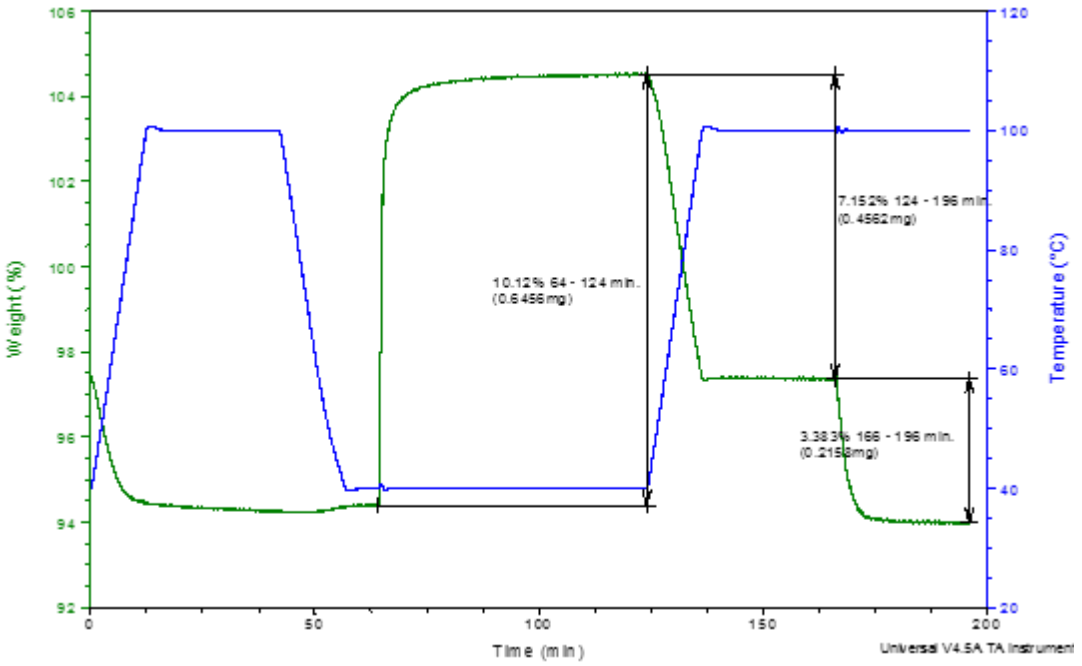

Figure 18. TGA of 65% BAS-1/35% AS-1 formulation showing working CO_2 capacity and total CO_2 capacity with 40 °C adsorption and 100 °C desorption.

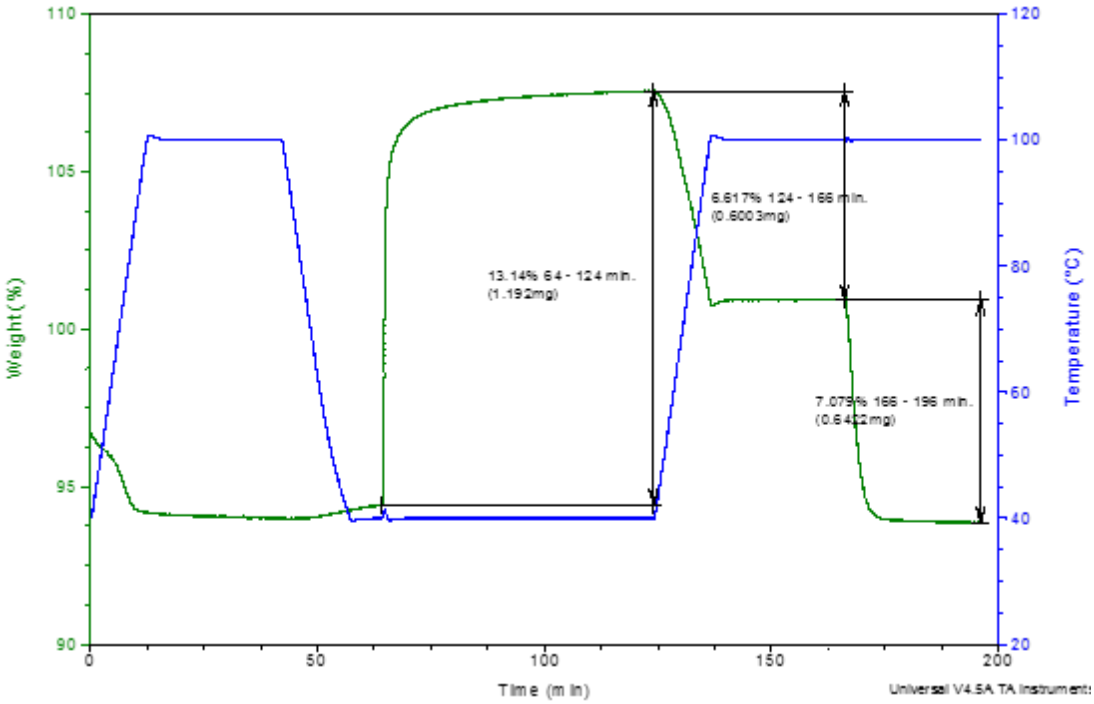

Figure 19. TGA of 75% BAS-1/25% AS-1 formulation with 0.9:1 (wt) PEI showing working CO_2 capacity and total CO_2 capacity with 40 °C adsorption and 100 °C desorption.

Table 4. Total and working CO_2 capacities based on TGA measurements.

AFA formulation	Total CO_2 capacity (wt%)	Working CO_2 capacity (wt%)	Working capacity as percentage of total (%)
75% BAS-1/25% AS-1	8.91	6.73	75.5
65% BAS-1/35% AS-1	10.54	7.15	67.8
75% BAS-1/25% AS-1 + 0.9:1 PEI	13.70	6.62	48.3

Porosimetry measurements indicate that increased AS-1 content causes a decrease in porosity, likely due to a weakening of the gel structure with less bridging amine (BAS-1) (Table 5). This loss of porosity actually corresponds to an increase in both total CO_2 capacity and mol CO_2:N. The addition of PEI also results in a decrease in porosity (Table 5), which is expected as PEI is not part of the aerogel structure but rather fills the pores. This loss of porosity does not seem to interfere with overall CO_2 uptake.

Table 5. Porosimetry measurements of BAS-1/AS-1 aerogel powders with varying AS-1 and PEI content.

AS-1 %	35	25	15	25	25	25
PEI wt ratio	**0**	**0**	**0**	**0.1**	**0.5**	**0.9**
surface area (m^2/g)	369	430	500	426	268	174
pore volume (cm^3/g)	1.70	2.15	2.48	2.48	1.78	1.18
avg pore diameter (nm)	17.5	19.1	19.0	22.3	25.4	26.1

3.1.3 AFA type # 2 sorbent using polyimine precursor

Another one of the promising sorbents from Aspen's previous effort[3] was IJ, which demonstrated high total CO_2 capacity (~22 % wt. i.e., 5 mmolCO_2/g-sorb) during the first cycle, but this CO_2 capacity dramatically decreased after 18 cycles (cycle: adsorption 40 °C, desorption 130 °C). Plus the kinetics of this sorbent was slow (the time to achieve 80% of equilibrium capacity was >40 minutes). Based on the data collected, we concluded that the amine on the sorbent was not stable and an improvement to make these AFA sorbents more stable was our main challenge with this sorbent type (AFA sorbent type # 2). By adjusting the ratio of different compounds and the order of addition during the sol-gel process, Aspen synthesized a series of sorbents labeled "CQ" and the first test results show high total CO_2 capacity (>14 wt.%) and fast kinetics, which is an important improvement.

This new family of sorbents was synthesized by the sol-gel process using two steps for the amine loading: 1) amine grafting by amino-alkoxysilane functionalization and 2) amine loading (coating) by polyimine (PEI) impregnation in a wet solution. The sorbents vary by their PEI content, water content in the sol-gel process, and their density. Table 6 groups the chemical and physical characteristics of selected CQ sorbents tested. The samples fabricated were sent to ADA-ES for CO_2 capture performance evaluation, and some of them were also sent to UA for structural characterization and pelletization process optimization.

Table 6. CQ family composition and gel quality.

Sorbent # ID	Density	PEI (%)	Water content (mole/mole SiO_2)	Gel quality
IJ*	0.065	60	8	Good
CQ17	0.1	25	4	Good
CQ15	0.1	10	4	Good
CQ30	0.15	12	4	Good
CQ31	0.15	10	4	Good
CQ28	0.15	8	4	Good
CQ20	0.2	12	4	Good
CQ29	0.2	10	4	Good
CQ26	0.2	8	4	Good
CQ27	0.25	12	4	Good
CQ22	0.25	10	4	Good
CQ23	0.25	8	4	Good
CQ25	0.1	8	4	Good
CQ24	0.1	5	4	Good

* Reference

Sorbent KY (CQ17) synthesized from PEI loaded hydrophobic aerogel was evaluated to have an 8.48 wt.% (1.92 mmolCO_2/g-sorb) working capacity with a desorption temperature of 130 °C. However, the sorbent showed poor stability when subjected to 18 cycles. Working capacity of the same sorbent was measured a third time with a lower temperature of desorption (100 °C), and it was found to have 3.95 wt.% working capacity (0.89 mmolCO_2/g-sorb). Figure 20 shows the percent change between the first cycle and second cycle at the three different desorption temperatures for KY.

Consequently, when not grafted to the silica matrix, the amine sites are very unstable at a temperature higher than 100 °C and the sorbent degrades rapidly. On the other side, it was found that a lower desorption temperature (i.e. 100 °C) for AFAs improved thermal cyclic stability, if the PEI is properly functionalized and grafted onto the silica hydrophobic aerogel matrix.

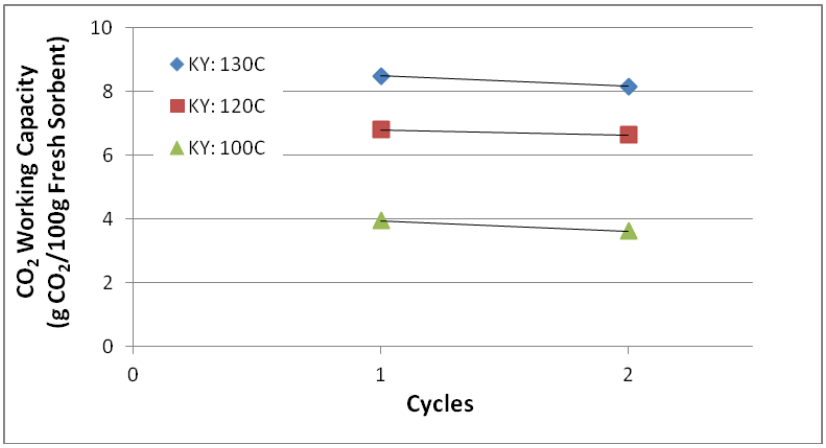

Figure 20. Difference between 1st and 2nd cycles at each different desorption temperature for sorbent KY (CQ 17).

In general, AFA sorbents type #2 have shown to develop significant total CO_2 capacity for adsorption, at 40 °C and a great working CO_2 capacity (8.48 wt.% (1.92 mmolCO_2/g-sorb)) when desorbed at 130 °C. However, these sorbents showed poor stability when subjected to 18 cycles. Consequently, when not grafted to the silica matrix, the amine sites are very unstable at a temperature higher than 100 °C and the sorbent degrades rapidly. Therefore, it was found that a lower desorption temperature (i.e. 100 °C) for AFAs improved thermal cyclic stability, if the *PEI is properly functionalized and grafted onto the silica aerogel matrix.*

Next, the goal was to improve the thermal stability of KY (CQ 17) type sorbent (PEI loaded) by chemically grafting PEI onto the silica aerogel matrix instead of a simple infiltration coating. A number of sorbents composed of an amine functionalized hydrophobic silica matrix were prepared via isocyanate cross-linking.

Another set of sorbents, labeled CQAXX, with target densities of 0.25 to 0.35 g/cc were prepared. PEI content varied between 30 – 65 wt.% and the ratio of the methylsiliconate precursor to the isocyanate precursor was fixed to 1:1. The CO_2 capacity proportionally increases as the silica/amine ratio decreases, in CQAXX sorbents. Sorbent CQA12 has the highest total CO_2 capacity adsorption (3.25 mmol/g-sorbent, ~ 14.3 wt.%), 8% greater than the UA standard sorbent (grey bar in Figure 21).

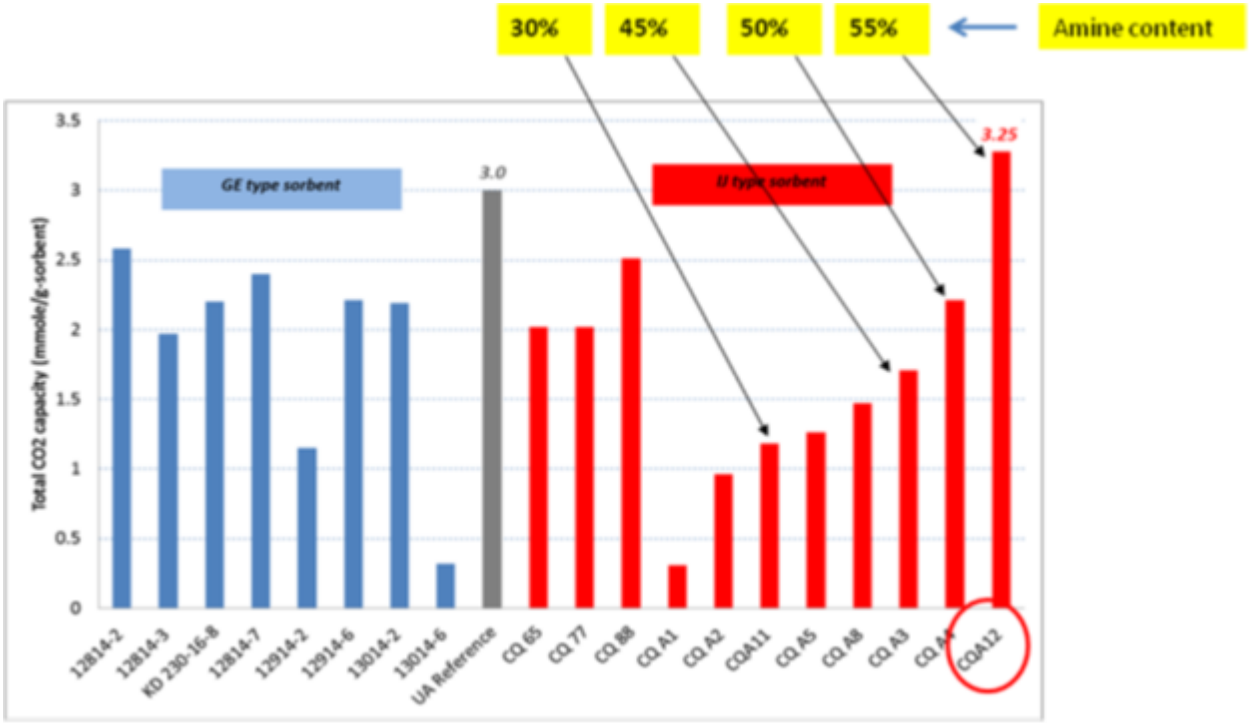

Figure 21. AFA sorbents screened by UA. Total CO_2 capacity measured as a function of synthesis route and amine content (AFA type # 2 sorbents: CQAXX).

Because of its fast-medium adsorption kinetics (15.58 minutes to reach 80% of total CO_2 adsorption) and high CO_2 adsorption capacity, other tests focused on CQA12 sorbent, such as working CO_2 capacity measurements, water uptake, and pellet optimization, which were performed at ADA-ES and UA respectively. This sorbent mainly has shown the highest working

capacity, 7.81 wt.%, and total CO_2 capacity of 19.87 wt.%, at 40 °C adsorption and 100 °C desorption cycles. As the temperature of desorption increases, the working capacity increases (as shown in Figure 22).

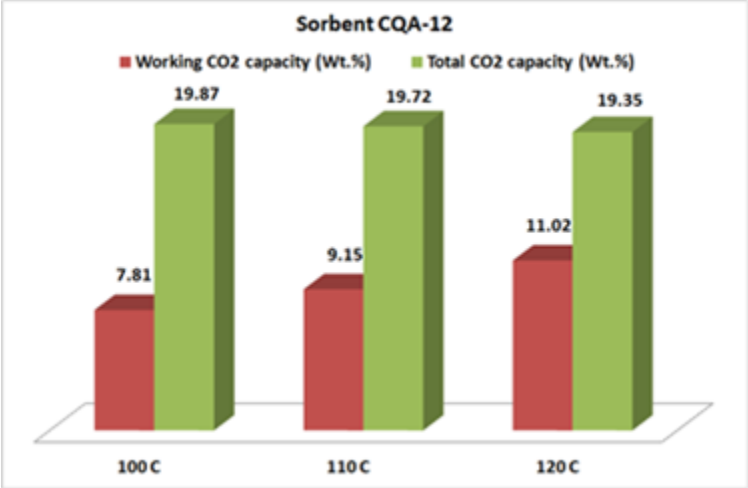

Figure 22. Sorbent CQA12 performance as a function of temperature of desorption.

Overall, the optimization of AFA sol-gel formulations led to two AFA-type sorbents with interesting CO_2 capture performance, as follow:

- AFA Sorbent Type #1-(type 90414-4 or KD-240-24 sorbents):
  - Direct amine grafting process, using amine-alkoxysilane and dipodal bridging alkoxysilane precursors and sol-gel process.
  - These sorbents have shown thermal stability (~ 190 °C) and relatively high CO_2 capacity (~ 14.3 wt.%) in powder form.

- AFA Sorbent Type #2 (type CQA-12 and CQ-XX):
  - "Double functionalization" process used by incorporating amino groups by grafting and impregnation methods.
  - These sorbents showed a very high CO_2 capacity (> 15.4 – 20 wt.%) and relatively good thermal stability up to 100 – 110 °C.

The degradation of sorbent type # 2, over time, is more likely to happen much faster than the sorbent type # 1.

3.2 Pelletization and SO_2 poisoning process optimization

The std. binder solution is water based while SRE is ethanol based. Depending on the hydrophobicity and solvent compatibility of the sorbents, some may not be pelletized or coated with either the std. binder or SRE coating.

Some AFA sorbent of type #1 (made from amino-alkoxysilane precursors) are incompatible with UA's std. binder solution. However, sorbent type # 2 such as CQA-12, are compatible with both the binder and the coating.

The 15% CO_2 adsorption/desorption processes of the samples were investigated by in-situ Fourier transform infrared spectroscopy (FTIR, Thermo Nicolet 6700) and mass spectrometry (MS, Pfeiffer Omnistar), in the presence of 40 ppm of SO_2. Two thermocouples were used to detect the temperature in the middle and the top surface of the sample to ensure that the whole sample was heated or cooled to a desired temperature. 20 cycles of CO_2 adsorption/desorption were completed on each sample. The compositions of the four samples are summarized in Table 7. These samples were prepared by mixing the CQA-12 powders with the ingredients following UA's SRE recipes. The mixing ratio of the SRE coating solution and the CQA-12 powders is 1.25:1 in weight. The SRE10-2 was prepared after we obtained an unexpected erroneous result for SRE10-1 due to a mistake in sample preparation.

Table 7. Compositions of the SRE coatings.

Sample (1 g)	Polyamines (gram)	Polymer Linkers	Antioxidant (gram)
SRE5	0.05	1.10 g, 5% sln.	0.09
SRE7	0.05	1.10 g, 7% sln.	0.09
SRE10-1	0.05	1.10 g, 10% sln.	0.09
SRE10-2	0.05	1.10 g, 10% sln.	0.09
SRE15	0.05	1.10 g, 15% sln.	0.09

Table 8 shows the CO_2 capture capacities of the sorbents in the presence of 40 ppm SO_2 in the first cycle and the 20th cycle. The CO_2 capture capacities in Cycle 1 are the initial CO_2 capture capacities that are measured by the weight-difference method (our rapid-screening method). Those in Cycle 20 are calculated by fitting the MS profile (CO_2 capture capacity decay curve, Figure 23) and the initial CO_2 capture capacities. The degradation of CO_2 capture capacity is calculated by:

$$\frac{C1-C20}{C1}\times 100\%$$

Table 8. CO_2 capture capacities in Cycle 1 (C1), Cycle 20 (C20), and % degradation.

Sample	Polymer Linker	Cycle 1 CO_2 capacity (Wt. %)	Cycle 20 CO_2 capacity (Wt. %)	Degradation
SRE-5	5% sln.	12.80	10.50	18.48%
SRE-7	7% sln.	11.88	10.52	11.48%
SRE-10	10% sln.	11.09	10.65	3.97%
SRE-15	15% sln.	10.82	10.47	3.18%
CQA-12	/	14.83	12.89	13.00%

The higher concentration of the active ingredient in UA's recipe results in a decrease in the initial CO_2 capture capacity, while slowing down the degradation of the coated sorbents. The CO_2

capture capacity decay curves are shown in Figure 23. Each curve was linearly fit to demonstrate the rate of decay, though the decay curves do not necessarily follow a linear trace. The slopes of the fitted curves are shown in the figure. The CO_2 capture capacity of SRE5 drops fastest while that of SRE15 does not change much. The degradation rate of SRE7 and newly prepared SRE10 are between SRE5 and SRE15. This provides evidence of the effectiveness of the SRE series SO_2 resistance coating.

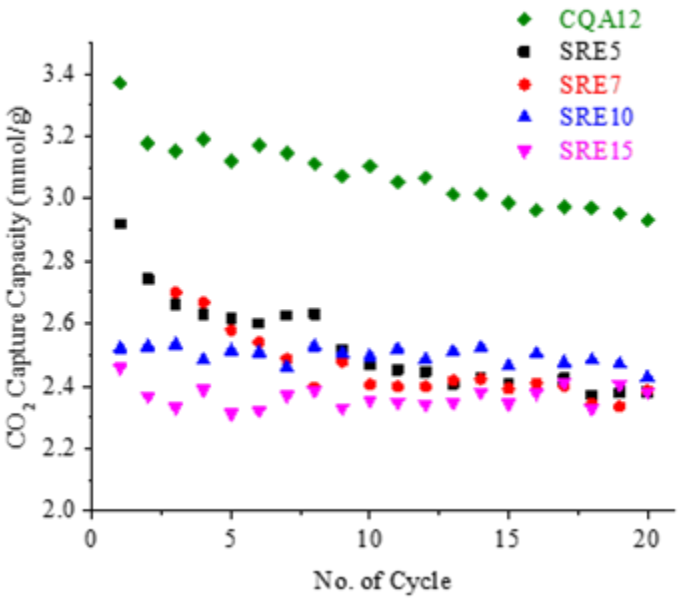

Figure 23. CO_2 capture capacity of the fresh and coated CQA-12 during cycling in 40 ppm SO_2.

The SRE-10 coating is proven effective to reduce the SO_2 poisoning of the aerogel sorbents. The concept of SO_2 resistance is based on the fact that the SRE recipe only contains tertiary amines. UA's study shows that tertiary amines are the only ones, unlike the primary and secondary amines, that reversibly interact with SO_2. Primary and secondary amine binds SO_2 more strongly than tertiary amines thus are easy to be poisoned, leading to sorbent degradation. To further verify the effectiveness of the SRE coating, we recently have initiated the study of SRE-coated silica (Rhodia amorphous precipitated silica) which does not contain amines. Results shown in Figure 24 verified that SO_2 reversibly adsorbs on the SRE coating while CO_2 hardly adsorbs on it. SRE10 coating alone adsorbs little CO_2. Most SO_2 is desorbed with Ar purging and fully desorbed at elevated temperature in TPD (temperature programmed desorption).

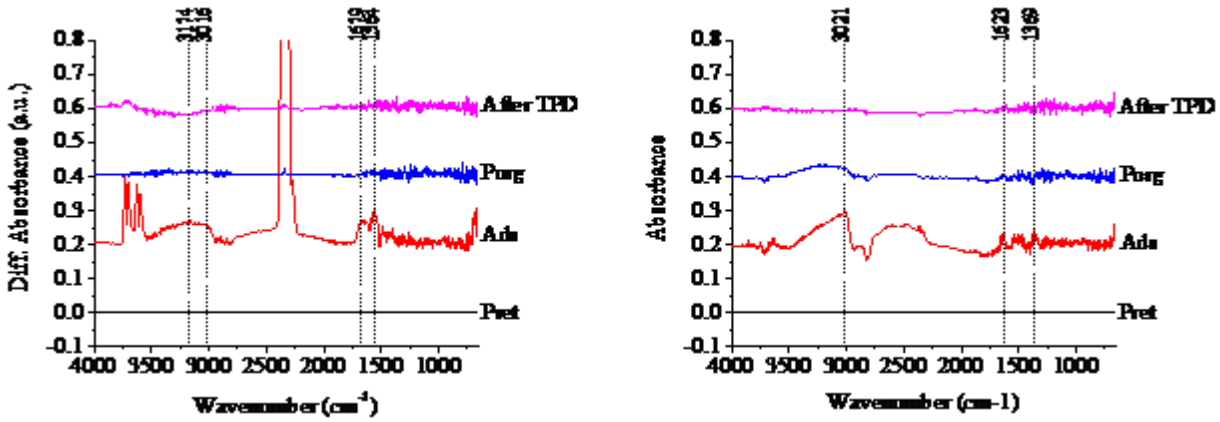

Figure 24. Diff. absorbance FTIR spectra of SRE10 coated on silica in 15% CO_2/air and 1% SO_2/air.

Figure 25 shows the MS profile of SRE5, as an example, and corresponding FTIR spectra at different stages (i.e., pretreatment, adsorption, Ar purging, and after TPD) in one CO_2 capture cycle. This figure includes single-beam spectra (the direct Fourier transform of IR interferogram), absorbance spectra (calculated from the absolute value of $\log(1/I_{\text{Single-Beam}})$), and difference spectra (calculated by subtracting the pre-treatment spectrum as a background).

The challenge in the current optimization is the drop in CO_2 capture capacity due to coating. SRE-10 decreased the CO_2 capture capacity of CQA-12 by ~ 25%. The poor homogeneity of the coating is the critical factor that causes the drop in the CO_2 capture capacity as the locally concentrated coating solution blocks the active amine sites on the aerogel sorbents. By optimizing the coating procedure and using solvents which have proper polarities, the local agglomeration can be eliminated and the homogeneity can be significantly improved. As a result, the drop of CO_2 capture capacity of the coated sorbents can be minimized. Table 9 summarizes the CO_2 capture capacity of some recently prepared CQA-12 sorbents using our improved procedures. These samples exhibited higher (due to the amine compensation composition in the recipe) or slightly lower CO_2 capture capacity than the uncoated sorbent.

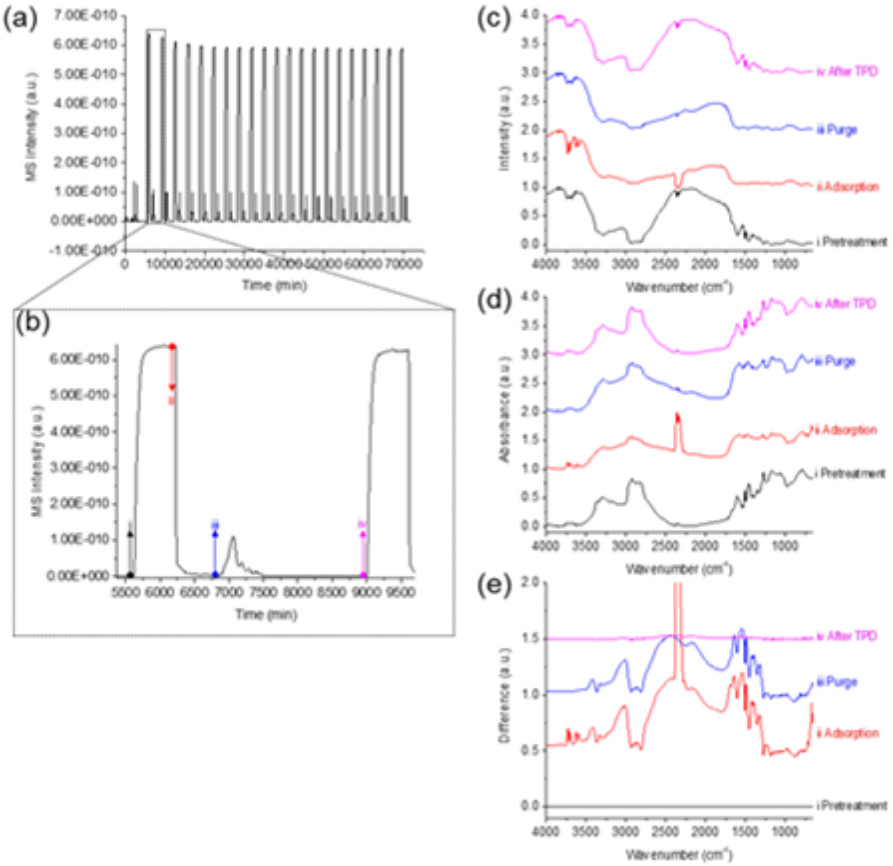

Figure 25. MS profile and FTIR spectra of SRE5 at different stages in a CO_2 capture cycle. (a) MS profile of whole 20 cycles; (b) MS profile of 1 cycle; (c) Single-beam spectra; (d) Absorbance spectra, $A=|\log(1/I_{\text{Single-Beam}})|$; (e) Difference spectra, $Diff=\log(I/I_{\text{Pretreatment}})$.

Table 9. CO_2 capture capacity of the SRE coated CQA-12 prepared via improved procedures and different solvents.

Sample (CQA-12 based)	40 °C/100 °C Capture Capacity		55 °C /130 °C Capture Capacity	
	Wt. %	mmol/g	Wt. %	mmol/g
SRE10	9.50	2.16	11.00	2.50
DIP5-SRE10	12.19	2.77	14.70	3.34
DIPW5-SRE10	10.74	2.44	12.63	2.87
DIT5-SRE10	9.90	2.25	11.31	2.57
DIT10-SRE10	10.25	2.33	11.40	2.59
DIA5-SRE10	11.97	2.72	13.46	3.06
DIA10-SRE10	9.02	2.05	10.74	2.44

Previous experiments revealed that pre-adsorbed CO_2 on CQA12 aerogel pellets prepared with SRE-7 (SRE-7 was used instead of SRE-10, which has the best performance in terms of SO_2 resistance, due to the insufficient sample amount of SRE-10) binder protects the sorbent from SO_2 poisoning at low SO_2 concentrations. 15% CO_2 in air containing 40 ppm of SO_2 was fed into a sealed FTIR (Thermo Nicolet 6700) reactor which held the SRE-7 aerogel pellet or CQA-12 (powder) samples. As evidenced by the FTIR spectra shown in Figure 26, fresh CQA-12 can be poisoned by 40 ppm SO_2. Figure 27 presents the IR spectra of SRE-7 aerogel pellets during the CO_2 adsorption process in the presence of 40 ppm and 1% SO_2 in the mixed gas. The adsorption peaks at 902 cm^{-1}, 958 cm^{-1}, and 1216 cm^{-1}, which are attributed to the sulfite species resulted from adsorbed SO_2, denote that the pre-adsorbed CO_2 is able to serve as a protection layer for the SRE-7 aerogel sorbent from SO_2 poisoning at low SO_2 concentration. The spectrum of the SRE-7 aerogel pellets with pre-adsorbed CO_2 exposed to 40 ppm SO_2 shows almost no sulfite peaks. However, the pre-adsorbed CO_2 is not able to protect the sorbent when the SO_2 concentration is 1%. Fresh CQA-12 showed better SO_2 resistance than fresh SRE-7 pellets, but pre-adsorbed CO_2 promoted the SO_2 adsorption on CQA-12 in contrast to its protection behavior on SRE-7 pellets.

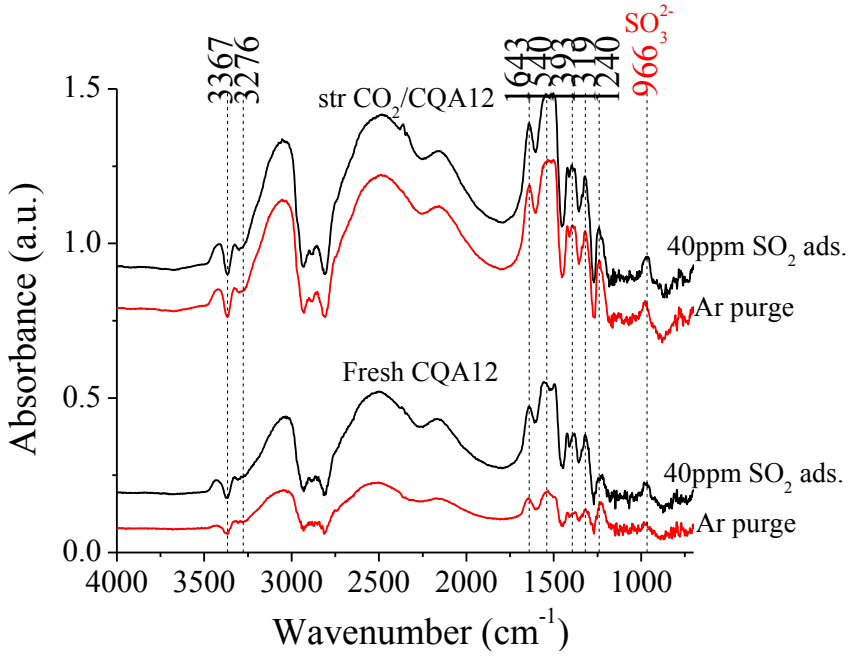

Figure 26. IR absorbance spectra of CQA-12 during 40ppm SO_2 adsorption, IR spectrum after pretreatment as bkg. str. CO_2 /CQA-12 refers to the CQA-12 with CO_2 strongly adsorbed.

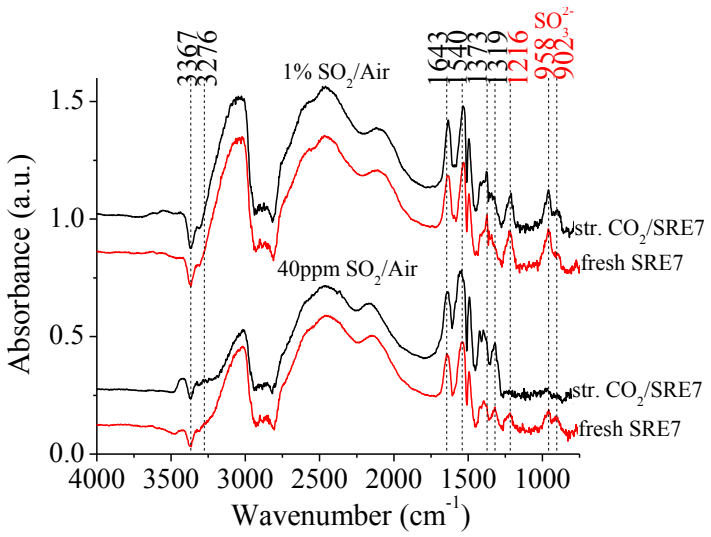

Figure 27. IR absorbance spectra of SRE-7 during 40ppm SO_2 and 1% SO_2 adsorption. The IR spectrum after pretreatment is subtracted as the background. Str. CO_2/SRE-7 refers to the SRE-7 with strongly adsorbed CO_2.

3.2.1 Proposed SO_2 removal process

As CO_2 and SO_2 competitively bond to amine functional groups on the sorbent, the presence of SO_2 in the flue gas stream may gradually decrease the sorbent capacity for CO_2 adsorption. So it is essential to the life of sorbent to remove SO_2 to a tolerable level. To comply with environmental regulations on acid gas, power plants treat flue gas in flue gas desulphurization units (wet or dry) before releasing into the atmosphere. The current regulations necessitate the limit of 0.2 lb SO_2/MM Btu (~90 ppmv SO_2). For new power plants, the standard is 0.1 lb/MMBtu. The current design of flue gas desulphurization (FGD) units can achieve more than 95 % removal of SO_2. For low sulfur coal (e.g., PRB coal), the SO_2 stack emission with implementation of efficient FGD is <20 ppm. If the sorbent tolerance to SO_2 is low, an additional SO_2 scrubbing unit before the CO_2 capture process is recommended. The additional SO_2 scrubbing unit serves several functions:

- Provide as much SO_2 removal as is practical.
- Removes trace fly ash and limestone from the flue gas.
- Cools the flue gas, condensing and removing a significant portion of the water from the flue gas stream

A cost-effective process to minimize the energy consumption, since the SO_2 poisoning is an accumulative process and SO_2 is desorbed at a higher temperature than CO_2, which consumes more energy, was proposed by the University of Akron (note: this idea is not part of this project). The proposed dual-column model is shown in Figure 28. The SO_2-contained flue gas goes through the first column in which the sorbents (or amine-free silica) are coated with a thick layer of SO_2-resistant coating, and then flows into the second column where the sorbents have a thin layer of SO_2-resistant coating. SO_2 is adsorbed and accumulated on the sorbents in the first column while little CO_2 is adsorbed due to the lack of primary and secondary amines. In the second column, only CO_2 is in the flow. The sorbents in the second column will be regenerated every cycle which produces high purity CO_2. The sorbents in the first column, however, will be desorbed only after a large number of cycles when the sorbents are saturated with adsorbed SO_2. This cycling limit could be determined by experiments (not part of this effort). The less frequent regeneration of the

sacrificing sorbents in the first column can significantly reduce the energy consumption and thus the operating cost of the whole process, and helps in generating high-purity CO_2 which is feasible for applications such as EOR.

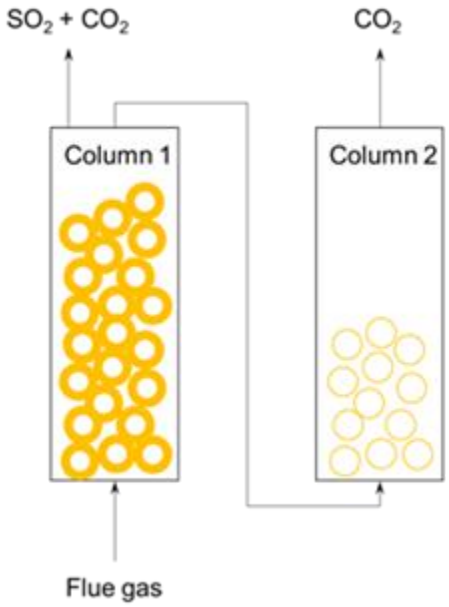

Figure 28. Schematic drawing of a proposed dual-column model (not part of this project).

3.3 AFA bead sorbents synthesis and CO_2 capture performance

Table 10 summarizes the conditions used to make gel beads with BAS-1 in a silicone oil medium. The aerogel target density was either 0.1 or 0.2 g/cc. BAS-1 was gelled alone or with another precursor to result in aerogels with 25 wt.% ethylene bis-siliconate. The beads were filtered, and rinsed with organic solvent. Some beads were aged at room temperature for a day prior to extraction, while some were aged at an elevated temperature for 15 h.

Table 10. Conditions for synthesis of gel beads with BAS-1 (samples KD240-24).

	target density (g/cc)	wt% amine precursor	gel time (min)	aging conditions*	size of dry beads (µm)
9A	0.2	100	3	RT	300-1100
12A	0.1	100	6.5	RT	300-900
1B	0.2	75	3.5	RT	200-1000
11A	0.1	75	11	RT	400-1000
5B	0.1	100	6.5	ET	60-450
14A	0.1	75	11	ET	80-800

RT: Room Temperature
ET: Elevated Temperature (40 – 60 °C)

All beads had high gel strength and were well defined (highly spherical without any fusing). After extraction with supercritical CO_2, all beads were heat treated. None of the beads appear to undergo a significant amount of shrinkage during extraction, and none of them crack or break apart Figure 29.

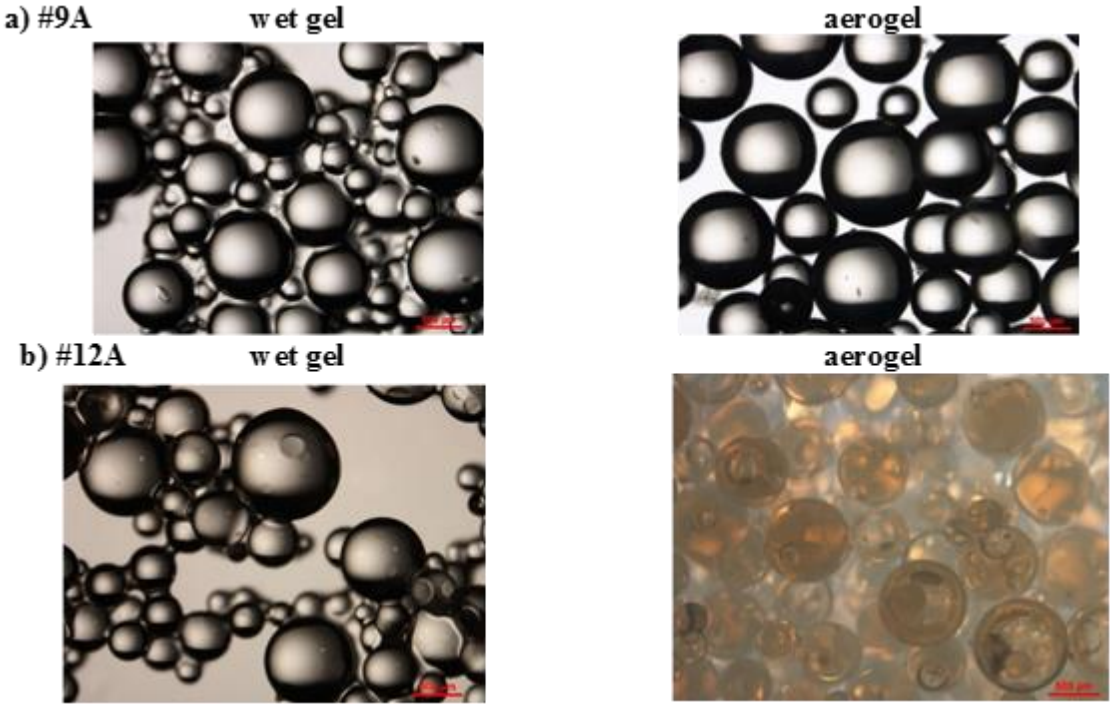

Figure 29. Microscope images of beads as wet gels (left) and aerogels (right).

Porosimetry was used to determine surface area, pore volume, and pore size of the aerogel beads (Table 11, Figure 30). The two samples made at the higher target density (0.2 g/cc) have no porosity. This is in contrast to monolithic samples of a similar density made previously with similar conditions, which were fairly porous. When aged at room temperature, the 100% BAS-1 beads have a surface area of 255 m^2/g, pore volume of 0.804 cm^3/g, and average pore size of 11.8 nm. Addition of 25% ethylene increases the surface area slightly to 283 m^2/g, increases the pore volume to 0.969 cm^3/g, and increases average pore size to 15.4 nm. Aging the 100% BAS-1 beads at 68 °C, rather than at room temperature, raises the surface area from 255 to 458 m^2/g and the pore volume from 0.804 to 0.896 cm^3/g. This surface area result is similar to that of powdered monolith aerogel made previously with similar conditions (449 m^2/g), however the pore volume and pore diameter for the powdered monolith were higher, 1.48 cm^3/g and 12.4 nm, respectively.

Table 11. Porosimetry measurements of AFA beads.

	9A	12A	1B	11A	5B
density (g/cc)	0.2	0.1	0.2	0.1	0.1
wt.% BAS-1	100	100	75	75	100
% -C_2H_4-	0	0	25	25	0
aging temp, (°C)	20	20	20	20	68
surface area (m^2/g)	0	255	2	283	458
pore volume (cm^3/g)	0	0.804	0.003	0.969	0.896
Avg. pore diameter (nm)	-	11.83	9.22	15.42	12.44

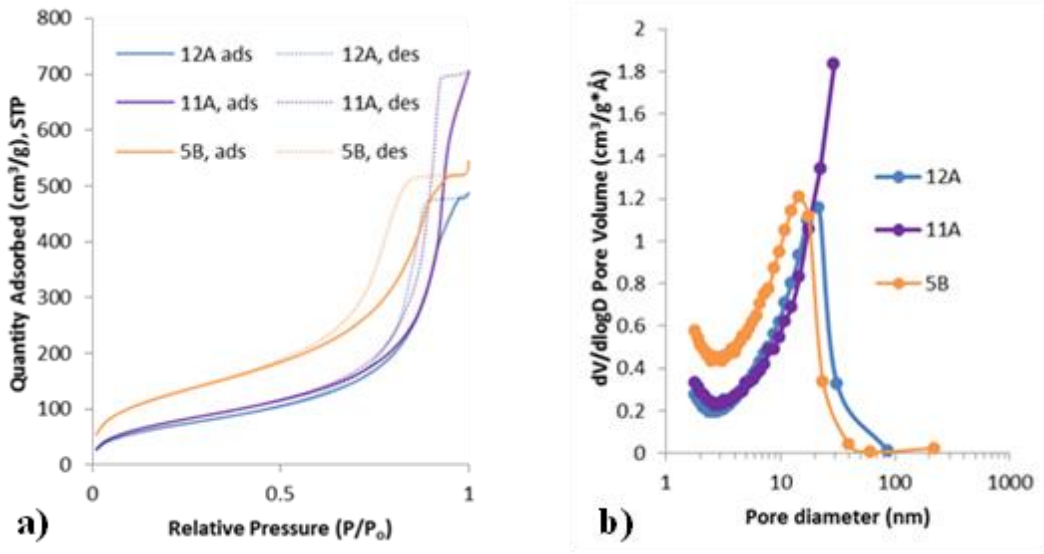

Figure 30. Adsorption isotherms (a) and pore size distributions (b) of aerogels.

CO_2 uptake was measured at Aspen using thermogravimetric analysis (TGA), which also allows the observation of adsorption/desorption kinetics. Adsorption took place at 40 °C (1st cycle) or 70 °C (2nd cycle). The CO_2-loaded sample was heated to 120 °C while maintaining a CO_2 atmosphere to determine working capacity, then the atmosphere was switched to N_2 to determine total capacity. One sample (5B) could not be measured at Aspen, but the total capacity was measured at the University of Akron using 10 min. at 40 °C for adsorption and 20 min. at 100 °C under N_2 for desorption. The total/working capacities for desorption at 120 °C could then be estimated based on this result, assuming the kinetics and the working:total capacity ratio are the same as the similar sample 12A. Table 12 summarizes the CO_2 uptake results. The two high-density (0.2 g/cc) samples had very low CO_2 uptake and slow kinetics due to their lack of porosity. As shown in Figure 31, the lower density (0.1 g/cc) sample made with 100% BAS-1 showed a total CO_2 capacity of 6.65 wt.% and working capacity of 6.17 wt.% using 40 °C adsorption and 120 °C desorption. As expected, the working capacity is a very high percentage (92.8%) of the total capacity. The kinetics are fairly quick, with adsorption reaching 88% completion at 10 min., while desorption reached 38% completion at 10 min. and 95% completion at 20 min. The total capacity corresponds to 0.307 mol of CO_2:N. Assuming that CO_2 forms carbamate with two amines required for each CO_2, this is only a fraction of the maximum of 0.5 CO_2:N.

The higher surface area and pore volume of the beads with 25 wt.% ethylene bis-siliconate improves amine availability, increasing the CO_2:N ratio to 0.36. However, this is not enough of an improvement to overcome the reduction of amine in the formulation, the total capacity is 5.86 wt.% and the working capacity is 5.48 wt.% (93.5% of total). The kinetics are very similar to the 100% BAS-1 sample, with adsorption reaching 86% completion at 10 min., while desorption reached 37% completion at 10 min. and 95% completion at 20 min. There was a large increase in surface area observed for beads aged at high temperature, and this corresponds to an increase in CO_2:N from 0.307 (20 °C aging) to 0.357. The working capacity for 40/120 °C ads./des. is estimated to be 7.18 wt%, based on a total capacity measurement at the University of Akron of 6.78 wt% for 40/100 °C ads./des.

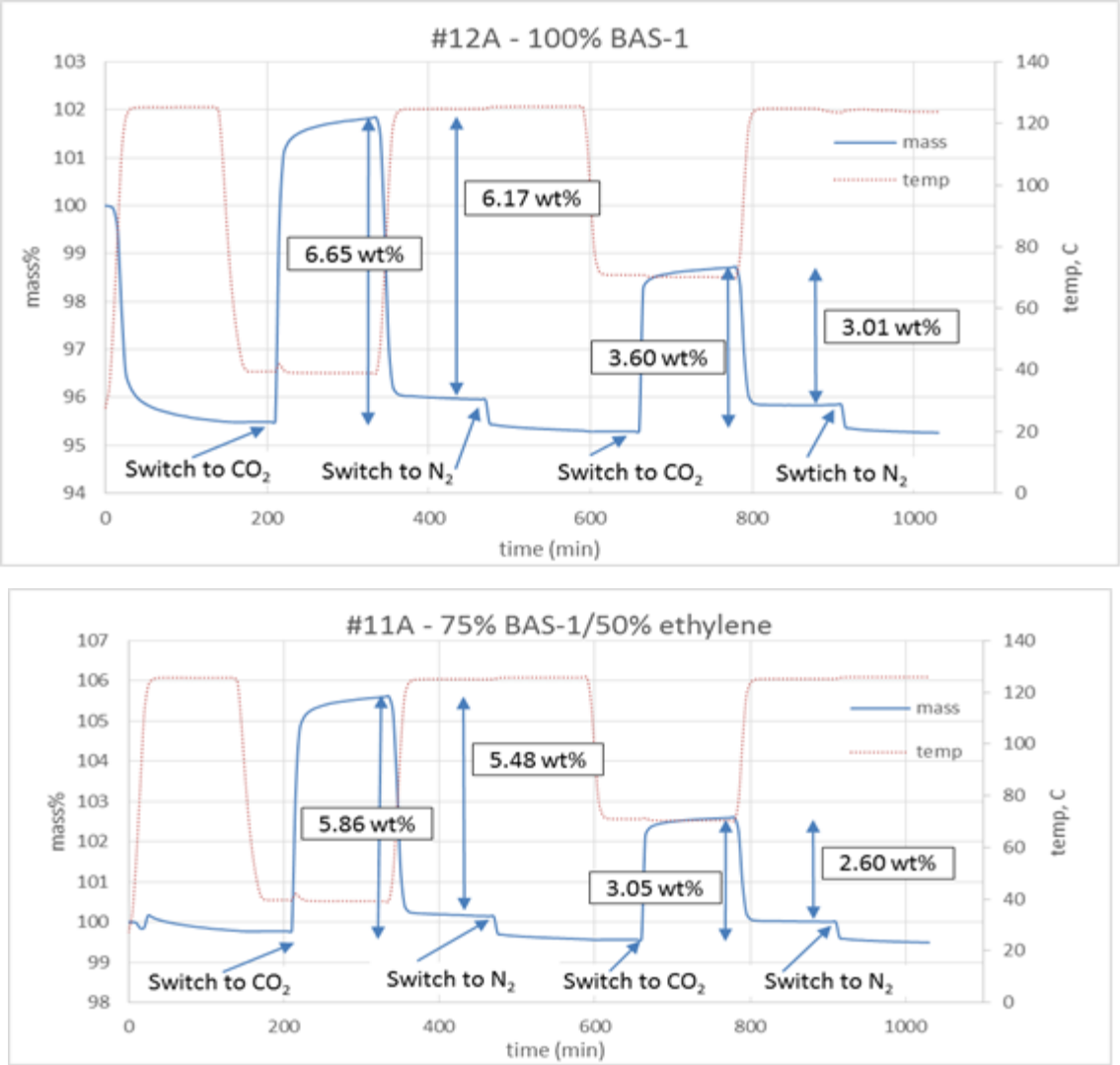

Figure 31. Total and working CO_2 uptake of BAS-based aerogel beads by TGA at Aspen, adsorption at 40/70 °C, desorption at 120 °C (samples KD240-24).

Table 12. CO_2 uptake results for aerogel beads.

	theoretical max CO_2 (wt.%)	CO_2, total (wt.%)	mol CO_2:N	CO_2, working (wt.%)	Working / total (%)	CO_2, total (wt.%)	CO_2, working (wt.%)	working / total (%)
Ads./des. Temp. (°C)→		40/ 120	40/ 120	40/ 120	40/ 120	70/ 120	70/ 120	70/ 120
9A	10.84	1.43	0.066	0.69	48.3	1.43	0.85	59.4
12A	10.84	6.65	0.307	6.17	92.8	3.60	3.01	83.6
1B	8.13	1.18	0.073	0.40	33.9	2.01	1.44	71.6
11A	8.13	5.86	0.360	5.48	93.5	3.05	2.60	85.2
5B	10.84	7.74*	0.357*	7.18*	92.8*			

***estimated based on University of Akron measurement of 6.78 wt% CO_2 at 10 min using 100 °C for desorption*

In another study, a monopodal precursor containing a primary amine, (amino siloxane AS-1) was added to BAS-1 as well to increase CO_2 capacity. As reported in Figure 31, AFA beads made with 100% BAS-1 had a working capacity of 6.17 wt% CO_2, which is 92.8% of the total capacity, when adsorption and desorption were performed at 40 and 120 °C, respectively. This working capacity is quite a large proportion of the total capacity, suggesting that CO_2 does not bind strongly and the pore structure facilitates desorption – both desired properties of a CO_2 sorbent. It has been observed before that higher amounts of primary amines (AS-1) in a sol leads to a weaker gel. The formulation with 25% AS-1 was made on both a small scale, sorbent 240-24-16 A (20 mL sol, similar to the others) and a large scale, sorbent 240-24-1C, (400 mL sol) in order to have enough material for extensive testing at UA and ADA-ES. Increasing the scale of the reaction 20x resulted in slightly larger beads, as the degree of turbulence caused by stirring the oil is not completely reproducible as volume is varied. All formulations resulted in well-defined beads that are highly spherical without any fusing. After extraction with supercritical CO_2, all beads were heat treated at 120 °C for 3 h.

The 100% BAS-1 beads have a surface area of 458 m^2/g, pore volume of 0.90 cm^3/g, and average pore size of 12.4 nm. Addition of 25% AS-1 decreases the surface area slightly to 389 m^2/g, increases the pore volume to 1.06 cm^3/g, and decreases average pore size to 10.2 nm. Porosity of the 25% AS-1 beads was lowered by increasing the reaction scale, an effect that is possibly related to the slightly different bead size or gel time. Table 13 summarizes the physical properties of the different batches.

Table 13. Porosimetry measurements of aerogel beads.

KD240-24	5B	16A	1C
wt% BAS-1	100	75	75
wt% other precursor	0	25% AS-1	25% AS-1
Surface area (m^2/g)	458	389	227
Pore volume (cm^3/g)	0.90	1.06	0.91
Avg. pore diameter (nm)	12.4	10.2	15.3

Total CO_2 capacity was measured at the University of Akron using 10 min. at 40 °C for adsorption and 20 min. at 100 °C under N_2 for desorption (Table 14). The beads made with 100% BAS-1 showed a total CO_2 capacity of 6.51 wt%, corresponding to a 0.357 CO_2:N molar ratio. Assuming that CO_2 forms carbamate with two amines required for each CO_2, this is 71% of the maximum theoretical CO_2 capacity of 10.84 wt%. Amine availability is slightly lower when 25% AS-1 is added (16A and 1C), likely due to the lower surface area, but the higher amine concentration in this formulation allows for higher total CO_2 capacity (9.11 wt% for 1C). Working capacity of the small-scale 25% AS-1 sample (16A) was measured at ADA-ES using 40 °C for adsorption under 0.15 bar CO_2 and 100-120 °C for desorption under 0.81 bar CO_2. *The working capacity was 6.63 - 7.17 wt% CO_2, depending on the desorption temperature, corresponding to 80-99% of the total capacity*. The kinetics of adsorption/desorption were considered medium to fast, taking 14-16 min. depending on regeneration temperature. TGA test results on sorbent KD240-24-16A, measured at ADA-ES, are reported on Figure 32.

Table 14. CO_2 uptake results for aerogel beads, measured at the University of Akron using 40 °C for adsorption and 100 °C for desorption.

KD240-24	CO_2, total (wt%)	mol CO_2:N	Theoretical max. CO_2 (wt%)
5B	6.51	0.357	10.84
16A	8.26*	0.315	13.13
1C	9.11	0.347	13.13

*measured at ADA-ES

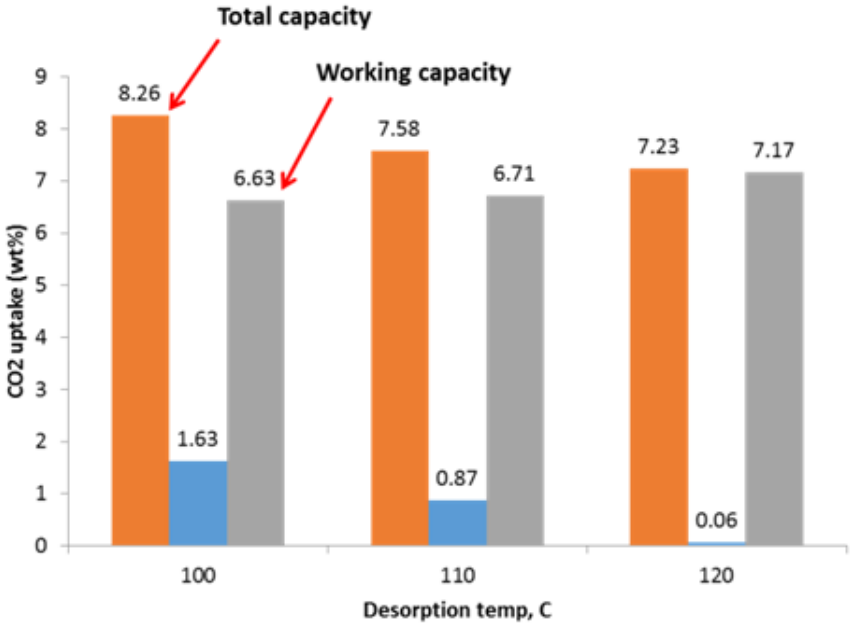

Figure 32. Total and working CO_2 uptake of BAS-1/AS-1 aerogel beads measured at ADA-ES (adsorption 40 °C, desorption 100/110/120 °C), orange bars are for the Total CO_2 capture capacity, grey bars are for the Working CO_2 capture capacity, blue bars indicated the amount retained by the sorbent during desorption .

This particulate formulation (75% BAS-1/25% AS-1) has led to AFA beads with very interesting CO_2 capture performance. The working CO_2 capacity (which is the important property in this study) is *80-99% of the total capacity*, which is unique for this formulation.

3.4 AFA pellets and beads performance comparison

Aspen and its team (ADA-ES and the University of Akron (UA)) completed several tests to compare the performance of Amine Functionalized Aerogel (AFA) beads and AFA pellets to determine which sorbent form would be used for bench scale production and testing. Aspen Aerogels supplied ADA-ES and UA with the aerogel material (beads and pellets) needed for the following tests comparison:

- Isobar testing
- Water uptake analysis
- Cycling stability
- Jet cup attrition and crush test

3.4.1 AFA pellets and beads performance evaluation at ADA-ES

3.4.1.1 Mass Spectrometer Fixed Bed

Fixed bed testing was performed to determine the sorbent selectivity between CO_2 and H_2O for sorbent beads and pellets. Breakthrough testing was also completed for the two sorbents to determine their selectivity of CO_2 vs H_2O. It appears that both sorbents have CO_2 breakthrough which occurs shortly after the sorbent is exposed to simulated flue gas and after only reaching between 20-40% of their total CO_2 capacity. The sorbents are initially loaded very rapidly during the first minute, but continue to take up moisture and CO_2 at a much lower rate for a significant duration of time of up to 1 hour.

When examining the period of time where over 90% CO_2 is captured in the bed, it appears that both the beads and the pellets adsorbed more CO_2 than water. The sample stream has to be substantially diluted due to the sensitivity of the mass spectrometer, so results are reported in partial pressure recorded by the mass spectrometer rather than absolute pressures. This still facilitates relative comparisons selectivity, but as seen in Figure 33, the y axis pressures are obviously post dilution.

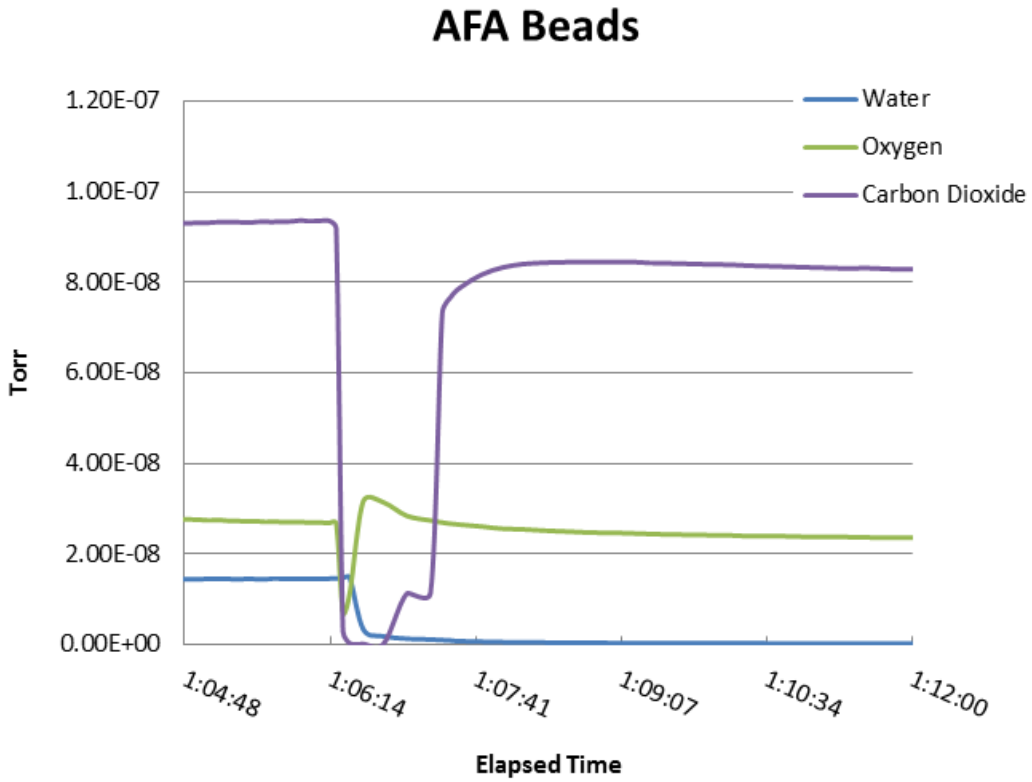

Figure 33. Breakthrough curve of AFA beads.

During the period of rapid adsorption of CO_2 when the sorbent is first exposed to simulated flue gas, as shown in Figure 33, the AFA beads were approximately 16 times more selective towards CO_2 than H_2O on a *mass* basis. However, during this time, the sample only adsorbed approximately 35% of its total CO_2 capacity. This performance exceeded the relative performance of the AFA pellets, which was approximately 13 times more selective towards CO_2 than H_2O on a

mass basis, but only adsorbed 20% of its total CO_2 capacity. This also matches results of moisture testing which indicated that the pellets adsorbed slightly more moisture than the beads. The breakthrough results of AFA pellets are shown in Figure 34.

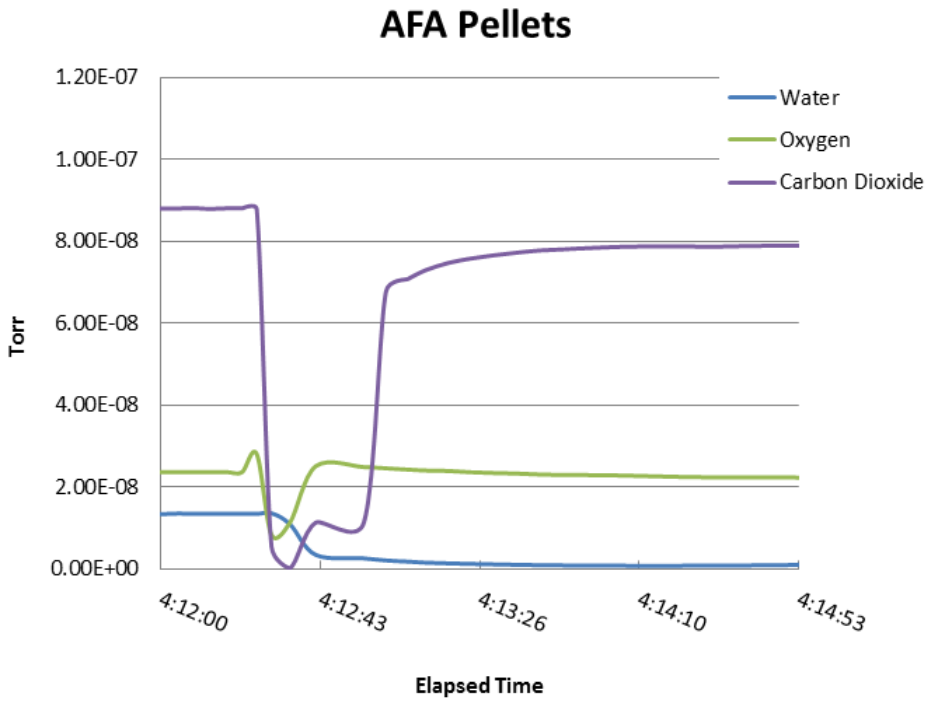

Figure 34. AFA pellet breakthrough curve.

3.4.1.2 Moisture Loading

Testing was also completed to allow moisture uptake comparisons at multiple moisture partial pressures to assess moisture uptake performance of AFA beads and pellets. The two sorbents indicated very similar behavior without a clear winner in performance. The beads appeared to have slightly less water uptake than the pellets, as shown in Figure 35. Due to limits in the TGA instrument, the moisture was limited to approximately 3% by volume, which at altitude in Highlands Ranch, Colorado limits the P_{H2O} to 0.027 bar. This is still considerably below the moisture level associated with coal derived flue gas, but provides a basis of comparison between the two sorbents. Furthermore, the moisture in the gas is a calculated value with gas being bubbled through a room temperature bubbler rather than directly measured. This adds to the uncertainty of the calculation, and is another reason why it is difficult to ascertain a clear performance advantage to the beaded sorbent in terms of moisture uptake.

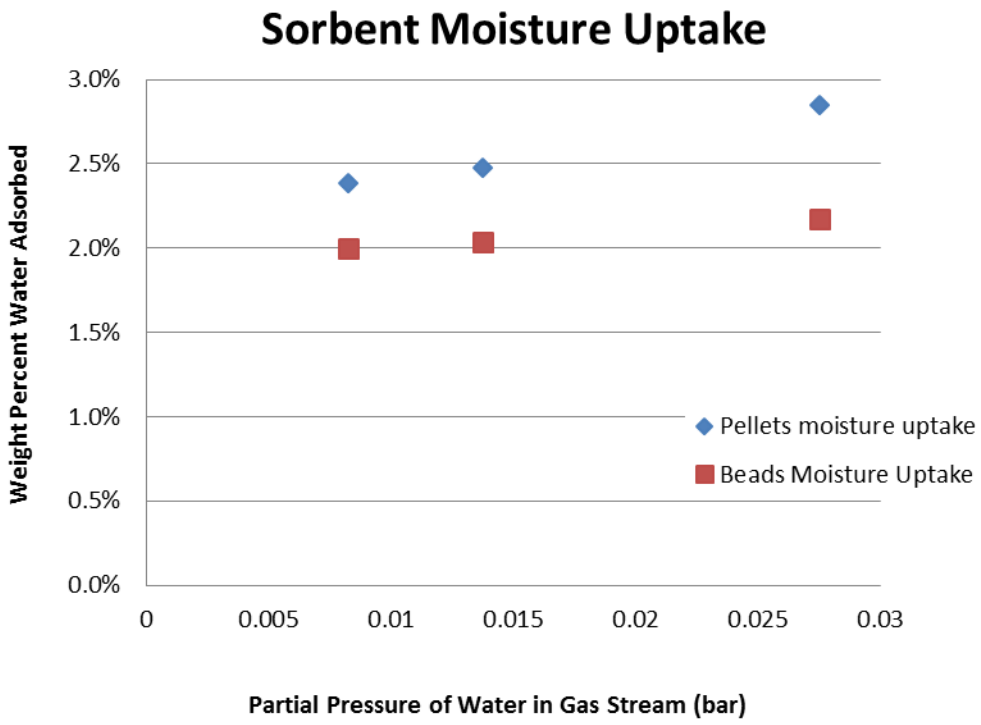

Figure 35. Moisture uptake of beads and pellets.

3.4.1.3 CO_2 Isotherms

One of the tests was an evaluation of sorbent isobars at temperatures from 40-120 ^{0}C at 10 ^{0}C increments. During these tests, approximate equilibrium values were obtained for both sorbents at four CO_2 partial pressures to allow for fitting of a Langmuir type isotherm. These data can be useful for design of a CO_2 capture system to optimize the adsorption and regeneration conditions.

When these data were collected, it was noticed that the sorbents had not completely dried during some of the tests, which will bias the amount of CO_2 adsorbed at lower temperatures slightly low. Also, some of the data for the beads at the P_{CO2} of 0.15 bar had data recording issues and may be subjected to a greater source of error. However, the data indicate the expected shape of an isotherm curve when plotted in Figure 36. The sorbent indicates an equilibrium working capacity of approximately 6% by weight when using the ADAsorb™ process with 40 ^{0}C adsorption and 120 ^{0}C regeneration.

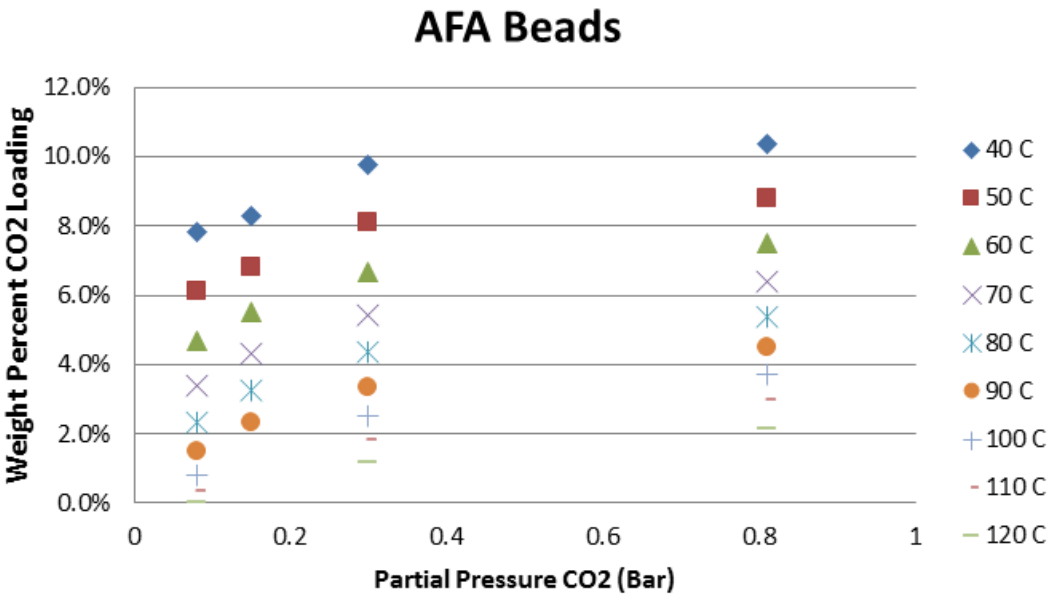

Figure 36. Isotherms for beaded sorbent based on isobaric testing.

The pellets exhibited similar performance in terms of ADAsorb™ working capacity, but adsorbed a higher total amount of CO_2. The working capacity of the pellets was slightly higher than the beads at just over 6.5%. But, a difference of half a percent is not conclusively better performance for the pellets since this is only one data point without the ability to perform statistical analysis. As was the case with the beads, the pellets exhibited the expected behavior during isobaric testing yielding Langmuir isotherm curves identifiable in Figure 37.

.

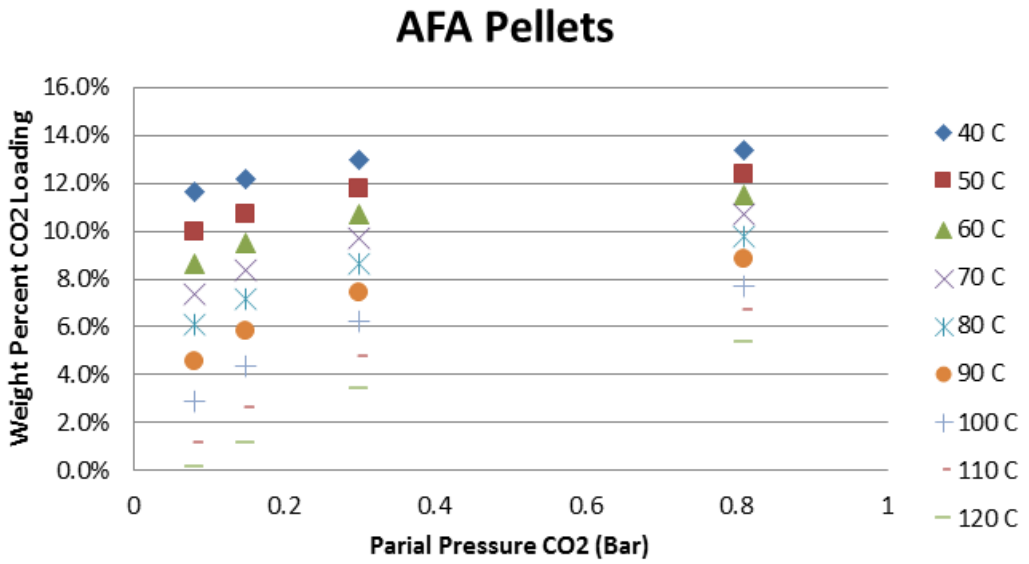

Figure 37. Pellet isobar data plotting Langmuir isotherms.

3.4.1.4 Cyclic Stability

The same two sorbents, AFA beads and AFA pellets, were also exposed to long term cycling between an adsorption condition of approximately 0.15 P_{CO2} bar and 0.034 P_{H2O} bar with a total

pressure of 0.81 bar balanced in nitrogen. The sorbent was then regenerated in nitrogen rather than CO_2 due to the CO_2 analyzer limitations. Thus, the results of these tests should be viewed as CO_2 adsorbed rather than CO_2 working capacity. Furthermore, this is a calculated value of CO_2 adsorbed based on a difference of volume calculation and is not as accurate as TGA analysis. However, these data are useful for assessing the long term stability of the sorbents when examining the ***slope of the curve*** plotted by the data rather than focusing on the adsorption capacity. As shown in Figure 38, the pellets displayed excellent stability without a significant reduction in working capacity. Adsorption conditions for both sorbents were 40 ^{0}C with 100 ^{0}C as the regeneration temperature. During the bead testing, some technical issues were encountered, which resulted in high fluctuations in the data. The beads showed a decrease in cycling stability, and was momentarily restored by attempting a set of cycles at a 110 ^{0}C regeneration temperature. For this test, the pellets showed better cycling stability compared to the beads, in terms of reliable and consistent stability throughout this test for long term CO_2 capture viability. However, due to the technical issues encountered during the test we cannot draw a final conclusion about the cyclic stability of AFA sorbent beads.

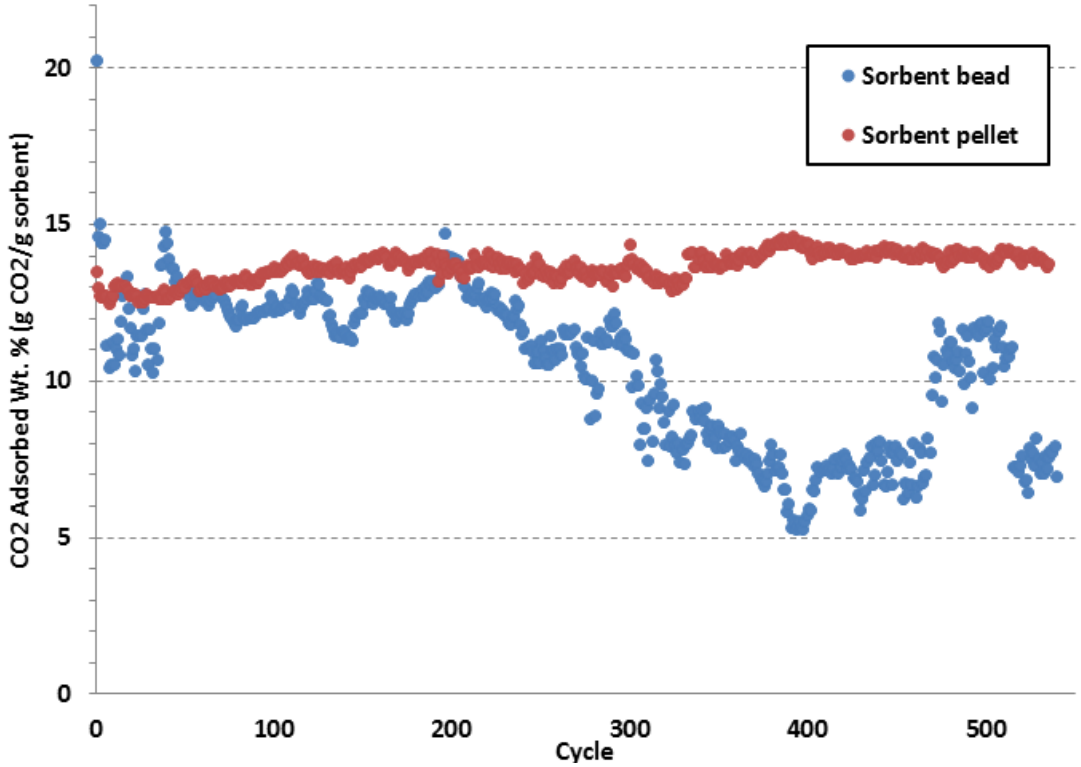

Figure 38. Cycling performance comparison sorbents bead and pellet.

3.4.1.4.1 Jet Cup Attrition and Crush Strength Testing

AFA pellet and AFA bead sorbents were also exposed to a jet cup attrition test and crush strength testing. Results from the attrition testing indicate that both the pellets and beads are subject to fragmentation; however the AFA beads were substantially more resistant to attrition than the AFA pellets. As shown in Figure 39, the pellets exhibited significant fragmentation with a corresponding attrition index (AI44) of 5.8. The beads were substantially more robust with an

AI44 of 0.31 and less fragmentation in the particle size distribution post testing as shown in Figure 40. The overall test results are shown in Table 15.

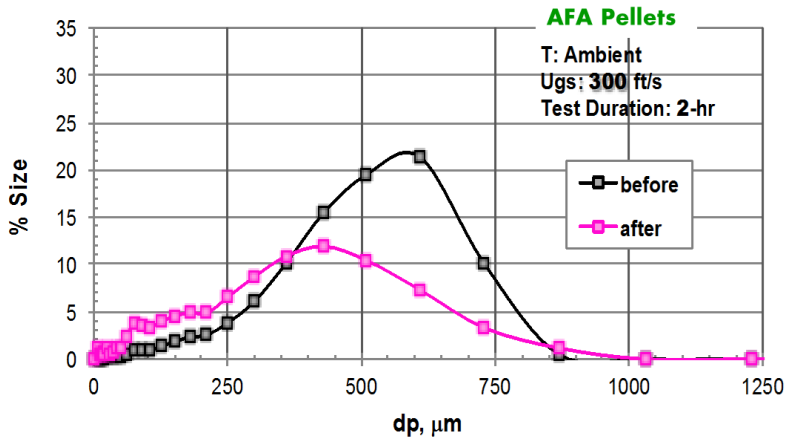

Figure 39. Pellet particle size distribution before and after jet cup attrition testing.

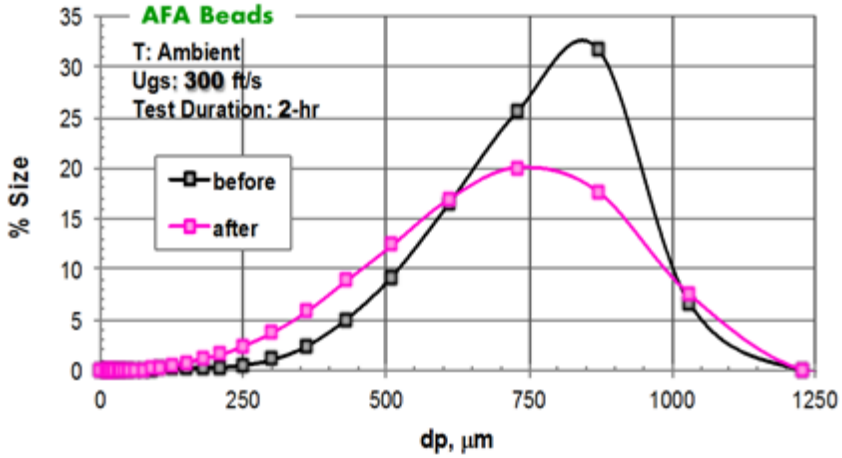

Figure 40. Bead particle size distribution before and after jet cup attrition testing.

Table 15. Attrition Index of bead and pellet sorbent by jet cup attrition testing.

Sorbents	Inventory (g)	AI (20)*	AI (44)**	Fine on filter (%)
Pellets	52.4	3.5	5.80	4.2
Beads	32.4	0.07	0.31	0.3

*: Attrition Index based on generation of material smaller than 20 microns
AI(20) = (Final F20) – (Initial F20)
**: Attrition Index based on generation of material smaller than 44 microns
AI(44) = (Final F44) – (Initial F44)
F44: Weight fraction of material smaller than 44 microns
F20: Weight fraction of material smaller than 20 microns

This indicates that the beads are more suitable for a fluidized bed process despite the fact that they had a lower crush strength of 8.4 lbf compared to pellets at 14 lbf. Results indicated that even though the binder may be stronger in the pellets, the beads were still much less likely to fragment in a fluidize bed. However, it is also important to note that the jet cup attrition testing is far more

violent than the ADAsorb™ fluidized bed process. The purpose of the jet cup attrition testing is also to cause some level of attrition so that an attrition index may be measured.

3.4.2 1 Kw system testing results.

Enough AFA sorbent material (KD-240 powder) was supplied to UA for pelletization and to be ran on the 1 Kw system testing. The system unit uses three thermocouples to monitor adsorption through the 3 L adsorber vessel. These measurements are made simultaneously with CO_2 purity measurements at the adsorber and desorber outlets. Figure 41 shows a sample adsorption cycle and the distribution of thermocouples A1/A2/A3 through the system.

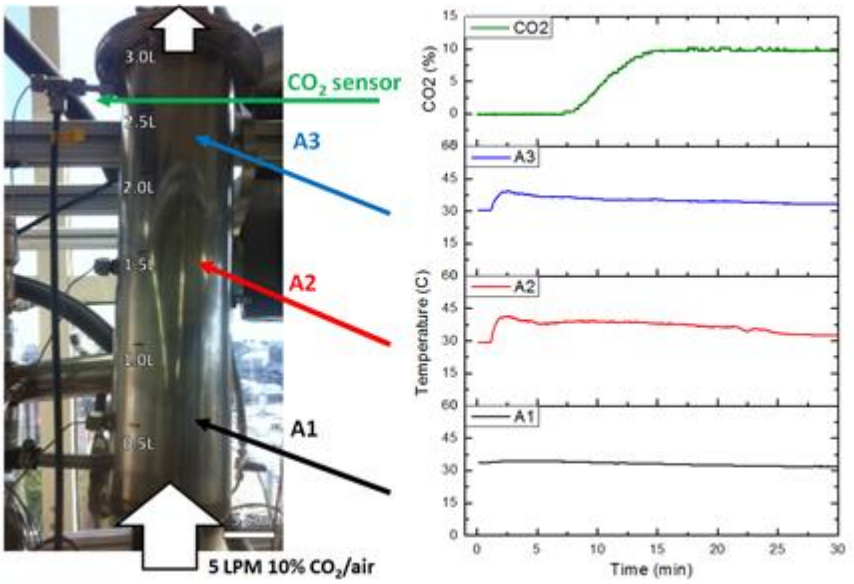

Figure 41.Temperature and thermocouple distribution.

Figure 42 A-C plot the %CO_2 measured from the outlet of the adsorber during continuous flow of 15% CO_2 at 5-20 LPM over 10 min. The sorbent bed for these trials is 500 g/1.5 L of AFA sorbent pellet. CO_2 breakthrough occurs within 1 min. of the start of adsorption. As the flow rate increases the time to observe a change in %CO_2 from 0 is reduced from 0.7 min. at 5 LPM to 0.35 min. at 20 LPM. Repeat trials show that this breakthrough time occurs reproducibly for a given condition. Breakthrough time is halved by quadrupling the flow rate. In Figure 42A, however, it is apparent that Cycle 2 possesses a longer breakthrough time (1.3 min.). This longer time disappears by Cycle 3. This longer adsorption period may occur from the drying of the sorbent bed after the steam leak. The 5 LPM trial represents the first testing after the samples baked at 60 ˚C overnight to dry.

The time to reach the 15% CO_2 plateau during the 10 min. adsorption is the most sensitive dependent variable observed in changing flow rates. The twelve cycles in each Figure 42A-C plot makes observing this change difficult – Figure 42D shows an average of each trial for comparison. The average time to reach 15% CO_2 out of the adsorber is 6.0 min. at 5 LPM which is reduced to 1.9 min. by 20 LPM. The slope of the %CO_2 curve between the point of CO_2 breakthrough and the plateau expectedly becomes steeper as flow rate increases.

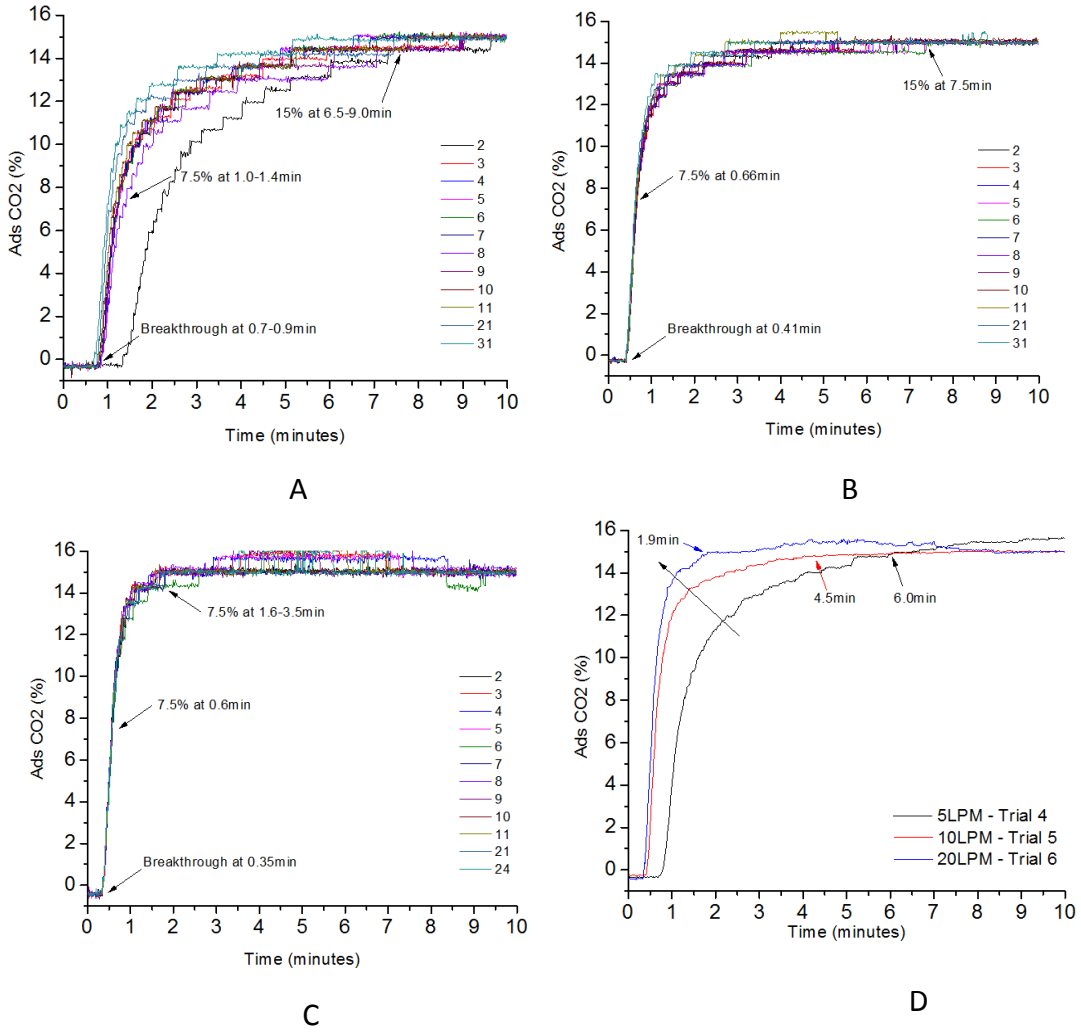

Figure 42. Different CO_2 profiles. A: 5 LPM, B: 10 LPM, C: 20LPM, and D: Averages of Figures A-C.

It is possible to estimate capture capacity of the sorbent bed based on the CO_2 breakthrough data from adsorption. However, measuring capture capacity as CO_2 extracted after desorption reveals the practical limits on CO_2 capture. The capacity measured from the desorption side of the cycle includes leaks to and from the system, remaining volumes of CO_2 that were not extracted by the vacuum, and unknown factors. The basis for calculating the amount of CO_2 released during desorption requires knowing the flow rate of gas from the desorber and its purity. Multiplying these two variables as a function of time and integrating with respect to time solves for the total liters of CO_2 released by the adsorption/desorption cycle. Figure 43 shows LPM of CO_2 from the desorber over several minutes during the CO_2 extraction step of the desorption process. This step ends when $\%CO_2$ reaches below 90% purity to ensure only high purity CO_2 is released by the process and that the system is able to cycle faster.

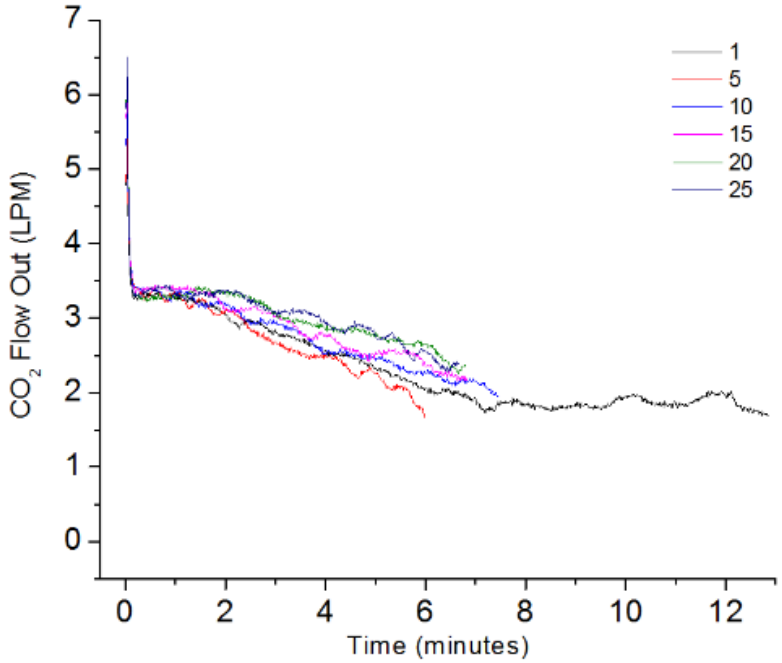

Figure 43. An example plot of LPM CO_2 from the desorber during extraction.

By integrating the LPM CO_2 plot in Figure 43 for 5-20 LPM, the average liters of CO_2 captured per 500 g of sorbent were obtained. Table 16 shows the calculated capture capacity from the 1 kW test system, which are lower than the values measured by TGA. This is due to some imperfections in the detection system. The vacuum pump only extracts gas with a pressure differential of 10 in. Hg (~1/3 atm), therefore, it does not remove all of the CO_2 during the extraction step, which affects the total CO_2 capacity measurement.

Table 16. Capture capacities from desorption.

Flow Rate	Liters of CO_2 Measured	Moles of CO_2 (at 22.4 L/mol) per 500g bed	Capture Capacity (mmol/g)
10	**14±3.2**	**0.62**	**1.25**
20	**21±4.5**	**0.94**	**1.89**

The exothermic reaction of amine and CO_2 on the sorbent requires considering heat mitigation. A steel cooling coil was placed within the bed to continuously draw away heat. Figure 44 shows the relation between %CO_2 out of the adsorber and the observed temperature rise in the bed. As flow rates increase from 5-20 LPM only a small reduction in peak temperature of the A1 thermocouple was observed. The A1 thermocouple is positioned closest to the gas inlet, and thermocouples A2 and A3 are equidistant throughout the adsorber vessel and do not contain the sorbent bed when it is half loaded (as shown in Figure 44).

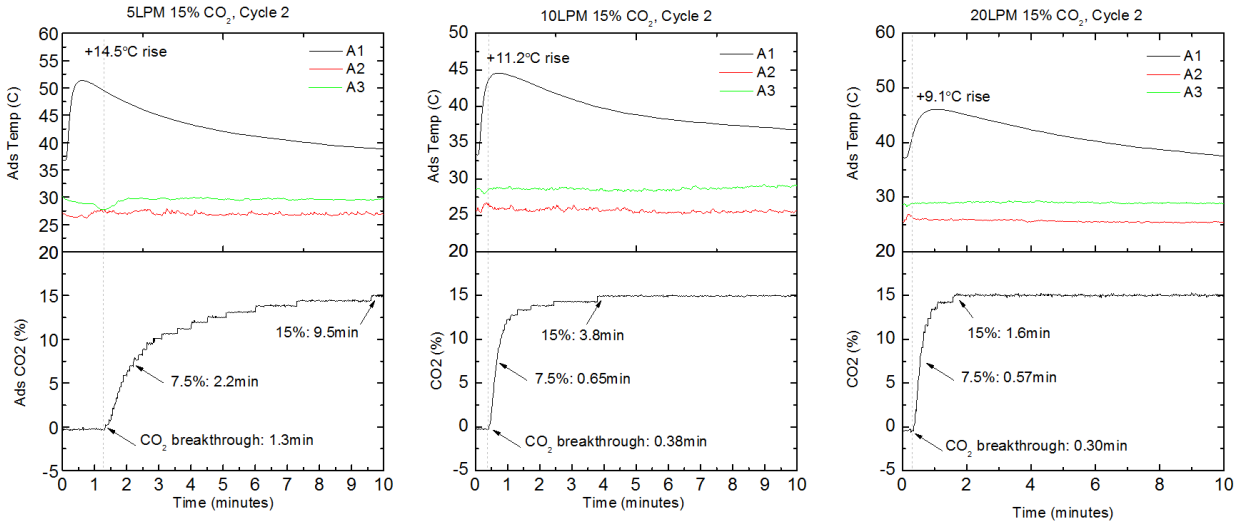

Figure 44. Combined temperature and %CO_2 plots during adsorption.

In a separate experiment, performed prior the upgrade of the 1 Kw system, CQA 12 pellets (AFA sorbent type # 2) were tested in the system. The pellet sorbent was only cycled eight times due to the observation of smoke and an intense amine smell coming from the desorber. Several temperature spikes in the desorber from 250 – 300 °C prompted ending the tests early. As shown in Figure 45, it is apparent that the pellet sample had begun to coat the upper section of the desorber and impede the flow of gas through the recirculation pathway. This would prevent proper fluidization of the pellets and lead to burning as the bed quickly reaches the temperature of the steam jacket (150 °C) well above the intended 100 – 120 °C desorption temperature. This desorption range is maintained, in part, due to balance of heat loss during fluidization and automation of the steam line pressure. With the temperature of the desorber rising above intended levels and the presence of O_2 in the desorber due to leaks it is possible some combustion of a component of the pellet occurred.

Figure 45. Pellet sample adhered to piping above the desorber and covers the vent to allow recirculation of the gases inside the desorber.

3.4.3 Sorbent form down-selection.

The test results showed that both product forms of AFA demonstrated comparable CO_2 capture performance, including good working CO_2 capacity (6 - 6.5 wt. %), low water uptake (< 3 wt. %), and cycling stability over 500 cycles (on a fixed bed and cycling between 40°C (adsorption), and 100 °C (desorption)). After reviewing all of the test results, the AFA pellet form was selected for the bench scale testing. This selection was primarily made based on the scale-up production capabilities of the aerogel at Aspen, and the pelletization capabilities at Akron for future large scale production.

3.5 AFA Bench scale testing results

3.5.1 AFA scale-up production (30 kg) for bench scale testing

AFA sorbent type # 1 (KD-240) was picked over AFA sorbent type # 2 (CQA 12) for pilot scale up production and pelletization processing. The assumptions were made regarding CO_2 capture performance and thermal stability for the sorbent type # 1. The un-successful test of the CQA 12 pellets on the 1 Kw system testing (see Figure 45) confirmed our choice to move on with AFA sorbent type # 2 for scale up production and bench scale testing.

A large amount (30 kg) of AFA sorbent powder type # 1 was prepared at Aspen, powderized into a fine powder (~70 micron particle size), and pelletized at UA for bench-scale fluidized bed testing. Figure 46 shows powderized AFA sorbent packed in plastic bags and put in 5 gallon containers that were shipped to the University of Akron for pelletization. Minor technical issues were encountered during sorbent pelletization on a large scale (30 kg), at UA. The sorbent binder solution was adjusted and strong pellets were produced.

Figure 46. AFA sorbent powder shipped in 5-gallons containers.

3.5.2 Solid Sorbent Capture Case

The solid sorbent capture case utilizing an Aspen Aerogel's sorbent was modeled using ADA-ES's general process design reported in their 1 MW pilot testing report (Figure 47) [13]. However, individual reactors were specifically designed and sized for use with the Aspen Aerogel's sorbent.

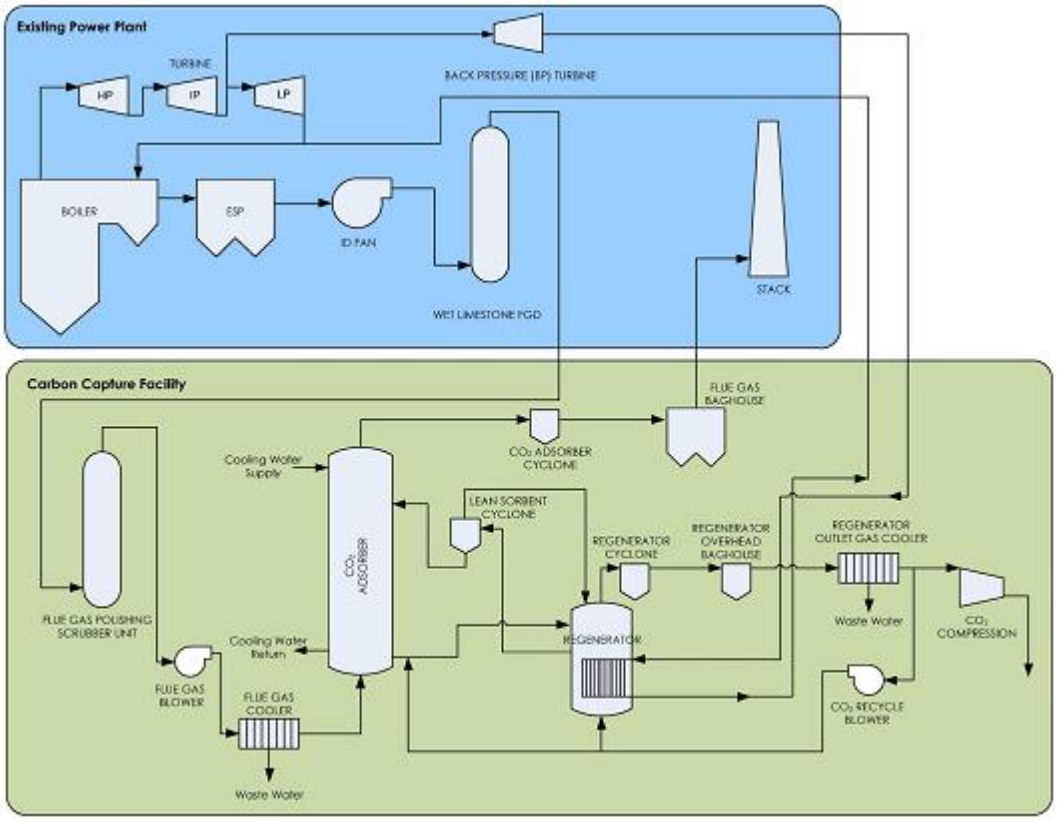

Figure 47. ADA-ES solid sorbent CO2 capture process flow diagram [13].

In this report, the "existing power plant" is increased in size and gross output to overcome the energy requirements of the "carbon capture facility" to maintain an equivalent 550 MW net generation output, schematically depicted in Figure 47. This is the same methodology used in the NETL baseline reports when scaling the "existing power plant" to a size necessary to produce 550 MW net generation output with the addition of the Cansolv™ capture system. For the solid sorbent case for this project, overall performance is similar to the MEA base case with a few notable differences. The most significant differences are that the steam extraction point for the sorbent/solvent regeneration in the NETL cases provides steam at a too high of a temperature and pressure to be utilized in the solid sorbent regenerator vessel.

Based on the extensive laboratory testing and characterization of the sorbent completed by Aspen in previous budget years, it was determined that the regeneration temperature should be 100˚C (212˚F) and that excessive temperatures could potentially cause sorbent degradation and/or functionalized amine deactivation. Therefore, the steam has to be reduced in temperature and pressure before it can be utilized in the regenerator. As a result, a back-pressure or let down turbine was installed in the process model to reduce temperature and pressure of the steam while extracting additional electrical energy as was also shown in the ADA-ES process flow diagram in Figure 47. These turbines are not as efficient as the primary generation turbines because these turbines do not typically have the same number of rotor stages.

During the ADA-ES program, the back pressure turbine was modeled using GateCycle™ software to determine an appropriate isentropic efficiency for the application investigated[13]. For the

purposes of this analysis, the isentropic efficiency was matched for the Aspen Aerogels sorbent, however the steam conditions were adjusted for the specific needs of this sorbent to determine specific power output of this turbine.

3.5.2.1 Sorbent CO_2 Langmuir Isotherm Analysis and Theoretical Capture Bounds

A thermo-gravimetric analysis (TGA) was performed on the amine functionalized pellets by ADA-ES in a previous phase of the project. Pellet mass was recorded as a function of CO_2 adsorption at nine temperatures from 40˚C to 120˚C in 10-degree increments, at all combinations of four CO_2 partial pressures: 0.081, 0.14904, 0.2997, and 0.81 bar. The data point of 0% CO_2 adsorption at 0 CO_2 partial pressure was also inserted. For each temperature set point, we used the method of least-squares function fitting to generate Langmuir isotherm curves between the gas CO_2 density ρ_g and pellet CO_2 density ρ_s of the form

$$\rho_s = \rho_{s,max}(T)\frac{K_{eq}(T)\rho_g}{1 + K_{eq}(T)\rho_g}, \qquad (1)$$

where the parameters to be fit were $K_{eq} = \frac{k_a}{k_d}$ is the adsorption equilibrium constant, expressed as the adsorption rate k_a over the desorption rate k_d, all of which are functions of temperature, and the maximum CO_2 sorbent density $\rho_{s,max}(T)$ (also a function of temperature).

The adsorption reactor vessel is expected to be operating in the range from a maximum of 0.128 bar down to 0.0128 bar and possibly lower CO_2 partial pressures in order to achieve a 90% capture rate or greater. However, the existing TGA data contained only one partial pressure (0.081) in that range. This presented a challenge because standard Langmuir curves are all decelerating (concave down), and without more data in the critical operating range, the curve fits will fit the most relaxed-slope line through the operating range with minimal concavity and will likely underestimate the true adsorption kinetics. To address this issue, an additional data point was derived at 0.04 bar, produced from TGA data from the raw non-pelletized sorbent powder from a previous phase of the project (Begag, et al., 2013). The powder had been tested at both 0.04 bar and 0.08 bar, each over the same temperatures as the pellets. To generate this derived data point, we computed ratio W of powder CO_2 mass fraction at 0.04 and 0.08 bar at each temperature. The derived pellet data point at 0.04 bar was computed as pellet CO_2 mass fraction at 0.08 bar times the powder mass fraction ratio W.

Using the supplemented data, a least-squares Langmuir isotherm curve fit was performed to obtain K_{eq} and $\rho_{s,max}$ parameter estimates for each of the nine temperatures. These parameter estimates were further fit, based on observation of the data trend (see Results), to an exponential and a linear curve least squares curve fit, respectively, for K_{eq} and $\rho_{s,max}$ to obtain reaction functions over a continuum of temperatures within the operating range:

$$K_{eq}(T) = K_{eq,0}e^{-\frac{T}{T_0}}, \quad \rho_{s,max}(T) = -\eta_1 T + \eta_0, \qquad (2)$$

where $K_{eq,0}$, T_0, η_0, and η_1 are parameters to be fit.

With the functions $K_{eq}(T)$, and $\rho_{s,max}(T)$ estimated (Equation 2), the Langmuir isotherm curve (Equation 1) then becomes a multivariate function of ρ_g and T that generates a Langmuir surface $LS(\rho_g, T)$. This function can also be expressed in terms of CO_2 partial pressure p in lieu of CO_2 density ρ_g through a linear change of variables via the ideal gas law: $LS(p, T)$.

The theoretical capture bound was be computed from this surface $LS(p,T)$ as follows: the regeneration vessel is set to a hot regeneration temperature T_{hot} and 100% CO_2 partial pressure $p(T_{hot}) = 1$ bar. There is a level curve defined by $\rho_{s,hot} = LS(1,T_{hot}) = LS(p,T)$ being constant, containing values $p = 1$ and T_{hot}, and other p-T-values satisfying the equation. The hot sorbent is then delivered quickly to the adsorber vessel where it is cooled to T_{cold}, and exposed to much lower partial pressures up to but not exceeding $p = 0.128$ (rich flue gas). When cooled, the equilibrium partial pressure p^* associated with T_{cold} will be on the aforementioned level curve, found by solving the following:

$$LS(p^*, T_{cold}) = \rho_{s,hot} = LS(1, T_{hot}) \quad (3)$$

for p^* given T_{cold} and T_{hot}. Geometrically, this point p^* is found by tracing back to T_{cold} on the regenerator's $\rho_{s,hot}$ level curve and recording the partial pressure. The capture proportion $P_{capture}$ is the proportion of p^* relative to the rich flue gas input:

$$P_{capture} = \frac{0.128 - p^*}{0.128}. \quad (4)$$

In general, $P_{capture}$ can be negative or positive, with positive values indicating a true capture of CO_2 whereas negative values indicate a non-functional process that emits more CO_2 into the flue gas stream than it captures.

3.5.2.2 Adsorption Reaction Kinematics: Linear Systems Timescale Analysis

The equilibrium constant $K_{eq} = k_a/k_d$ can be estimated from the isotherm experiments (see previous Section) but the individual adsorption and desorption rate constants k_a and k_d, respectively, cannot be determined from equilibrium isotherm data. However, the rates can be estimated to an order of magnitude based on isobar experiments.[9] In these experiments, the kinetics and CO_2 capacity of the isolated amine powder were studied. The amine powder is distinct from the amine-functionalized aerogel sorbent pellet, however the kinetics of both should be highly related. In previous research project[9], the amine powder exposed to a constant 15% CO_2 partial pressure and temperature was varied over 9 holding temperatures (120 to 40 ˚C), with fast 10 ˚C temperature changes that occur within a 1-2 minute window followed by 60 minute hold time. Amine powder mass was measured with sampling frequency ½ Hz, providing sufficiently a fine-grained time resolution of the dynamics of CO_2 adsorption as a function of temperature. The principal interest is the dynamics of the amine powder mass change in response to quick changes in temperature.

In order to estimate the parameter related to the amine-CO_2 binding/unbinding reaction, one must use the time-series isobar data (explained further below) to form a model of the dynamic response of adsorption to dynamic changes in temperature input. We used standard linear systems theory to estimate the transfer function of the binding/unbinding dynamics and showed a good fit with a proportional-integrator model (explained further below). The transfer function is defined as the ratio of the Laplace transforms of the output time-series over the input time-series (see Eqn. 5). The Laplace transform is integral to linear systems analysis and is a standard tool used in process and control engineering.

Let $\theta(t)$ denote the mass fraction and $T(t)$ denote temperature, both as functions of time t. The goal was to establish the nature of the dynamic relationship between these observed variables. The sampling rate of the experiment was $f_s = 30$ (1/min), so a dynamic analysis will be able to resolve dynamic features in the data up to the Nyquist frequency---half the sampling rate $f_s/2 = 15$ (min-

[1]). Likewise, for the long timescale, we may resolve dynamic changes on the order of the half experimental time window of 30 minutes. For every 60-minute holding temperature time window, the mean-subtracted the mass fraction was defined as $\theta_{ms}(t) = \theta(t) - \bar{\theta}$, and temperature $T_{ms}(t) = T(t) - \bar{T}$ (equations are not numbered since they are part of the text). The Laplace transform of each was computed: $\mathcal{L}[\theta_{ms}](s)$, $\mathcal{L}[T_{ms}](s)$. The resulting transfer function was

$$H(s) = \frac{\mathcal{L}[\theta_{ms}](s)}{\mathcal{L}[T_{ms}](s)}. \quad (5)$$

We constructed transfer functions for each of the nine holding temperatures. As the results will show, the shape of the transfer function is suggestive of a proportional-integrator (PI) linear model

$$\theta_{ms}(t) = A\, T_{ms}(t) + B \int_0^t T_{ms}(\eta) d\eta, \quad (6)$$

with constants A, B, and approximate transfer function

$$\widehat{H}(s) = A + \frac{B}{s}. \quad (7)$$

The constants A, B were fit to the empirically computed transfer function $H(s)$ yield the approximation $\widehat{H}(s)$ (Equation 7). The magnitude of the constant A represents the contribution of a very fast (proportional) response of $\theta_{ms}(t)$ to fluctuations in temperature$T_{ms}(t)$, whereas magnitude of the constant B represents the contribution of a slower-timescale response of $\theta_{ms}(t)$ to the averaged past values of $T_{ms}(t)$ (integrative response). To assess the relative contribution of these components, the influence fraction (IF) of $|A|$ relative to the total variation $|A| + |B|$ was defined:

$$influence\ fraction = IF = \frac{|A|}{|A| + |B|}. \quad (8)$$

Large IF values near unity are reflective of fast processes that respond quickly and proportionally to changes in the input signal. Conversely, a low IF value near zero indicates a process that slowly changes in response to long-timescale integrated effect of past input values.

3.5.2.3 Effective Heat Capacity of Aerogel Pellets

Aerogel pellets are built on silica aerogel matrix with functionalized amine. Silica aerogel is a novel material because the silica skeletal material that makes up the gel matrix possesses a fairly conventional heat capacity 860 J/(kg K); however, the spatial heat conductance κ of silica aerogel is one the lowest measured in the world, on the order of $\kappa \sim 10^{-2}$ W/(m K). That is, while its theoretical heat capacity is conventional, the timescale required to thoroughly heat the aerogel solid is very long.

Heat transfer in fluidized beds is primarily through direct pellet-to-heat-exchanger contact. Mean pellet contact times with heat exchanger for typical fluidized particle beds have been recorded on the order of seconds, before they are circulated off the heat exchanger through turbulent mixing and into the vessel volume[10]. That is, the heating and cooling of the entirety of the fluidized bed is primarily mediated through rapid particle exchange in and out of the heat exchanger boundary layer.

With contact times on the order of seconds[10], and a very low silica aerogel heat conductivity, it is expected that any volume of aerogel material in contact with a heat exchanger should exhibit rapid

surface heating but very slow and incomplete penetrance to the depth ℓ of the volume. Moreover, the amount of energy ΔJ imputed per unit of surface area over a fixed time window τ, to cause a surface temperature change $\Delta T_{surface}$ will be smaller compared to the energy and time required to heat thoroughly the entire solid volume. Importantly, because the gas-to-amine contact also occurs near the surface of the pellet, it stands to reason that the adsorption and desorption reactions will be driven primarily by surface temperature swings $\Delta T_{surface}$ rather than through heating if the entire volume. Therefore, we define the effective heat capacity of the aerogel to be

$$c_{eff} = \frac{\Delta J}{\rho_a \ell \Delta T_{surface}}, \quad (9)$$

where ρ_a is the pellet apparent mass density and ℓ is the characteristic material depth. As the results will show, the mean pellet diameters are within a range from 500-1500 microns with a mean of about 848 microns across multiple gas velocities, hence ℓ is on a several hundred micron scale.

An effective heat capacity c_{eff} was computed using a simplified model system to simulate the effect of aerogel heat conductivity on surface temperature swings as a function of the time scale τ of contact heating and cooling. The characteristic length scale was set to $\ell = 500$ microns, a typical radius of a pellet. Without loss of generality, it was assumed this volume is a flat slab of material with depth ℓ and contact area of 1 meter squared. Heat conduction within the volume with temperature $T(x,t)$ is governed by the heat equation

$$\frac{\partial T}{\partial t} = \frac{\kappa}{c\rho_a}\frac{\partial^2 T}{\partial x^2}, \quad (10)$$

with a Fourier's law heat flux term $\phi(x,t) = -\kappa\frac{\partial T}{\partial x}(x,t)$. At $x = \ell$, the test volume we take to be non-conductive: $\kappa\frac{\partial T}{\partial x}(\ell,t) = 0 = \phi(\ell,t)$. At the other end $x = 0$, the test volume is in contact with the heat exchanger with uniform temperature $T_{he}(t)$ that alternates between 40 and 100°C, with each temperature exposure for a duration of τ seconds. The heat flux at this contacting surface is proportional to the temperature difference across the boundary, with heat transfer coefficent K_f yielding a boundary condition

$$K_f T_{he}(t) = K_f T(0,t) - \kappa\frac{\partial T}{\partial x}(0,t). \quad (11)$$

The solution $T(x,t)$ was computed for a range of ten half-cycle times τ from 0.1 s up to 100 s on a logarithmic scale. The computed solution began with an initial condition of $T(x,0) = 70$ and included five alternating cold-then-hot cycles which allowed the solids temperature to approach a steady state oscilation with consistent trough-to-peak temperatures. The solution was computed analytically via Fourier series eigenfunction expansion using 200 terms.

To calculate the effective heat capacity c_{eff}, both the heat flux ΔJ into the material was measured and temperature swing $\Delta T_{surface}$ on the last τ-cycle. On this cycle, the solid's temperature transitioned from a minimum (cold) surface temperature at time t_{start} to the end of the cycle

reaching a peak (hot) temperature at time $t_{start} + \tau$, we computed the net heat flux into the volume as

$$\Delta J = K_f 100\,\tau - K_f \int_{t_{start}}^{t_{start}+\tau} T(0,t)dt. \qquad (12)$$

The resulting surface temperature swing was

$$\Delta T_{surface} = T(0, t_{start} + \tau) - T(0, t_{start}). \qquad (13)$$

Equations (36-37) were inputed to Equation (33) to compute c_{eff} over a range of τ-cycles.

3.5.2.4 Multiphase Gas-Solid Breakthrough Model for the Adsorbtion Reactor System

As a result of kinetic rate investigation, isotherm functions, and initial process modeling, it was possible to examine the necessary equipment for the post combustion CO_2 capture system. The key components of the adsorber-desorber unit are depicted in the schematic drawing in Figure 48. The desorber accepts CO_2 rich cold particles into the top of the bed. The bed is fluidized using recycled CO_2 product gas and CO_2 is desorbed from the incoming sorbent particles as a result of the heat provided by boiler steam. The lean hot particles are then removed from the desorber and transferred to an intermediate position of the adsorber bed. The hot particles undergo advective flux downward in addition to bi-directional turbulent mixing while they are cooled by heat exchangers.

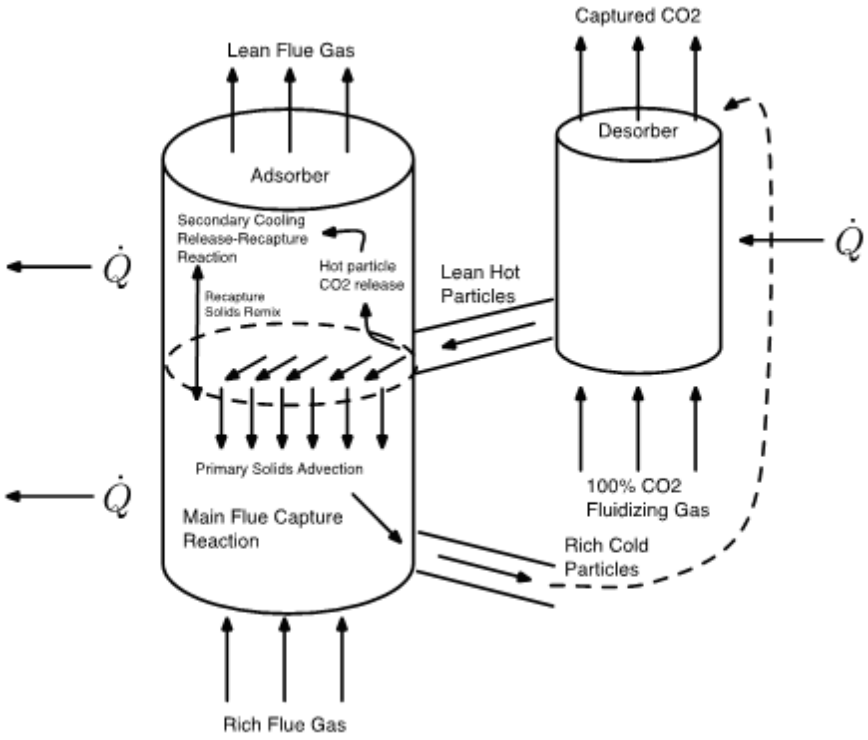

Figure 48. Schematic diagram of the turbulent fluidized bed adsorber and desorber reactor units with key internal processes.

The lower half of the adsorber bed contains the primary adsorption reaction, where flue gas is stripped of a majority of its CO_2, rich cold particles are shunted back to the desorber while leaner flue gas fluxes upward. Above the primary reaction, this leaner flue gas comes into contact with hot-but-cooling sorbent particles. When the lean hot particles are brought in contact with lean gas, the particles desorb an additional amount of CO_2, thereby making the hot particle extra lean. This secondary release of CO_2 gas then advects upward through the upper section of the absorber column and adds CO_2 back to the lean flue gas, thereby making the flue gas slightly richer. However, this secondary gas release is mostly recaptured in the upper bed as the newly introduced hot particles are cooled, and the gas readsorbs into these leaner cool particles before leaving the top of the column. This secondary recapture onto particles in the upper column eventually remixes into the main lower column through turbulent diffusion and exit to the desorber. *The ability to sufficienty cool hot particles in the upper bed and the speed of remixing of cooled particles to the lower bed is critical to determine the overall capture rate*. These factors are critical because the upper section of the fluidized bed is the last opportunity to adsorb CO_2 before it leaves to the stack, and because solids in the top vessel volume do not undergo advective transport, diffusive mixing and reactor geometry are critical factors.

In addition to CO_2 capture, moisture uptake from the sorbent is critically important. Excessive moisture content in the sorbent can greatly increase the heat duty of the regenerator due to the latent heat of vaporization of water. One potential method of mitigating moisture uptake in the adsorber is to design a residence time that promotes maximum CO_2 uptake while minimizing moisture uptake. In order to perform this calculation, Aspen Aerogels provided moisture uptake measurements so that moisture uptake could be determined for practical time scales and moisture partial pressures.

Breakthrough curves for both moisture and CO_2 were provided. As shown in Figure 49, the CO_2 uptake and loading of the sorbent to a near equilibrium value occurs much more quickly than with H_2O. In addition, moisture equilibrium data was provided in Figure 50. These data allowed for extrapolation of expected moisture loading on the sorbent at a given residence time and water vapor pressure for incorporation in the process model and economic analysis.

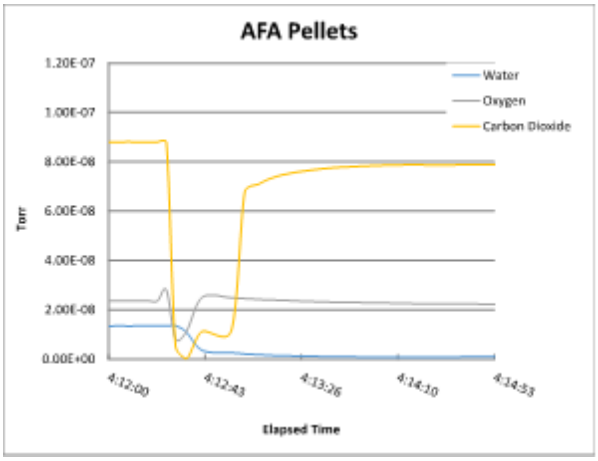

Figure 49. Breakthrough data for pelletized sorbent showing rapid uptake and equilibration with CO_2 while moisture loading occurred over a much longer time scale.

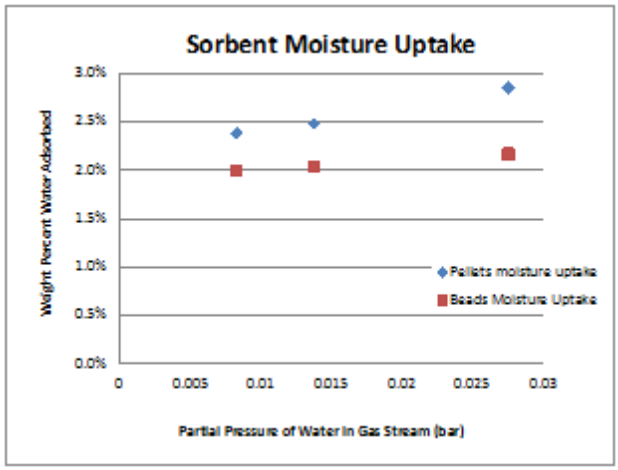

Figure 50. Moisture uptake for sorbent pellets as a function of moisture partial pressure.

3.5.2.5 Adsorber Multiphase Breakthrough Model

The adsorber unit is a cylinder with flow in the vertical z-direction. A test volume of the bed is depicted horizontally in Figure 51. Homogeneous behavior for all x and y points in a fixed z-plane is assumed for the sake of simplicity, and can be modeled as an effectively one-dimensional process. This one-dimensional reduction entails that all extensive quantities are for a test volume of one meter-squared of cross-sectional area. Such a simplifying reduction is appropriate at this early stage of technology development.

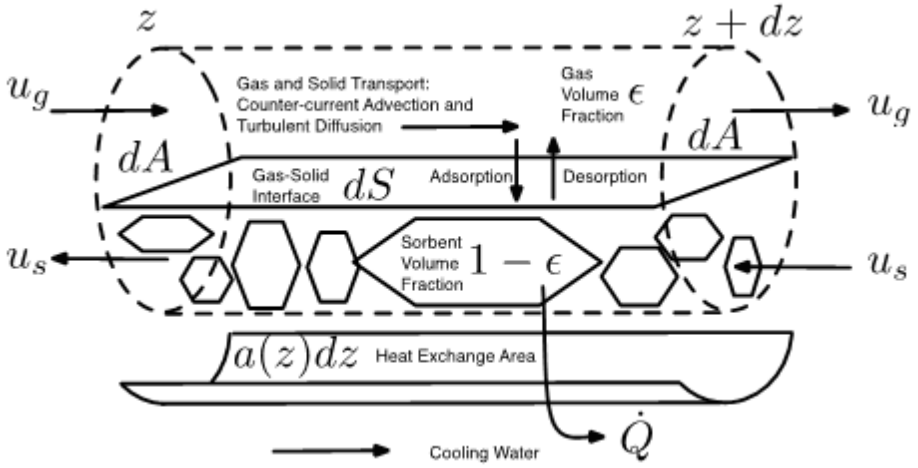

Figure 51. Multiphase model schematic of key features of a primary reacting bed test volume dV=dzdA, including gas and solids advection velocity u_g and u_s, gas and solids volume fraction ϵ and 1-ϵ, respectively and adsorption and desorption processes through the gas-solid interface dS. The solids volume also exchanges heat $\dot{Q}$ through heat exchange surface coupled to 15C cooling water, with area $a(z)dz$.

The adsorber unit has length L, which is comprised of two sections, the bottom L_b and top L_t section lengths ($L = L_b + L_t$), where primary and secondary reactions take place, respectively (see Figure 48). The test volume is dV Figure 51 is a small cylinder with cross sectional area dA and

length dz, and volume $dV = dA\,dz$. The gas volume is given by ϵdV. Flue gas flows into the volume on the left face and exits on the right face by advective flux at fixed velocity u_g. Conversely, solid sorbent particles reside in the volume $(1-\epsilon)dV$. Diffusive transport also occurs to approximate the average transport in turbulent gas and solid flows, which are modeled by diffusivity coefficients D_g and D_s, respectively.

In addition to advective and diffusive transport of gas and solids, adsorption and desorption occur at the gas-solid interface dS, where CO_2 binds or unbinds. The binding (adsorption) process is an exothermic reaction which increases the sorbent material temperature. The advection, dispersion, adsorption, and thermal dynamics, paired with mass conservation principles, determine a set of governing equations[6], written as follows.

At a point z and time t, let $\rho_g(z,t)$, and $\rho_s(z,t)$ be the gas and solid mass density of CO_2 and let $T(z,t)$ be the sorbent temperature. We do not model the temperature of the gas phase as the gas energy density is very small relative to the solids; moreover, to a first approximation, the heat transfer is primarily through solids contact with the heat exchanger[10]. In the volume $dV = dAdz$ depicted in Figure 51, the mass in each phase is then $\epsilon\ dV\ \rho_g$ and $(1-\epsilon)dV\rho_s$. The reaction to and from the two phases is by the law of mass action. The time rate of change of the two phases, and the temperature is given by the system of three coupled nonlinear partial differential equations:

$$\frac{\partial \rho_g}{\partial t} = -u_g \frac{\partial \rho_g}{\partial z} + D_g \frac{\partial^2 \rho_g}{\partial z^2} + X k_d [\rho_s - K_{eq}(T)(\rho_{s,max}(T) - \rho_s)\rho_g], \tag{14}$$

$$\frac{\partial \rho_s}{\partial t} = -U_s(z) \frac{\partial \rho_s}{\partial z} + D_s \frac{\partial^2 \rho_s}{\partial z^2} + k_d\left[K_{eq}(T)(\rho_{s,max}(T) - \rho_s)\rho_g - \rho_s\right] + u_s \rho_{s,lean} \delta_{L_b}(z), \tag{15}$$

$$\frac{\partial T}{\partial t} = \frac{K_f a}{c\rho_a}(T_{ahe} - T) + \frac{h}{c\rho_a M(CO_2)} k_d\left[K_{eq}(T)(\rho_{s,max}(T) - \rho_s)\rho_g - \rho_s\right] + T_{hot} u_s \delta_{L_b}(z), \tag{16}$$

where $X = (1-\epsilon)/\epsilon$ appears in the gas Equation (14) to account for density conversion of the mass flux between phases due to the different-sized gas and solid volume fractions.
The sorbent superficial advection velocity $U_s(z)$ of Equation (15) is a function of z because the adsorber vessel has advective flux in the lower part of the vessel where the primary reaction occurs, while in the upper section of the vessel the sorbent transport is driven solely by turbulent diffusion of the fluidized bed:

$$U_s(z) = \begin{cases} u_s, & 0 \le z < L_b \\ 0, & L_b \le z < L \end{cases}. \tag{17}$$

The delta functional source term $u_s \rho_{s,lean} \delta_{L_b}(z)$ in Equation (15) sets the input rate of the sorbent into the reactor vessel, where the Dirac delta functional $\delta_{L_b}(z)$ is the point source term with the property that $\int_{a_1}^{a_2} \delta_{L_b}(z)\mathrm{dz} = 1$ if and only if the point L_b is contained in the interval $[a_1, a_2]$.
The source term $T_{hot} u_s\ \delta_{L_b}(z)$ in Equation (16) sets the energy input rate from the hot sorbent in, while the heat exchanger dynamically affects solids temperatures in proportion to the solids-

cooling water temperature difference $T(z,t) - T_{ahe}$, where $T_{ahe} = 15$°C, with proportionality constant formed by the coefficient K_f, the heat exchanger surface area a per cubic meter of fluidized bed (bed cross sectional area), sorbent heat capacity c, and the apparent pellet mass density ρ_a. The reaction heat affects solids temperature through the coefficient $\frac{h}{c_s \rho_a M(CO_2)}$, consisting of the heat of adsorption h J/(mol), specific heat c, apparent density ρ_a, and CO_2 molar mass $M(CO_2)$.

3.5.2.6 Boundary Conditions of the Multiphase system (9-11)

Let ϕ_g be the flux of the gas phase per unit cross sectional area of the adsorber vessel. The gas flux within the interior of the reactor vessel is

$$\phi_g(z,t) = \epsilon u_g \rho_g(z,t) - D_g \frac{\partial \rho_g}{\partial z}(z,t). \qquad (18)$$

At $z = 0$ the CO_2 mass flux per unit cross sectional area of the adsorber reactor vessel is the product of the flue gas density times the advective velocity, times the void fraction:

$$\phi_g(0^-,t) = \epsilon u_g \rho_{flue}. \qquad (19)$$

At $z = L$ the gas condition is

$$\phi_g(L^-) = -D_g \frac{\partial \rho_g}{\partial z}(L^-,t) + u_g \rho_g(L^-,t) = \phi_g(L^+) = u_g \rho_g(L^+,t) \quad (20)$$

implying a zero-derivative boundary condition:

$$\frac{\partial \rho_g}{\partial z}(L^-,t) = 0. \qquad (21)$$

The boundary conditions for the solid phase can be deduced from a similar argument:

$$\frac{\partial \rho_s}{\partial z}(0^+,t) = \frac{\partial \rho_s}{\partial z}(L^-,t) = 0. \quad (22)$$

Let ϕ_s be the flux of the solid phase. At the point of hot sorbent input $z = L_b$, the flux has a jump condition owing to the point source:

$$\phi_s(L_b^-) - \phi_s(L_b^+) = -u_s \rho_{s,lean}, \quad (23)$$

where $\rho_{s,lean}$ is the hot lean sorbent density and the negative sign in the above indicates that the flux is leftward. Boundary conditions for solids temperature $T(z,t)$ mirror that of solids density with the modification that input flux is in proportion to input hot solids energy density. Equilibrium solutions were computed as a limiting solution of a temporal finite difference simulation using a first-order forward explicit scheme using 1,000 spatial grid points[7].

3.5.2.7 Desorber Lumped System Model

The desorption process occurs in up to 100% CO_2 gas partial pressure depending on the moisture present on the sorbent and thus the vessel spatial dynamics are less complicated. The worst-case scenario for desorption is 100% CO_2, so the model uses 100% CO_2 to provide a bound of desorber performance. This is the worst case from a sorbent perspective because the sorbent will regenerate more readily under a lower partial pressure CO_2 environment. As discussed in the section Multiphase Gas-Solid Breakthrough Model for the Adsorbtion Reactor System, moisture will be loaded on the sorbent which will likely reduce the concentration of CO_2 to below 100% on an absolute basis. However, from a modeling perspective, assuming a 100% CO_2 atmosphere is a reasonable assumption.

Furthermore, the adsorption-desorption kinetics are very fast relative to the thermodynamics. Therefore, a reduced, lumped system model to characterize the desorber reactor was chosen that uses equilibrium adsorbed-desorbed values as a function of the average solids temperature within the reactor $\bar{T}(t)$.

The average solids temperature $\bar{T}(t)$ within the desorber reactor is dynamically coupled to the following energy fluxes: energy flux solids input from the adsorber $\dot{e}_{s,in}$, energy flux of exiting solids $\dot{e}_{s,out}$, gas exiting the adsorber $\dot{e}_{g,out}$, the heat exchange flux between boiler steam to the desorber solids $\dot{e}_{he}$, and the endothermic desorption heat of reaction $\dot{e}_{desorb}$. Because the desorber reactor is dynamically coupled to the adsorber reaction, we model each of these fluxes *per adsorber cross-sectional area* (J/(s m^2)). The energy density within the desorber vessel is $e_s = c\rho_a\bar{T}(t)$, where c and ρ_a are the heat capacity and apparent mass density, respectively. The time rate of change of e_s is equal to the sum of all inward energy fluxes minus outward energy fluxes:

$$c\rho_a\frac{d\bar{T}}{dt} = \dot{e}_{s,in} + \dot{e}_{he} - \dot{e}_{s,out} - \dot{e}_{desorb} - \dot{e}_{g,out}\,. \quad (24)$$

It is assumed the adsorber unit reaches equilibrium in which the CO_2 solid sorbent density $\rho_{s,loaded} = \rho_s(z=0)$ and cold sorbent input temperature $T_{cold} = T(z=0)$ are constant. In equilibrium, the solids energy influx is

$$\dot{e}_{s,in} = (1-\epsilon)u_s\left(\rho_a + \rho_{s,loaded}\right)cT_{cold}\,. \quad (25)$$

The lean sorbent loading on upon exit of the desorber is the equilibrium loading $\rho_{s,lean}$ at the desorber temperature set point $T_{hot} = 100$°C, yielding an outward solids energy flux

$$\dot{e}_{s,out} = (1-\epsilon)u_s\left(\rho_a + \rho_{s,lean}\right)cT_{hot}. \quad (26)$$

The energy density flux of outflowing gas is

$$\dot{e}_{g,out} = (1-\epsilon)u_s\left(\rho_{s,load} - \rho_{s,lean}\right)c_{co_2}T_{hot}\,. \quad (27)$$

The desorbed gas is produced through an endothermic reaction with reaction heat h J/mol, divided by the CO_2 molar mass $M(CO_2)$:

$$\dot{e}_{desorb} = (1-\epsilon)u_s\left(\rho_{s,load} - \rho_{s,lean}\right)\frac{h}{M(CO_2)}. \quad (28)$$

The heat exchanger energy flux is the product of the fluidized bed heat transfer coefficient K_f, the heat exchange total surface S, and the temperature differential between the solids and the approach temperature of the heating steam T_{steam}:

$$\dot{e}_{he} = K_f S\left(T_{steam} - \bar{T}(t)\right). \quad (29)$$

In equilibrium ($d\bar{T}/dt = 0$) the desorber temperature is required to be at its set point $\bar{T} = T_{hot}$. This equilibrium state is attained through the correct-sized heat exchange surface area. Solving $d\bar{T}/dt = 0$ for S we get

$$S = \frac{\dot{e}_{s,out} + \dot{e}_{g,out} - \dot{e}_{s,in}}{K_f(T_{steam} - T_{hot})}. \quad (30)$$

3.5.2.8 Particle Residence Times in the Adsorber and Desorber

The adsorber residence time is defined by the function $r(z)$ to be the mean time it takes for a particle to reach the bottom of the adsorber given a starting position z within the adsorber vessel. Because all particles enter the vessel at the sorbent input port at position $z = L_b$, the residence time of interest is $t_{res\,time} = r(L_b)$. Naturally, it is required that

$$r(0) = 0, \quad (31)$$

and because no particles can pass through the top of the adsorber we require the residence time to cease changing there:

$$\frac{\partial r}{\partial z}(L) = 0. \quad (32)$$

The above are boundary conditions for the residence time differential equation (Gardiner, 2004)

$$-U_s(z)\frac{\partial r}{\partial z} + D_s\frac{\partial^2 r}{\partial z^2} = -1, \quad (33)$$

with flux

$$\phi_r(z) = -U_s(z)r - D_s\frac{\partial r}{\partial z}, \quad (34)$$

where and jump condition at the sorbent input port position $z = L_b$

$$\phi_r(L_b^-) - \phi_r(L_b^+) = -u_s. \quad (35)$$

The above conditions yield a solution

$$r(z) = \frac{x}{u_s} + \left(\frac{D_s}{u_s^2} - \frac{L_t}{u_s}\right) e^{-Pe_{L_b}} \left(1 - e^{\frac{u_s x}{D_s}}\right), \qquad (36)$$

where $Pe_{L_b} = \frac{u_s L_b}{D_s}$ is the Peclet number over the lower bed length. At $z = L_b$, and bed parameters inserted, the average residence time is then

$$t_{res\,time} = r(L_b) = \frac{L_b}{u_s} + \left(\frac{L_t}{u_s} - \frac{D_s}{u_s^2}\right)\left(1 - e^{-Pe_{L_b}}\right) = 300.01\ s\ (5.00\ min). \quad (37)$$

This residence time is applied to both the adsorber and the desorber.

3.5.3 Sorbent pellet physical characterization and fluidizing regime

Sorbent characterization and fluidization testing was performed by PSRI Inc. of Chicago, IL USA. The results of this testing was incorporated into the process model to facilitate the techno-economic analysis.

Density and size distribution: Sorbent pellet apparent density was measured $\rho_a = 1147$ kg/m^3. Figure 52 shows the pellet diameter size distribution with minimum pellet sizes between ~500 and ~1470 microns, and median diameter$dp_{50} = 848.3\ \mu m$. The surface-volume diameter dp_{sv} is broadly similar.

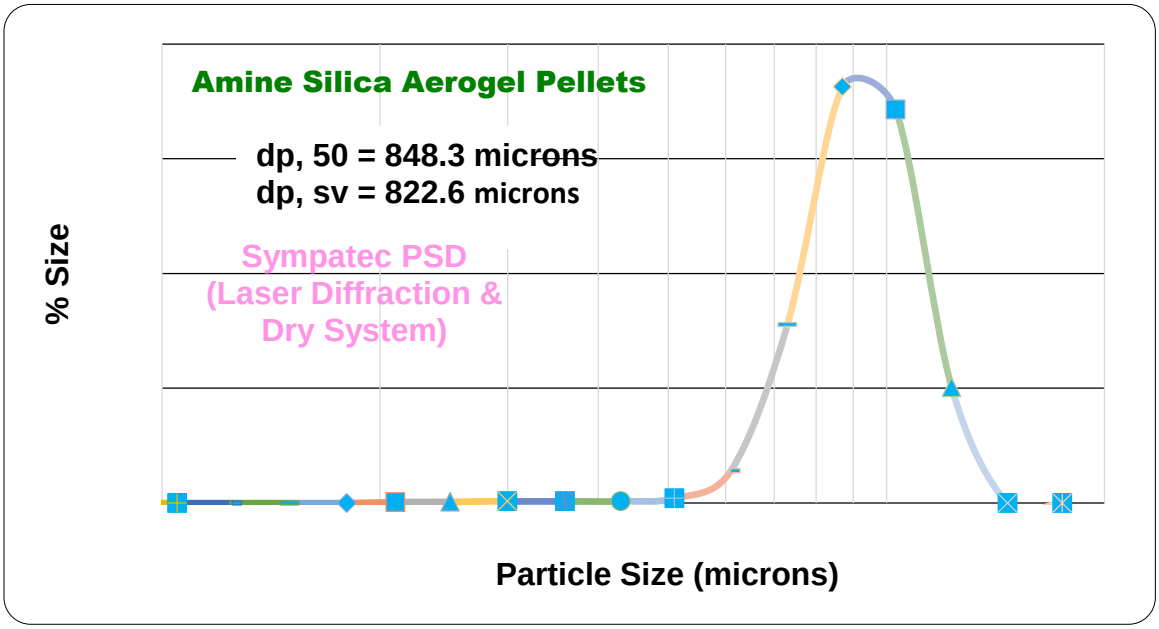

Figure 52. Particle size distributions (microns) of aerogel pellets.

Fluidization velocity: Figure 53 shows the pressure drop (psi/ft, left abscissa) and bed expansion (bed height percentage of resting height) as a function of the superficial gas velocity (ft/s) for both ascending and descending velocity sweeps (Produced by PSRI, Chicago Il). The theoretical pressure drop is given by the Ergun equation prediction indicated by the dashed line in Figure 53[8]. Consistent with standard theory and practice, increasing gas velocity from zero produces a quasi

linear increase in pressure, up to the minimum fluidization velocity $U_{mf} = 1.141$ ft/s, upon which bubbles and then slugging appear, while the pressure drop across the bed peaks and begins declining slightly. Reducing gas velocity from above the fluidization point yeilds similar pressure values as the asscending phase, however the peak pressure drop at the fluidization point is slightly reduced.

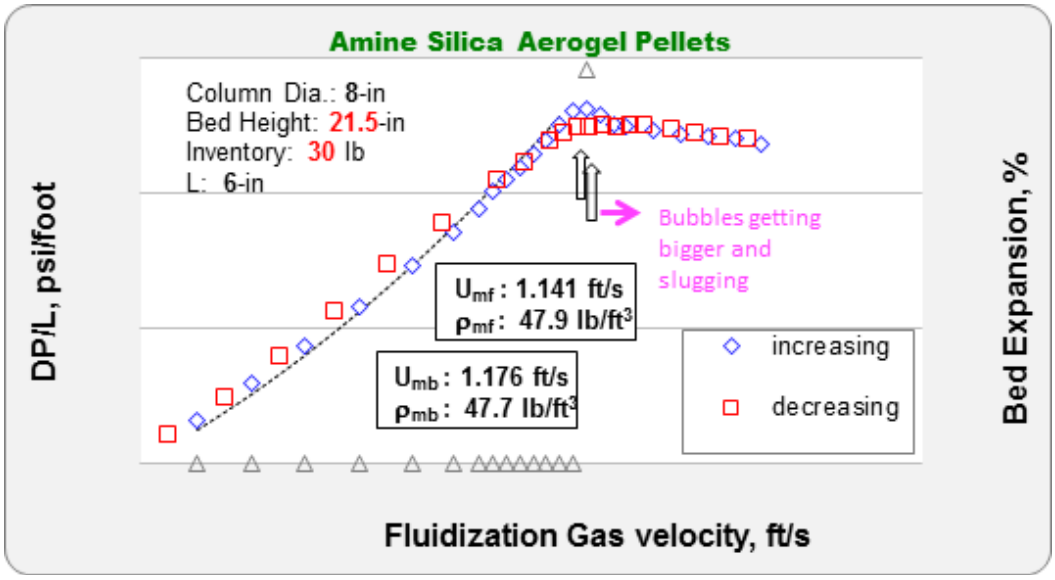

Figure 53. Particle bed pressure drop (psi/ft, left absicssa) and bed expansion percent (right abscissa) as a function of gas velocity (ft/s). Ascending and descending sequence of applied gas velocities are shown (blue diamonds, red squares, respectively), as is the theoretical Ergun equation (dashed line), and bed expansion (triangles).

Bed density and void fraction: In the non-fluidized bed, the void fraction was measured to be $\epsilon_0 = 0.4$. Bed density was measured directly from bed height relative to its loose bulk density over gas velocities from 0 to 6 ft/s in mostly half-foot increments, as shown in Figure 54. Minimum fluidization occurs slightly above 1 ft/s, and so the first fluidized bed density measured was at 1.5 ft/s. Based on many simulation scenarios of the multiphase model adsorption reactor (see below), it was determined that 1.5 ft/s was the ideal velocity for reactor function because higher velocities induced significant reaction heat that required an onerously large heat exchanger surface area for cooling. Based on these observations, void fraction of the fluidized bed was

$$\epsilon = 1 - (1 - \epsilon_0)\frac{V_0}{V_{1.5}} = 0.56, \quad (38)$$

where the volume fraction in Equation (34) is computed by the ratio of the bed densities at 1.5 ft/s over the loose bulk density $\frac{V_0}{V_{1.5}} = \frac{35}{48}$, read from Figure 54.

Heat transfer coefficent measurement: The heat transfer coefficient, also called the film coefficicient K_f was measured at three fluization velocities 2, 4.5, and 6 ft/s shown in Figure 55. Because it was determined that 1.5 ft/s gas velocity was ideal for system operation, the measured heat transfer coefficient at the nearest tested velocity, 2ft/s, was used: $K_f = 30$ BTU/(hr ft^2 °F), or rather, in SI units $K_f = 170.12$ W/(m^2 K).

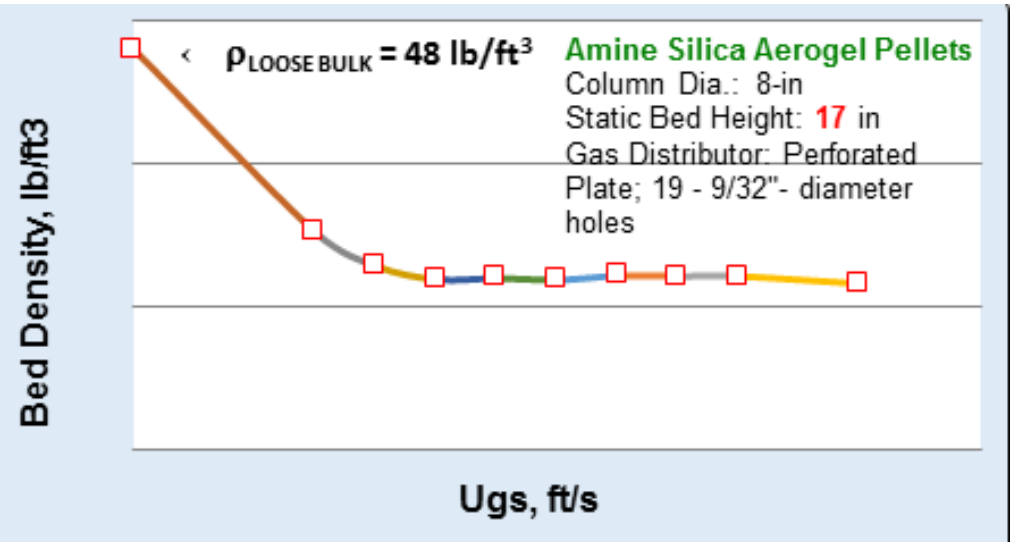

Figure 54. Bed density (lb/ft^3) as a function of gas velocity (ft/s).

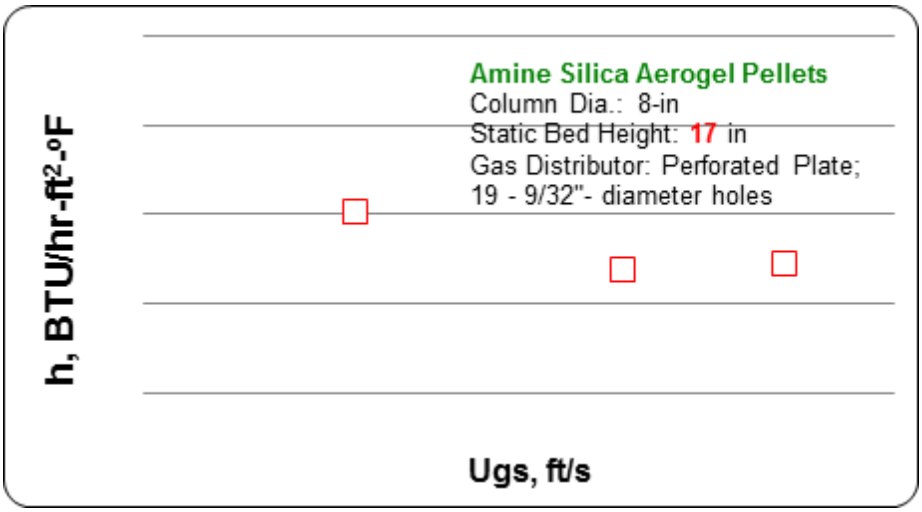

Figure 55. Heat transfer coefficient K_f(BTU/(hr ft^2 F) measured at three gas velocities (ft/s).

3.5.3.1 Sorbent Pellet Attrition Analysis

In order to determine a sorbent's suitability for use in a fluidized bed process, jet cup attrition testing was conducted to determine which mechanism is the dominant cause of sorbent attrition. Attrition of sorbent pellets is caused by two primary mechanisms: abrasion and fragmentation. Sorbents which undergo fragmentation are rapidly reduced in size and are not viable for fluidized bed CO_2 capture processes where the sorbent must withstand thousands of cycles between adsorption and regeneration. Fragmentation of sorbent particles would lead to rapid changes in the particle size distribution disrupting bed fluid dynamics and causing the loss of sorbent mass through entrainment of fine particles. Sorbents which are dominated by an abrasion attrition mechanism may be suitable for use in a fluidized bed environment.

The attrition index (AI) was lower for pelletized sorbent relative to a reference of FCC catalyst in three out of four measured attrition indices. The attrition index was higher for < 20 micron particles at 300 ft/s than the reference fluidized catalytic cracker sample. The AI index indicate that the

sorbent is suitable for a fluidized bed process where it will not only encounter mechanical attrition from the fluidized bed at relatively low velocities, but it will also be subject to high gas velocity cyclones needed to separate the sorbent from the gas flow. Results of the attrition testing are shown Table 17.

Table 17. Particle size distribution of baseline and attrited sorbent samples

Sample ID	Inventory g	Jet Velocity ft/s	Test Duration hr	AI (20)	AI (44)
Aspen Aerogel Sorbent (350 - 500 μm)	35 35	300 450	2 3	1.82 4.44	2.13 6.16
CQA12 pellets KD 240-24-5C (Test done in 2015)	52 52	300 300	2 2	3.50 0.07	5.80 0.31
GE-06 (Test done in 2013)	57 57	300 450	2 3	6.57 16.15	9.18 27.31
PSRI Std FCC Eq. (for Reference Purpose)	100 100	300 450	2 3	0.9 11.6	4.5 21.3

The test results show that the sorbent will be able to survive many cycles in a multiple fluidized bed system without excessive degradation from mechanical attrition. A small shift in particle size distribution with an increase in fine particles was observed as a result of abrasion during the 300 and 450 ft/s attrition tests. The initial particle size distributions as well as the post testing samples are shown in Figure 56. It should also be noted that these tests are intended to induce attrition and actual process conditions will be less severe.

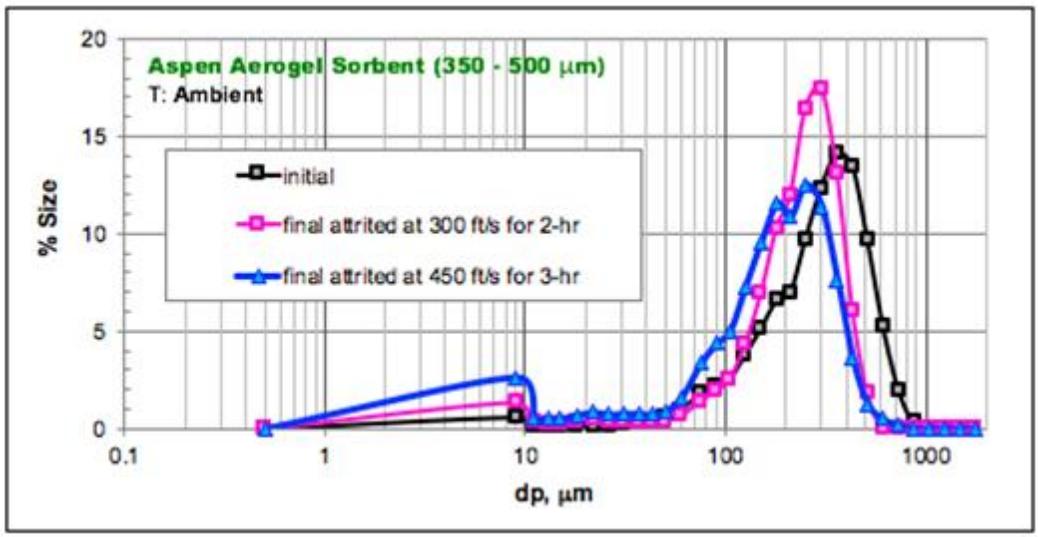

Figure 56. Particle size distribution of baseline and attrited sorbent samples.

Further bench scale testing would be needed to determine an exact attrition rate under practical process conditions and determine whether mechanical attrition or chemical deactivation would be the limiting factor for the sorbent. However, these initial attrition tests indicated that sorbent is sufficiently robust to warrant further examination and testing in a practical setting such as bench scale or small pilot testing.

3.5.3.2 Heat of Reaction of Sorbent Pellets

The heat of reaction, measured by DSC-TGA, was calculated to be $h = 52$ kJ/mol CO_2 under dry CO_2 conditions by Hazen Research. The thermograph is shown in Figure 57. Tests were also performed to determine a heat of reaction with water vapor. However, this test is typically very challenging as water vapor can easily condense in the small capillary lines in the TGA-DSC instrumentation leading to erroneous results. During testing, results were significantly lower than expected indicating the probability of water condensing on cold spots of the gas transport lines. For this reason, the results of the dry CO_2 experiments were used to determine the heat of reaction with CO_2, and the value of 40 kJ/mol H_2O was used for the heat of reaction with moisture as this is the latent heat of vaporization of water and has been reported in similar literature[13]. The results of the dry CO_2 test experiment and data corresponding to the thermograph in Figure 57 are reported in Table 18.

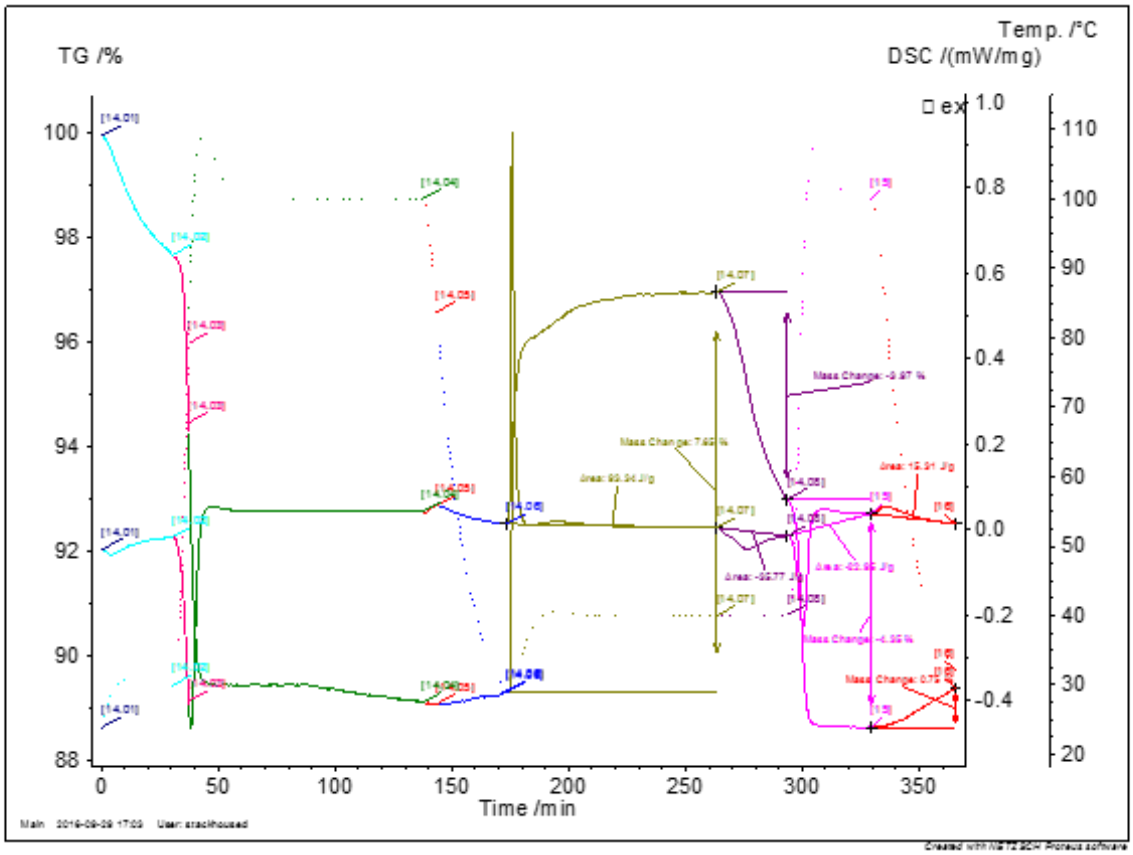

Figure 57. Dry CO_2 thermograph.

Table 18. Dry CO_2 heat of reaction sorbent pellet test results.

Sample	Temp	Action	Step	Atmosphere	Mass change	Enthalpy	
	°C		#		% wt	J/g	
Aspen Pellets	40	Isothermal	7	Dry CO2	7.65	93.3	Exothermic
	40	Isothermal	8	Dry N2	-3.97	-35.8	Endothermic
	100	Heating/Isothermal	9, 10	Dry N2	-4.35	-23.0	Endothermic

	40	Cooling/Isothermal	11, 12	Dry N2	0.75	15.3	Exothermic
				Net Values	0.08	49.9	

3.5.4 Sorbent CO_2 Langmuir Isotherm Analysis and Theoretical Capture Bounds

The isotherm data and Langmuir curve fits are shown in Figure 58. The curve fits with the supplemented data and recorded data are both shown. Over all temperatures, both supplemented and recorded curves are broadly similar, but at low temperatures (~40˚C) present in the reactor vessel, the supplemented fits that include the derived data point are slightly higher and more concave. Over the range of temperatures, the asymptotic values $\rho_{s,max}$ are reduced for increased temperature. At the higher temperatures of 110˚C and 120˚C, the curves are adequate but appear to yield inaccurate asymptotes (see below for more on this).

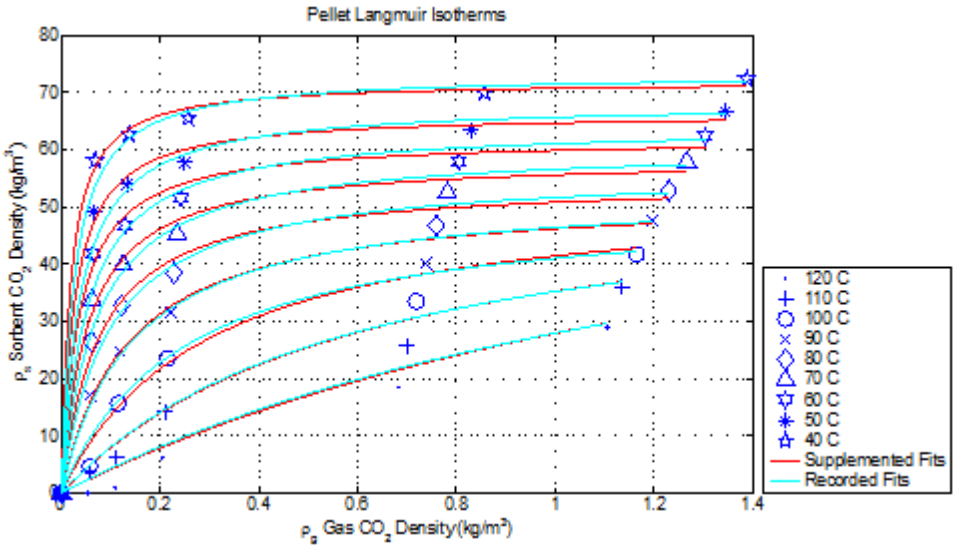

Figure 58. Langmuir isotherm data for 9 temperatures from 40 C to 120 C and Langmuir curves fit using supplemented data and recorded data (see legend).

The supplemented data Langmuir fits shown in Figure 58 yielded parameter estimates for $K_{eq}(T)$ and $\rho_{s,max}(T)$ over the nine temperatures from 40˚ to 120˚C (10˚C increments). Figure 59 (left panel) shows these point estimates over the full range of experimental temperatures for both the supplemented data and recorded data. As suggested, the equilibrium constants were estimated to be higher for the supplemented data relative to the recorded data, particularly for lower temperatures. Both data sets also exhibited a decaying exponential relationship. The supplemented equilibrium fit was:

$$K_{eq}(T) = K_{eq,0}e^{-\frac{T}{T_0}} = 265.58\, e^{-\frac{T}{25.76}}. \qquad (39)$$

The saturation constants $\rho_{s,max}(T)$ are also shown in Figure 59 (right panel). There is a clear linear declining relationship for lower temperatures. However, because the aforementioned poor modeling fits at high temperatures, saturation estimates sharply rise for high temperatures 110˚C and 120˚ these estimates appear spurious. Moreover, the temperatures from 40˚C to 100˚C make up the operating range of the adsorber and desorber reactors. Hence, linear fits were performed

only on this lower temperature range and the data points at 110˚C and 120˚C were excluded. The linear supplemented saturation fit is:

$$\rho_{s,max}(T) = -0.7894\,T + 149.89. \quad (40)$$

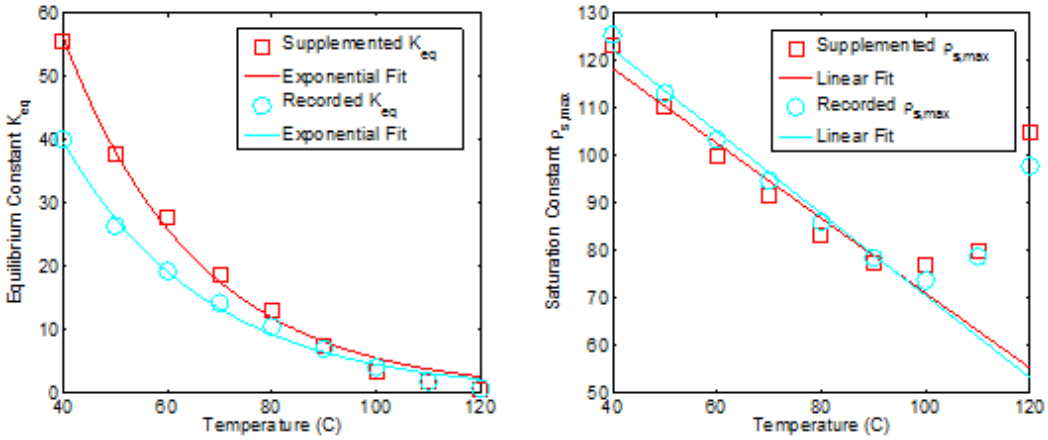

Figure 59. Left: Langmuir equilibrium constant data $K_{eq}(T)$ as function of experimental temperature values for both supplemented and recorded data. Also shown are exponential fits to these data. Right: $\rho_{s,max}(T)$ data and fitted lines for both supplemented and recorded data.

The parameter fits generated a Langmuir surface as a function of both CO_2 partial pressure p and temperature T: $LS(p,T)$. The level curves of this surface $LS(p,T)$ are shown in Figure 60 (left panel). This surface enables the computation of a theoretical upper bound on CO_2 capture proportion as a function of the hot desorber/regeneration vessel temperature and the cold adsorber vessel temperature, shown in Figure 60 (right panel). Note that in Figure 60 right panel shows that the sorbent pellets can achieve 90% or better capture for adsorber and desorber reactor temperatures at or near the point $(T_{cold}, T_{hot}) = (40,100)$ specified by the design criteria. Note also that the level lines exhibited slopes that are greater than 1:1 lines, which indicates that for lower cold temperatures that additional gains in capture proportions can be achieved for the same 60-°C temperature swing (blue dashed line in Figure 60 right panel). That is, a T_{cold} smaller than 40˚C may improve capture proportion for the same 60-°C temperature swing.

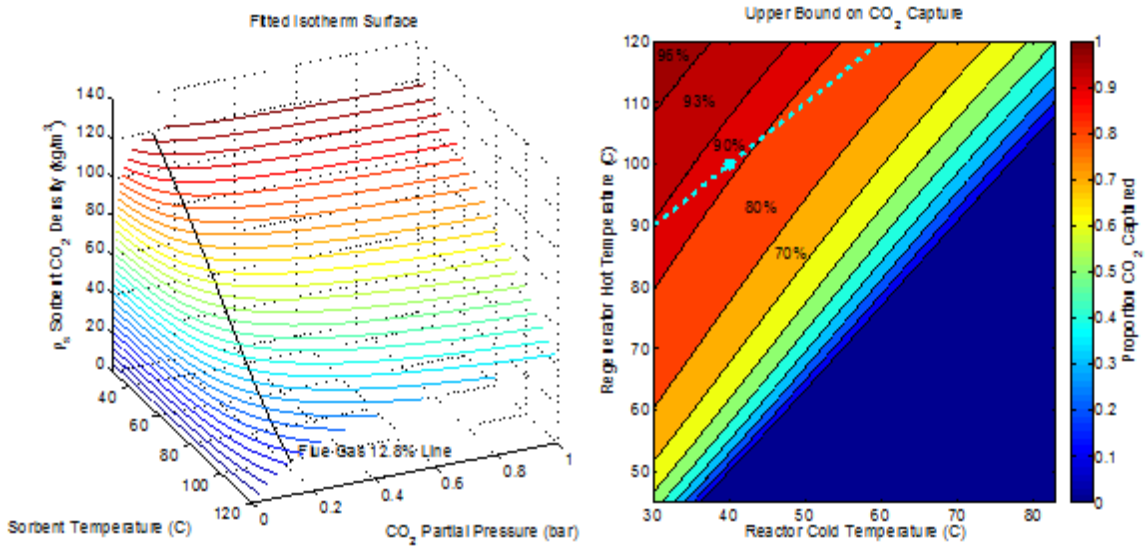

Figure 60. The Lanmuir pressure-temperature surface function for sorbent CO_2 mass density. Right: the theoretical upper bound on CO_2 capture rate as a function of cold and hot temperature. A few regions' capture rate are indicated, bordered by black isocapture lines, which have a slope greater than 1:1 lines. An example 1:1 line (light blue) that passes through the point (40,100) is shown.

In practice, the adsorber and desorber reactors will not reach the theoretical *maximum* capture bound. In the adsorber, the failure to reach the bound could be due to a number of factors. Principal factors include the following: (a) slow reaction timescales that occur at very low partial pressures on the order of $p \sim 0.0128$–a timescale is too slow when it is longer than the average particle residence time in the adsorber reactor; (b) inadequate thermal control, where the required heat exchanger surface area is too large for the vessel size.

3.5.5 Adsorption Reaction Kinematics: Linear Systems Timescale Analysis

The temperature change dynamics of the CO_2 mass fraction in the isobar experiments, over the 9 holding temperatures are shown in Figure 61. The graphs are excised six-minute time sections of the mass fraction (left abscissa) and temperature transitions (right abscissa). The initial temperature started at $T(0)$ = 130˚C and transitioned to 120 ˚C (upper left panel) followed by a 60 hold time (not shown), resulting in a rapid increase in the mass fraction $\theta(t)$. Subsequent temperature drops are shown from left to right descending.

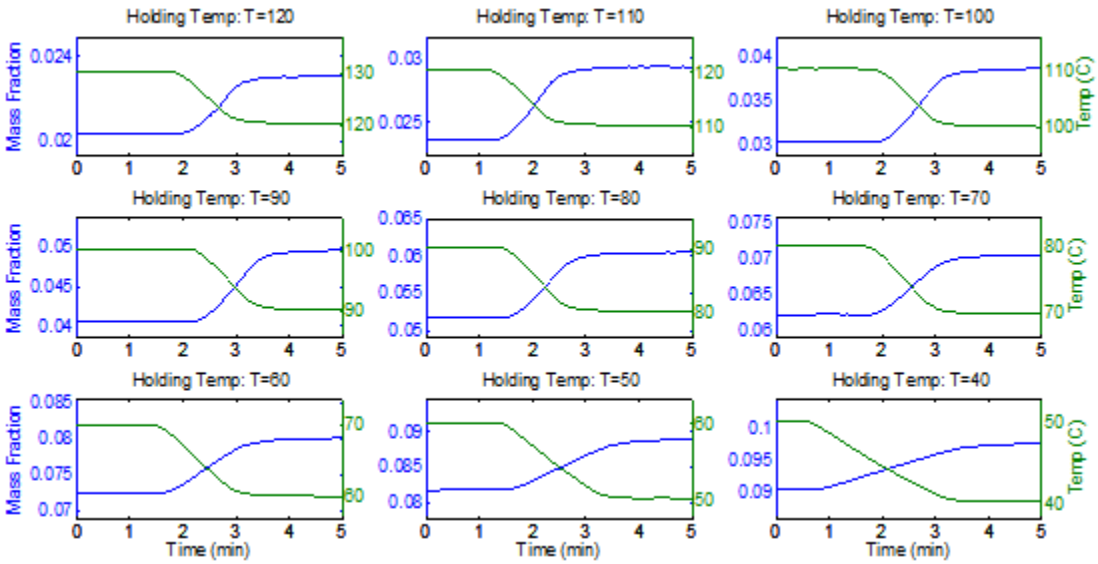

Figure 61. Isobar experiments with 0.15 atm CO_2 partial pressure over 9 descending holding temperatures from 120C to 40C (green line) and the resulting amine sorbent CO_2 mass fraction (blue line)[9].

Notably, for each of the nine temperature changes, the resulting mass fraction changes are seemingly in lockstep with temperature, and when the temperature reaches the holding temp, the mass fraction ostensibly stops changing. Over the subsequent 60-minute holding time window (not shown in Figure 61), the mass fraction does continue to slowly rise a small amount (not shown). However, in each of the 9 holding temperatures, 93-98% of the mass fraction gain had occurred immediately when the temperature leveled off to its holding temperature, and critically 97% for the 40˚C set point (98.99% 97.46%, 95.72%, 93.62%, 94.64%, 95.44%, 95.72%, 96.57%, 96.95%, 97.25%, for holding temperatures 120-40C, respectively). This secondary slow rise in mass fraction is likely from both ultra-slow kinetics near equilibrium, and a small number of amine binding sites that are either diffusion-limited, or thermally-insulated, and thus take considerably longer for CO_2 to become available to the binding sites or to cool down.

Based on isobar experiments depicted in Figure 61, k_a and k_d are deduced to be very fast, with reaction timescales on the order of seconds. However, visual inspection may not detect slow dynamic changes. To confirm the visual analysis, a rigorous linear systems analysis of the temperature-mass fraction dynamics is needed. As detailed in the Methods, empirical transfer functions $H(s)$ were computed for the temperature change and 60-minute holding periods for each of the nine temperature conditions. Based on inspection, it was determined that a proportional-integrator (PI) linear model, with transfer function

$$\widehat{H}(s) = A + \frac{B}{s}, \qquad (41)$$

for constants A and B, was a very good approximation to the empirical transfer functions. For each of the nine temperature conditions, the PI transfer function the parameters were fit to the empirical transfer functions as shown in Figure 62.

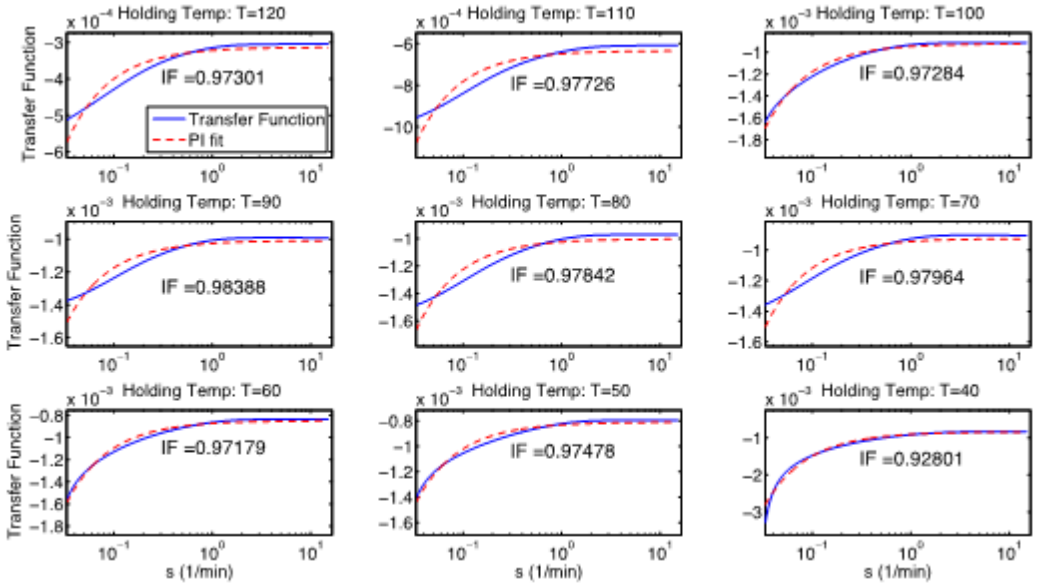

Figure 62. Empirical transfer functions H(s) (blue line) and fitted PI transfer functions $\hat{H}$(s (dashed red line)) over the nine sequential temperature-change epochs from 120 to 40˚C, and associated influence factor IF (Equation 7).

The fitted PI transfer function parameters give information about kinetics of the adsorption process: the magnitude of the constant A represents the degree or instantaneous response of the sorbent CO_2 mass fraction $\theta(t)$ to the *current* temperature $T(t)$ while the constant B represents the relative amount of slow-timescale response to a time-average of the *past* temperatures on the current mass fraction. The relative magnitude of A to B is given by the influence fraction IF = $|A|/(|A| + |B|)$. For each of the nine temperature transitions, the IF values were between in the ranges of 0.927 to 0.983, as listed in Figure 62, meaning that mass fraction is overwhelmingly accounted for by the current temperature and only weakly by long-timescale past temperatures. This linear systems analysis is consistent with visual inspection that the adsorption reaction has incredibly fast kinetics, on the order of seconds or faster, so fast that the conclusion is limited by the sampling frequency. Therefore, as per best practices, the kinetic rate of desorption is conservatively estimated to be the Nyquist frequency, defined as half the sampling rate of the data (15 per minute), hence:

$$k_d = \frac{15}{60} = 0.25 \ (\text{sec}^{-1}). \qquad (42)$$

The adsorption constant is given then $k_a = K_{eq}(T)k_d \ (m^3 kg^{-1}\text{sec}^{-1})$.

3.5.6 Effective Heat Capacity of Aerogel Pellets

To investigate the role of aerogel pellet heat capacity, a heat transfer model was constructed to investigate to what extent the very low heat conductance of silica aerogel pellet material $\kappa \sim 10^{-2}$– one of the lowest measured conductance values in the world–impacts the pellet surface temperature changes that control the favorability of the adsorption-desorption reaction. Of principal interest is to determine if; 1) the heat exchanger energy transfer to aerogel pellets, over the relevant timescale τ of pellet-heat exchanger contact times produces an isothermal pellet, or, alternatively, 2) the

thermal effects are limited to the outer surface of the pellet. Particle contact times in fluidized beds are reported to be on the order of seconds (τ~1 s;)[10]. If during these timescales the pellet becomes near isothermal, then temperature change is limited by the material heat capacity of aerogel pellet material, which is measured to be 860 J/(kg K). If, however, there is weak thermal penetrance, then the heat transfer ΔJ is not distributed evenly through the pellet depth ℓ, and should result in a greater change in the surface temperature $\Delta T_{surface}$ than otherwise, which will result in an lower effective heat capacity c_{eff} relative to the measured (isothermal) heat capacity ($c_{eff} < 860$).

To investigate this question, temperature distributions $T(x,t)$ were computed for a volume of material with aerogel-level heat conductance $\kappa = 10^{-2}$, with material depth $x = \ell = 500\ \mu m$, which is comparable to the mean measured pellet radius (see Figure 52). This volume was contacted by a heat exchanger at $x = 0$, and underwent an alternating cycle of 60-°C holding temperature swings between 40°C and 100°C. The holding temperature had duration of τ and timescales ranging from sub second to 100-second were investigated. Figure 63 (left panel) shows the solution $T(x,t)$ over five temperature cycles for $\tau = 1$, which shows a thermal penetrance for only the outside 100 microns of the volume ($0 \leq x \lesssim 100\ \mu m$), with large temperature deviations on the outside surface ($x = 0$) but leaving the remainder of the material effectively unperturbed at the mean holding temperature ~70°C.

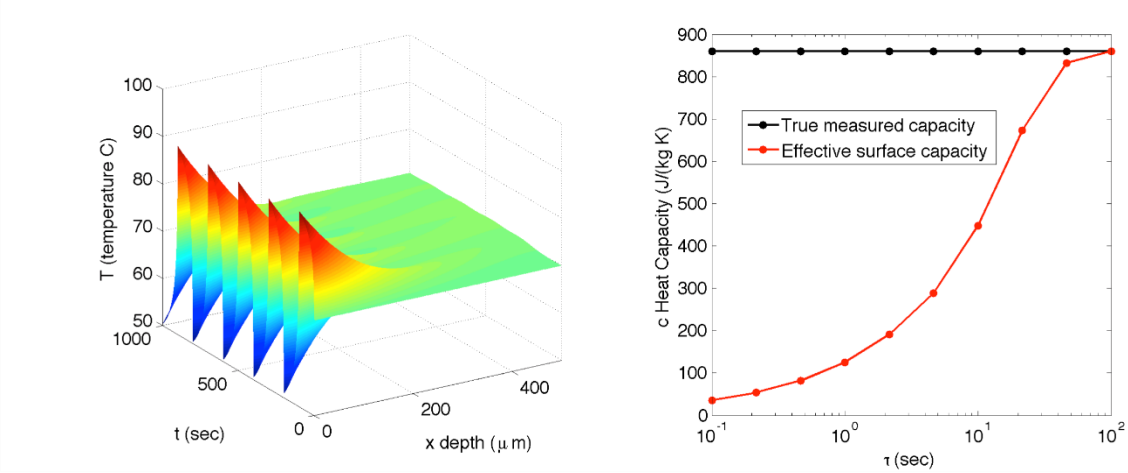

Figure 63. Left: Temperature solution T(x,t) to Equations (34-35) in response to alternating 1-second duration hot-cold heat-exchanger contact for a volume of material 500 microns in depth. Right: effective heat capacity (Equation 33).

The effective heat capacity was computed to be $c_{eff} = \frac{\Delta J}{\rho_a \ell \Delta T_{surface}}$ (see Equation 9) as a function of τ-cycle time is shown in Figure 63 (right panel). For short τ-cycles on the order of a second or less, the effective heat capacity was much smaller than the measured capacity, on the order of 14.5% for the one-second cycle, and 51% at 10 seconds. By $\tau = 100$ seconds of exposure, the effective capacity reached pairity with the measured (isothermal) capacity, meaning the entire thermal volume was in equilibirum.

Because (i) contact time and particle exchange from the heat exchanger surface is the primary driver of heat transfer in the fluidized bed, and (ii) the pellet surface temperature is the primary

driver of favorable adsorption and desorption reactions for CO_2 capture applications, *it is concluded that the measured heat capacity of the aerogel pellets overestimates the required energy to drive the necessary temperature changes for adsorbtion-desorption reactions*. However, the model used in this analysis does not provide explicit prescriptions because it posesses a simplified geometry. Moreover, the measured heat transfer coefficent K_f for the heat exchanger-fluidized bed interface is based on existing data of the entire turbulent mixing fluidized bed system and not a single pellet-heat exchanger interface, although the coefficient should be in the same order of magnitude.

Therefore, a conservative heat capactiy estimate was taken for the aerogel pellets: $c = 500$ J/(kg K). This effective heat capacity is an intermediate value, less than the measured value of 860 J/(kg K), but much greater than the effective heat capacity results of Figure 63 typical of 1-2 second contact times that a pellet would experience within the fluidized bed.

3.5.7 Multiphase Adsorber Breakthrough Model and Desorber Results

3.5.7.1 Parameter values for multiphase model:

The following is a listing of model parameters, some of which are summaries of results discussed in previous Sections.

Bed depth: $L = 10$ meters, and $L_b = 5$, $L_t = 5$ meters.

Void fraction: $\epsilon = 0.56$.

Advection velocities: $u_{tot} = 0.808$ m/sec, is the total or relative velocity of gas and solids, where $u_g + u_s = u_{tot}$, and $u_g = 0.7887\ m/s$, $u_s = 0.0194\ m/s$.

Turbulent dispersion constants: D_g and D_s, were derived from Peclet numbers based on meta analysis survey of mixing parameters[11,12].

$$Pe_s = 71.86(1-\epsilon)^{0.67}Re^{0.23} = 107.6328, \quad Pe_g = 10, \quad (43)$$

where $Re = 47.17$ is the Reynolds number. The nondimensional Peclet numbers give the ratio of the advective velocity times characteristic length scale of the reactor over the diffusivity. Because we know u_{rel} and L, the diffusivity parameters are

$$D_s = \frac{u_{tot}L}{Pe_s} = 0.0751\ \frac{m^2}{s}, \quad (44)$$

$$D_g = \frac{u_{tot}L}{Pe_g} = 0.8081\ \frac{m^2}{s}. \quad (45)$$

Reaction kinetics parameters: $k_d = 0.25\ (\text{sec}^{-1})$,

$$K_{eq}(T) = K_{eq,0}e^{-\frac{T}{T_0}} = 265.58\, e^{-\frac{T}{25.76}}\ \frac{m^3}{kg}, \quad (46)$$

$$\rho_{s,max}(T) = -0.7894\,T + 149.89\ kg/m^3. \quad (47)$$

Thermal parameters: Cooling water $T_{ahe} = 15$°C; Heat transfer coefficient: $K_f = 170.12$ W/(m^2 K); heat exchange surface area per cubic meter of adsorber bed: $a = 21.75\ m^2$; apparent pellet density: $\rho_a = 1147\ kg/m^3$; $c = 500\ J/(kg\ K)$; heat of reaction: $h = 52\frac{kJ}{mol}$.

Adsorber simulation results: Figure 64 shows the equilibrium solution of Equations (14-23). Gas flows left to right through the bed and sorbent particles flow leftward due to advection in the lower

bed. The CO_2 gas density (panel A) exhibits a decreasing trend from $z = 0$, beginning on the left where 12.8% CO_2 rich flue gas enters and declines till about the 2.5-meter bed depth, at which point the gas density rises slightly as z approaches the hot sorbent input port at $z = 5$. The increase in gas density at the input port is a result of the secondary desorption of CO_2 from the newly injected hot sorbent. Beyond $z = 5$, the hot sorbent, as it is mixed and cooled, re-adsorbs much of the released gas. This process is also observed in the CO_2 gas flux (panel B), where the initial rich flue gas flux at $z = 0$ rapidly declines till $z = 5$, where hot sorbent desorption gas release causes a secondary peak. The gas flux that decays further above the input port, resulting in a low gas exit flux that was 90.07% less than the input gas flux.

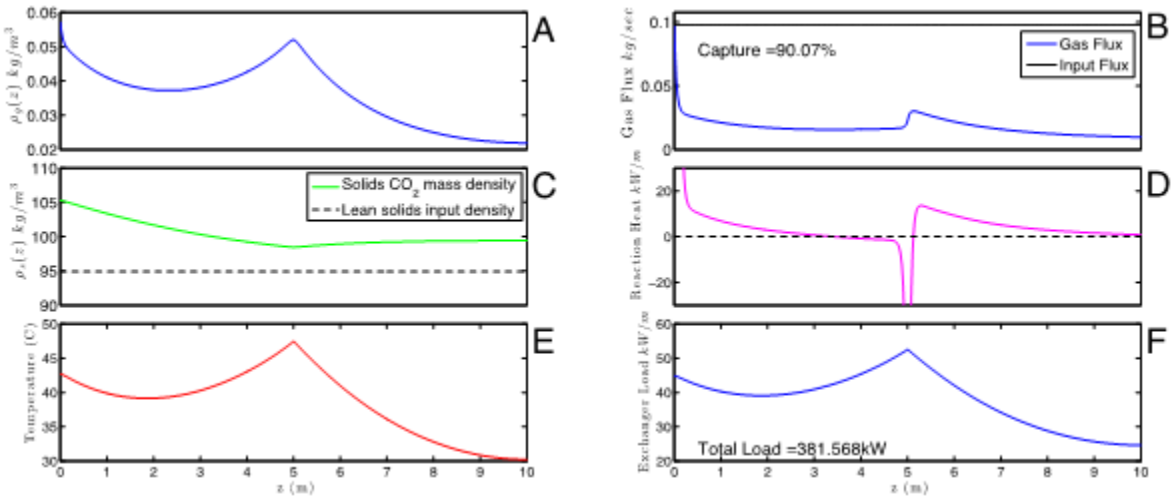

Figure 64. Equilibrium solution of the thermally coupled multiphase reaction-advection-diffusion equation along the 10-meter fluidized bed with sorbent input at z=5 m. A: gas CO_2 density. B: CO_2 gas flux. C: solids CO_2. D: Reaction heat (exothermic) from solids. E: Solids temperature. F: Heat transfer load from cooling water of heat exchanger to solids.

The solid sorbent CO_2 density shown in Figure 64C exhibits a similar decreasing shape, where lean particles flowed from the right to left from the input at $z = 5$ to left exit at $z = 0$. Turbulent diffusive mixing occurred throughout the entire bed in addition to advective flux that occurs only in the lower section of the bed ($z < 5$). The solids CO_2 density slightly rises from $z = 5$ through to the top of the bed, due to the re-adsorption of hot-solids-desorption gas release from the solids input.

The reaction heat shown in Figure 64 reveals the high exothermic rate of reaction near $z = 0$ where rich flue gas contacted the exiting sorbent, but the rate declined rapidly as adsorption reduces CO_2 partial pressure. At the hot-sorbent input port ($z = 5$) the aforementioned hot-desorption release caused a spatially localized endothermic (negative) reaction that served to cool the hot sorbent. The released gas mixed and underwent advection to the left, where the gas was readsorbed producing a secondary exothermic reaction in the top of the bed ($z > 5$) until most of the gas was readsorbed.

The combined coupling of three processes resulted in a spatial distribution of solids temperature $T(z, t)$ shown in Figure 64E: (a) exothermic-endothermic adsorption-desorption reactions, (b) hot

input sorbent, and (c) heat exchanger cooling. Naturally, the sorbent particle temperature was highest at $z = 0$, where rich flue gas first mixed with sorbent, and there was another secondary peak at the hot sorbent input port.

Without the cooling input of the heat exchanger surface pipes distributed through the bed, the solids temperature $T(z,t)$ would be much higher and the adsorption reaction would self-limit, resulting in an overall capture rate well below 90%. The distributed heat exchanger load is shown in Figure 64F. The heat exchanger load exhibited two distinct peaks. Naturally, there was one at gas input and one at hot sorbent input.

The reactor equilibrium solution shown in Figure 64 was the result many simulations where the heat exchange surface area a was titrated upward until the adsorption reaction was sufficiently favored and 90% capture was achieved. The optimal surface area was determined to be a =21.7 square meters of contacting area per cubic meter of fluidized sorbent bed.

Other critical parameters that required optimization were the fluidization velocities u_g and u_s and the length of the top reactor section L_t where the hot-sorbent-desorption-then-readsorption reaction occurred. A relatively low gas velocity (1.5 ft/s) near the minimum fluidization velocity was selected because higher velocities required higher counter current sorbent velocities to achieve 90% capture. When investigated, these higher sorbent velocities introduced both greater hot sorbent flux and reaction heat, resulting in larger required heat exchanger surface areas. The required surface areas were far beyond what could be realistically placed in a reactor vessel. The top reactor section L_t parameter also required careful tuning: too short and the released gas readsorption reaction could not be completed before the gas left the top of the vessel, causing CO_2 gas breakthrough before achieving 90% capture. If L_t were set too long, the sorbent mix out of solids from the top of the bed to the lower bed would take excessively long, resulting in significantly longer particle residence times. The long-waiting stagnant particles in the top of the vessel would become increasingly loaded. These excessively loaded particles could not adsorb any more CO_2, and CO_2 gas would breakthrough and exit the top of the bed vessel without achieving 90% capture.

The multiphase adsorber model gives a powerful insight into realistic reactor function. The results show that in order to achieve 90% capture, the upper section of the vessel had to be cooled far below the theoretically predicted 90%-capture target temperatures $T_{cold} = 40^{\circ}\text{C}, T_{hot} = 100^{\circ}\text{C}$ derived from the kinetics analysis (see Figure 60). The sorbent temperature $T(z,t)$ varied across the bed length, with an average temperature $avg\big(T(z,t)\big) = \frac{1}{L}\int_0^L T\, dz =$ 38.57˚C, which is very near the target adsorber cold temperature $T_{cold} = 40^{\circ}\text{C}$. However, the upper bed, due to the aforementioned slow mix out and overloading limitations that can cause breakthrough, required much greater cooling. Solids at the top of the bed were required to be cooled to $T(L,t) = 25^{\circ}\text{C}$! Without this low temperature, 90% capture levels could not be achieved. Note, however, the required low temperatures in the upper bed are not necessarily energetically expensive because very little reaction heat is generated in the upper bed because only a small fraction of the overall adsorption occurs there. Additionally, slow mix out limits the hot-for-cold particle exchange in the upper bed. Hence, while the effective temperature swing required of 100˚C -25˚C = 75˚C the energy requirements are not too severe. In fact, the overall energy load of the reactor vessel (per square

meter cross section) was computed to be 381.56 Kw, while the energy load of the desorber model was comparable at 387.2 kW.

Desorber results: In equilibrium ($d\bar{T}/dt = 0$, see Equations 24-37) the desorber temperature is required to be at its set point $\bar{T} = T_{hot} = 100$. This equilibrium state is attained through the correct-sized heat exchange surface area S. Solving $d\bar{T}/dt = 0$ (Equation 24) resulted in the correct value for S (Equation 30):

$$S = \frac{\dot{e}_{s,out} + \dot{e}_{g,out} - \dot{e}_{s,in}}{K_f(T_{steam} - T_{hot})} = 121.04\, m^2. \quad (48)$$

Particle Residence Times in the Adsorber and Desorber

Using the average residence time calculated from Equation (37), with bed parameters inserted, the average residence time is

$$t_{res\,time} = r(L_b) = \frac{L_b}{u_s} + \left(\frac{L_t}{u_s} - \frac{D_s}{u_s^2}\right)\left(1 - e^{-Pe_{L_b}}\right) = 300.01\, s\ (5.00\, min). \quad (49)$$

This residence time was used for both the adsorber and the desorber for a total roundtrip time of 10 minutes. For the purposes of this model, the transfer time between adsorber and desorber is considered small and negligible compared with the required residence times which dominate the time requirements.

3.6 Techno-Economic Assessment of AFA sorbent

The ultimate goal of the TEA is to determine a cost estimate for the technology being evaluated. The basis for the costing analysis is described in section 2.7 of the NETL baseline report[2] and was followed to provide the cost estimates for this solid sorbent technology. This report details costs of financing, land, geographic location, and all other variables necessary to determine costs on an equivalent basis for various post combustion CO_2 capture technologies. The guidance is lengthy and referenced rather than reproduced.

Using the NETL report guidance, the designed CO_2 capture system was analyzed on a cost basis to determine relative cost estimates between the benchmark MEA system and the AFA sorbent system. It should be noted that although the MEA system is a benchmark system, it has not been demonstrated at a 550 MWe scale and the costs should be regarded as estimates only. Costs for the CO_2 capture system were scaled based on reported data of other similar systems[13]. Due to the inherent uncertainty of costing a system which has never been built before, these figures are considered to be very rough estimates only and should be viewed as such. However, due to the simple mild steel construction of the solid sorbent vessels as opposed to the corrosion resistant materials required for the solvent system, it is expected that the overall cost of the vessels on an equivalent volume basis will be substantially less expensive for a solid system rather than a solvent system. Also, a contingency of 30% was used for the CO_2 capture system even though large bench or pilot studies have not been performed for this particular sorbent, no full scale system would ever be built without such studies. Furthermore, solid sorbents have been tested at a pilot scale[13]. This contingency factor is in line with the NETL guidelines[2] and was used for this analysis. Base power plant items and components were scaled linearly with a factor using the amount of coal required

in mass per hour for the solid sorbent CO_2 capture power plant divided by the listed coal consumption for the MEA base case 12B plant listed in the NETL baseline study[2]. A complete assessment of capital costs can be found in Appendix 1.

3.6.1 Plant Process System Model Comparison

The sorbent-based model system detailed in the previous sections was integrated into the model plant process system and compared to the benchmark MEA capture system from the NETL report[2]. The flue gas flow rate that was optimized for adsorber capture function was then scaled to match flue gas production from the plant model, provide requisite parasitic steam to the adsorber, parasitic electricity for fans to meet flue gas pressurization to meet fluidized bed pressure drops in the adsorber-desorber units, parasitic electricity for CO_2 compression for storage, and other miscellaneous loads required for plant operation. As stated previously, a let-down turbine was required to achieve safe steam temperatures in the desorber unit. The power generation from the let-down turbine offset a significant amount of the aforementioned parasitic electrical loads, as shown in Table 19. Parasitic power loads were adjusted linearly based upon an increase in the coal burn from the MEA to sorbent capture system. A flue gas polishing scrubber was used to reduce SO_2 concentration to 10 ppmv. This was scaled from the ADA-ES report which required 1-2 ppmv SO_2 concentrations because the sorbent investigated did not use Aspen Aerogel's proprietary SO_2 resistant coating[13].

Table 19. Power plant performance adapted from NETL and ADA-ES reports[2,13].

Plant Performance			**NETL 12B Capture Case MEA**		**Sorbent Capture**
Gross Power Output			641,276		748,427
Parasitic Power		Unit			
	Coal Handling and Conveying	kWe	480		565
	Pulverizers	kWe	3,370		3,970
	Sorbent Handling and Reagent Preparation	kWe	1,070		1,261
	Ash Handling	kWe	780		919
	Primary Air Fans	kWe	1,670		1,967
	Forced Draft Fans	kWe	2,130		2,509
	Induced Draft Fans	kWe	8,350		9,837
	SCR	kWe	60		71
	Activated Carbon Injection	kWe	27		32
	Dry Sorbent Injection	kWe	108		127
	Baghouse	kWe	100		118
	Wet FGD	kWe	3,550		4,182
	Miscellaneous Balance of Plant	kWe	2,000		2,356
	Steam Turbine Auxiliaries	kWe	400		471
	Condensate Pumps	kWe	640		754

	Circulating Water Pump	kWe	7,750		9,130
	Ground Water Pumps	kWe	710		836
	Cooling Tower Fans	kWe	4,010		4,724
	Transformer Losses	kWe	2,380		2,804
	Sub Total	kWe	39,585		46,636
	Flue Gas Polishing Scrubber Unit				
	Recirculation Pump	kWe			953
	Recirculation Pump	kWe			953
	Bleep Pump	kWe			238
	Bleep Pump	kWe			238
	Sub Total	kWe			2,381
	CO2 Capture				
	Econamine FG Plus Auxiliaries	kWe	16,000		-
	Condensate Return Pump	kWe			196
	Cooling Tower Fan Power	kWe			1,509
	Circulating Water Pump	kWe			2,895
	Flue Gas Compressor	kWe			64,243
	CO2 Recycle Compressor	kWe			17,718
	Lean Sorbent Lift Compressor	kWe			17,576
	Sub Total	kWe	16,000		104,137
	CO2 Compressor				
	CO2 Compressor	kWe	35,690		69,258
	Sub Total	kWe	35,690		69,258
	Total Aux Power	kWe	91,275		220,030
	Total Parasitic Power	**kWe**	**91,275**		**198,427**
Back Pressure Turbine Generator Output		kWe	0		21,604
Net Power Output		kWe	550,001		550,001
Net Power Reduction		kWe	-		-
Boiler Efficiency		%	89%		89%
Coal HHV		Btu/lbm	11,666		11,666
Coal Flow Rate		lbm/hr	495,582		583,854
Thermal Input		kWth	1,694,348		1,996,071

	Power Plant	kWth	1,320,598		1,541,258
	CO2 Capture	kWth	373,750		454,813
Gross Output to Thermal Input to PP		%	55		55
Net Plant HHV Efficiency		%	32.5		28
Net Plant HHV Heat Rate		Btu/kWh	10,512		12,384
Capacity Factor		%	85		85
Net kWh @ 85% Capacity Factor		kWh-net	4,095,304,095		4,095,303,902
CO2 Capture Profile					
CO2 Produced		lbm/hr	1,176,915		1,386,543
CO2 Captured		lbm/hr	1,059,224		1,247,889
CO2 Emissions		lbm/hr	117,692		138,654
CO2 Removal System Parameters					-
Sorbent Regeneration Energy		Btu/lbm CO2	1,073		1,244
Total Energy Requirement		MMBtu/hr	1,275		1,552
Steam Pressure		Psia	73.5		73.5
Steam Enthalpy		Btu/lbm	1290		1,290
BP Steam Enthalpy		Btu/lbm			1,195
Heat Exchanger Steam Enthalpy		Btu/lbm			1,167
Condensate Enthalpy		Btu/lbm	273		217
Steam Extraction Flow		lbm/hr	1,253,971		1,633,564

In addition to the back pressure turbine, other performance data was interpolated or scaled from the ADA-ES pilot data report. One significant issue is the compression of the flue gas to overcome the pressure drop in the adsorber bed. This is the single largest electrical energy auxiliary for this process. An assumption of 9 psia (62 kPa) was used for the pressure drop. This was based on data from testing at Particulate Solid Research Incorporated and ADA-ES reported data[13]. The pressure drop was so high because the apparent particle density was unexpectedly high, possibly due to production challenges. Typically aerogel materials are very low density, but PSRI measured an apparent particle density of 71.76 lb/ft^3 (1150 kg/m^3) as well as high pressure drops of 0.24 psia per foot of bed depth. This large particle density and corresponding pressure drop caused significant power requirements for fans and is the most significant contributing factor to the overall energy penalty of the system. With further refinement in the production process, the lightweight aerogel substrate may be optimized with reduced binder content to potentially reduce pressure drop by up to 50%.

Another significant variance is the increased CO_2 compression load. According to the baseline report, the MEA system delivers CO_2 from the stripper at a pressure of ~2 bar[2]. In this process,

similar to the ADA process, the sorbent regenerator provides a CO_2 stream to the compressors of ~ 1 atm[13]. This requires additional compressor power when compared to the NETL baseline. However, ADA's pilot plant report does not take this into account, and underestimated the parasitic energy penalty in their report[13].

However, a second ADA report indicates approximately twice the compressor energy penalty than the NETL baseline report[13]. Work by Charles and Levy, in Appendix 2 of this report indicates an appropriate compressor model for the ADA system, and thus the Charles and Levy model was used in this report due to the greater degree of accuracy when compared with the published data from ADA's 1 MW TEA [13].

3.6.2 Water Usage

Water usage is reduced as a result of using the solid adsorbent system for several reasons. The most important reason is that adsorption takes place at ~40˚C (104˚F) rather than 30˚C (86˚F) and this substantially reduces cooling water load for the flue gas cooler. However, this is offset by increased cooling requirements for the adsorber due to the higher cooling duty requirement of the adsorber in the solids system compared with the absorber in the Cansolv™ system as well as the increased water consumption of the base power plant. Overall, water consumption is essentially the same between the two systems[2] at 23 m^3/min. An updated estimate of water usage is found in Table 20.

Table 20. Updated water consumption table for solid sorbent case.

Water Use	**Water Demand**	**Internal Recycle**	**Raw Water Withdrawal**	**Process Water Discharge**	**Raw Water Consumption**
	m3/min (gpm)	m3/min (gpm)	m3/min (gpm)	m3/min (gpm)	m3/min (gpm)
FGD Makeup	4.88 (1,288)	–	4.67 (1,234)	–	4.88 (1,288)
CO2 Drying	–	–	–	0.01 (2.2)	-0.01 (-2.2)
Capture System Makeup	0.022 (5.6)	–	0.022 (5.6)	–	0.022 (5.6)
Deaerator Vent	–	–	–	0.079 (20.2)	-0.079 (-20.2)
Condenser Makeup	**0.079 (2.23)**	**–**	**0.079 (2.23)**	**–**	**0.079 (2.23)**
BFW Makeup		–	0.079 (2.23)	–	0.079 (2.23)

	0.079 (2.23)				
Cooling Tower	**29.5 (7,800)**	**4.68 (1,234)**	**24.9 (6,566)**	**6.64 (1,754)**	**18.2 (4,812)**
FGD Dewatering	–	2.52 (664)	-2.52 (-664)	–	-2.52 (-664)
CO2 Capture Recovery	–	1.64 (435)	-1.64 (-435)	–	-1.64 (-435)
CO2 Compression KO	–	0.06 (14.6)	-0.06 (14.6)	–	-0.06 (14.6)
BFW Blowdown	–	–	–	–	–
Total	**34.5 (9,096)**	**4.68 (1,234)**	**29.67 (7,808)**	**6.73 (1776)**	**23.1 (6,102)**

After tabulating the capital costs, it was possible to calculate total overnight costs (TOC) and total as spent costs (TASC) based on the NETL methods. These values are important in determining the overall cost of electricity based upon capital expenditures since a power plant cannot be built instantaneously. The TOC and TASC costs and breakdowns are given in Table 21.

Table 21. Solid sorbent system owner's costs.

Solid Sorbent Owner's Costs		
Description	**$/1,000**	**$/kW**
Pre-Production Costs		
6 Months All Labor	$ 12,156	$22
1 Month Maintenance Materials	$ 2,090	$4
1 Month Non-fuel Consumables	$ 11,427	$21

1 Month Waste Disposal	$ 635	$1
25% of 1 Months Fuel Cost at 100% CF	$ 14,606	$27
2% of TPC	$ 42,233	$77
Total	**$ 83,147**	**$151**
Inventory Capital		
60 day supply of fuel and consumables at 100% CF	$ 51,353	$93
0.5% of TPC (spare parts)	$ 10,558	$19
Total	$ 61,911	**$113**
Other Costs		
Initial Cost for Catalyst and Chemicals	$ -	$0
Land	$ 900	$2
Other Owner's Costs	$ 316,750	$576
Financing Costs	$ 57,015	$104
Total Overnight Costs (TOC)	**$ 2,486,333**	**$4,521**
TASC Multiplier (IOU, high-risk, 35 year)		

	1.14	
Total As-Spent Cost (TASC)	**$ 2,834,420**	**$5,153**

In addition to capital costs, there are fixed and variable operating costs which are associated with operating the power plant. Again, the NETL procedures were used to determine the fixed and variable operating costs for the plant utilizing the sorbent capture system. Fixed operating costs consist of the costs of operators at the plant as well as maintenance. For the purpose of this analysis, the number of personnel and their hours is matched to those figures used in the NETL 12B case[2]. A 650 MW gross and 700 MW gross power plant typically have the same number of operating personnel and it was not possible to justify a significant difference in these costs.

The variable operating costs are largely a function of the amount of coal burned as they include consumables used to keep the power plant in environmental compliance. Variable operating costs also include disposal costs for fly ash and other byproducts. For the solid sorbent case, sorbent attrition was assumed to be 1 kg/10,000 kg or the sorbent would last for 10,000 cycles. This assumption will have to be verified in a practical pilot or bench scale device, however the jet cup attrition testing performed by PSRI indicated that the sorbent was relatively robust. However, even at this assumed lifespan, with a sorbent cost estimate of $8.29/kg, the sorbent replacement costs add a significant cost burden to plant operations. The fixed and variable operating costs as well as fuel costs are broken down in Table 22.

Table 22. Fixed and variable operating costs for the solid sorbent CO_2 capture case

Case: Solid sorbent CO2 capture	B12B	Supercritical PC w/ CO2 Capture		Cost Base:	Jun-11
Plant Size (MW, net):	550	Heat Rate-net (Btu/kWh):	10,508	Capacity Factor (%)	85
Operating and Maintenance Labor					
Operating Labor			**Operating Labor Requirements per Shift**		
Operating Labor Rate (base)	39.70	$/hr	Skilled Operator:	2	
Operating Labor Burden	30	% of base	Operator	11.3	
Labor O-H Charge Rate:	25	% of labor	Foreman	1	
			Lab Tech's etc.	2	
			Total:	**16.3**	
Fixed Operating Costs					
			Annual Cost		
			$		**$/kW-net**

	Annual Operating Labor:			$ 7,384,208		$13.43
	Maintenance Labor:			$ 12,065,150		$21.94
	Administrative & Support Labor:			$ 4,862,340		$8.84
	Property Taxes and Insurance:			$ 38,782,850		$70.51
	Total:			**$ 63,094,548**		**$114.72**
Variable Operating Costs						
				$		**$/MWh -net**
	Maintenance Material:			$ 20,345,817		$4.968
Consumables						
	Consumption					
	Initial Fill	**Per Day**	**Per Unit**	**Iniitial Fill**	**Cost ($)**	
Water (/1,000 gallons):	0	5,707	$1.67	$-	$2,964,248	$0.72
Makeup and Waste Water Treatment Chemicals (lbs):	0	27,627	$ 0.27	$ -	$ 2,295,719	$ 0.56
Limestone (ton)	0	693	$33.48	$-	$7,195,526	$1.76
Hydrated Lime (ton)	0	141	$155.00	$-	$6,798,494	$1.66
Activated Carbon (ton)	0	3.3	$1,255.00	$-	$1,265,737	$0.31
CO2 Capture System Chemicals	Proprietary				$83,264,547	$20.33
Triethylene Glycol (gal)	0	464	$6.57	$-	$946,153	$0.23
Ammonia (19% NH3, ton)	0	103	$330.00	$-	$10,536,388	$2.57
SCR Catalyst (m3)	0	0.46	$8,938.80	$-	$1,287,617	$0.31
Subtotal:				**$-**	**$116,554,429**	**$28.46**
Waste Disposal						
Fly Ash (ton)	0	694	$25.11	$-	$5,408,449	$1.32
Bottom Ash (ton)	0	137	$25.11	$-	$1,063,895	$0.26

Amine Purification Unit Waste (ton)	0	24	$-	$-	$-	$-
Thermal Reclaimer Unit Waste (ton)	0	2	$-	$-	$-	$-
Prescrubber Blowdon Waste (ton)	0	53	$-	$-	$-	$-
Subtotal:					**$6,472,345**	**$1.58**
By-Products						
Gypsum (ton)	0	95	$-	$-	$-	$-
Subtotal:				**$-**	**$-**	**$-**
Variable Operating Costs Total:				**$-**	**$144,347,990**	**$35.25**
Fuel Cost						
Illinois Number 6 (ton):	0	7,006	$68.54	$-	$148,983,257	$36.38
Fuel Total:				**$-**	**$148,983,257**	**$36.38**

The last component in the NETL cost of electricity calculation is the CO_2 transportation and storage cost. In the report, the cost is given as $11/ton of CO_2. This cost is then compiled along with the capital costs, fixed and variable operating costs, and fuel costs to determine the overall cost of electricity as shown in the procedures of the NETL report[2].

The total cost of electricity for the solid sorbent system was calculated to be $173.6/MWhr, while the MEA baseline case was listed as $142.8/MWhr. The difference in costs for the solid sorbent system are attributed driven primarily by the variable operating costs associated with sorbent attrition. However, this is also a very significant unknown as the sorbent may last a greater or lesser number of cycles in a practical environment, highlighting the need for bench scale testing under practical conditions. Additionally, the cost of the fuel increased because a substantial parasitic load was imposed on the plant as a result of the high particle density and corresponding large pressure drop across the adsorber. The capital costs were higher for the sorbent system because the increase in base plant capacity more than offset any potential savings by reducing the costs of the CO_2 capture system with a simpler design and lower costs of construction materials. The breakdown of the contributions to the cost of electricity are shown in Table 23.

Table 23. Cost of electricity breakdown for the solid sorbent capture case as well as NETL case 12B[2].

NETL's Exhibit 3-67 Case B12B COE breakdown		
Component	Value, $/MWh	Percentage
Capital	72.2	51%
Fixed	15.4	11%
Variable	14.7	10%

Fuel	30.9	22%
Total (Excluding T&S)	133.2	N/A
CO_2 T&S	9.6	7%
Total (Including T&S)	142.8	N/A
Solid Sorbent Case		
Component	Value, $/MWh	Percentage
Capital	75.3	43%
Fixed	15.4	9%
Variable	35.2	20%
Fuel	36.4	21%
Total (Excluding T&S)	162.3	N/A
CO_2 T&S	11.3	7%
Total (Including T&S)	173.6	N/A

The costs per ton of CO_2 captured as a result of this study was $80.52/ton versus $62.83/ton for the MEA Case 12B base case[2]. The cost per ton of CO_2 captured is an important metric because it indicates the market price of CO2 as an emissions credit or as a bulk commodity product for enhanced oil recovery or other applications that would be required for commercial competitiveness of the CO_2 capture technology. This is shown in Figure 65.

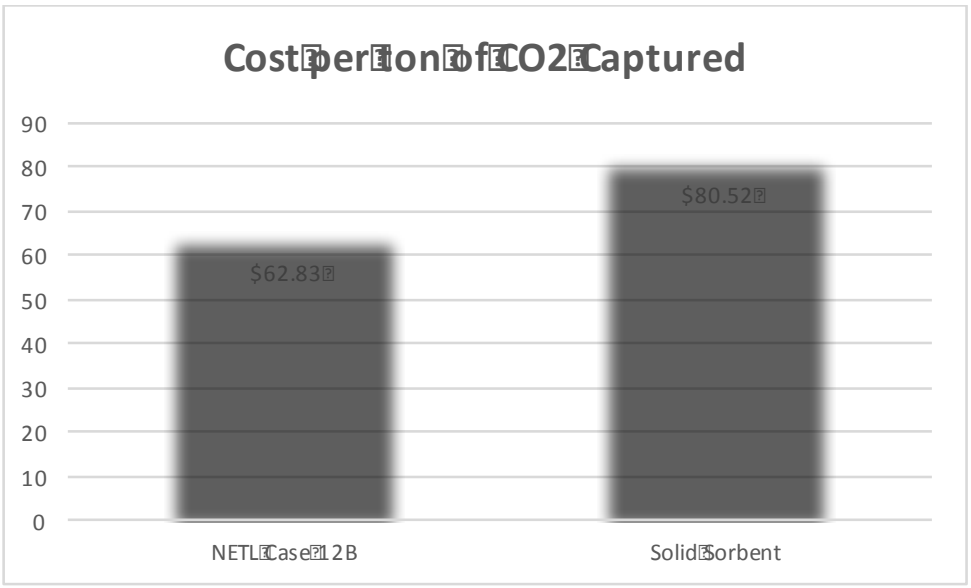

Figure 65. Cost per ton of CO_2 captured in 2011 dollars for the MEA NETL Case 12B and the aerogel solid sorbent utilized in this study.

However, this analysis was completed with the sorbent that was available understanding that it may not fully represent the complete potential of the material. As such, the performance summary of the analyzed sorbent and the NETL cases is presented in Table 24.

Table 24. Performance and cost estimates for NETL cases and Aspen Aerogel's solid sorbent CO_2 capture case[2].

Estimated performance and cost results for PC cases					
	Pulverized Coal Boiler				
	PC Subcritical		PC Supercritical		
	Case B11A	Case B11B	Case B12A	Case B12B	Solid Sorbent Case
PERFORMANCE					
Nominal CO2 Capture	0%	90%	0%	90%	90%
Capacity Factor	85%	85%	85%	85%	85%

Gross Power Output (MWe)	581	644	580	642	748
BP Turbine Output (MWe)	0	0	0	0	21.6
Auxiliary Power Requirement (MWe)	31	94	30	91	220
Net Power Output (MWe)	550	550	550	550	550
Coal Flow rate (lb/hr)	412,005	516,170	395,053	495,578	583,854
Natural Gas Flow rate (lb/hr)	N/A	N/A	N/A	N/A	N/A
HHV Thermal Input (kWt)	1,408,630	1,764,768	1,350,672	1,694,366	1,996,071
Net Plant HHV Efficiency (%)	39.00%	31.20%	40.70%	32.50%	28%
Net Plant HHV Heat Rate (Btu/kWh)	8,740	10,953	8,379	10,508	12,384
Raw Water Withdrawal, gpm	5,538	8,441	5,105	7,882	9,170
Process Water Discharge, gpm	1,137	1,920	1,059	1,813	2,120
Raw Water Consumption, gpm	4,401	6,521	4,045	6,069	7,030
CO2 Emissions (lb/MMBtu)	204	20	204	20	20
CO2 Emissions (lb/MWh-gross)	1,683	190	1,618	183	185
CO2 Emissions (lb/MWh-net)	1,779	223	1,705	214	252
SO2 Emissions (lb/MMBtu)	0.085	0.000	0.085	0.000	0.000

SO2 Emissions (lb/MWh-gross)	0.700	0.000	0.673	0.000	0.000
NOx Emissions (lb/MMBtu)	0.085	0.075	0.088	0.078	0.078
NOx Emissions (lb/MWh-gross)	0.700	0.700	0.700	0.700	0.700
PM Emissions (lb/MMBtu)	0.011	0.010	0.011	0.010	0.010
PM Emissions (lb/MWh-gross)	0.090	0.090	0.090	0.090	0.090
Hg Emissions (lb/TBtu)	0.363	0.321	0.377	0.333	0.377
Hg Emissions (lb/MWh-gross)	0.000003	0.000003	0.000003	0.000003	0.000003
Cost					
Total Plant Cost (2011$/kW)	1960	3467	2026	3524	3839
Bare Erected Cost	1582	2665	1646	2716	2925
Home Office Expenses	158	257	165	263	285
Project Contingency	220	427	216	430	454
Process Contingency	0	118	0	115	177
Total Overnight Cost (2011$/MM)	1336	2346	1379	2384	2486
Total Overnight Cost (2011$/kW)	2429	4267	2507	4333	4521
Owner's Costs	469	800	480	809	945
Total As-Spent Cost (2011$/kW)	2755	4865	2842	4940	5153
COE ($/MWh) (excluding T&S)	82.1	133.5	82.3	133.2	162.3
Capital Costs	37.8	71.1	39	72.2	75.3
Fixed Costs	9.3	15.1	9.6	15.4	15.4
Variable Costs	9.2	15.1	9.1	14.7	35.2
Fuel Costs	25.7	32.2	24.6	30.9	36.4
COE ($/MWh) (including T&S)	82.1	143.5	82.3	142.8	173.6
CO2 T&S Costs	0	10	0	9.6	11.3

3.7 Environmental Health and Safety Evaluation

Aspen performed an Environmental Health & Safety (EH&S) evaluation on the process of AFA sorbent fabrication and assessed all the risks (environmental, health) related to the process of fabrication and to the sorbent material. Aspen took the appropriate measures to mitigate (or minimize) any EH&S risk during pilot scale up production. The following required elements for the EH&S assessment were conducted and evaluated:

- Potential risks related to the process of AFA manufacturing
- Potential toxological risks related to manufacture of AFA sorbent
- Assessment of physical and equipment risks by handling the AFA sorbent
- The compliance and regulatory implications of the technology
- Process optimization study to minimize use of toxic/hazardous substances
- Safe handling and safe storage of AFA sorbent.

3.7.1 Potential risks related to the process of AFA manufacturing

In order to assess the potential exposure impact of AFA manufacturing on operators, personal monitoring was conducted in the laboratory setting. Two employees were monitored for their personal exposure to airborne total dust, inhalable dust, and respirable dust while performing pulverizing activities related to the AFA sorbent development. The personal exposure results indicated that:

- Both employees monitored for airborne total dust had exposure concentrations below the enforceable 8-hour OSHA PEL of 15 mg/m^3. Since the total dust personal exposure results were below the 8-hour OSHA PEL, there are no regulatory requirements.
- Both employees monitored for airborne inhalable dust had exposure concentrations below the recommended 8-hour ACGIH TLV of 10 mg/m^3. Since there is no OSHA PEL established for inhalable dust, there are no regulatory requirements.
- Both employees monitored for airborne respirable dust had exposure concentrations below the enforceable 8-hour OSHA PEL and recommended ACGIH TLV of 5 and 3 mg/m^3. Since the respirable dust personal exposure results were below the 8-hour OSHA PEL, there are no regulatory requirements.

The pulverized AFA sorbent is a silica based-aerogel material; therefore, additional personal sampling is recommended to determine amorphous silica exposures. Due to the silica content of the milled material, it is recommended that the employees continue to wear respiratory protection while milling the silica gel.

3.7.2 Potential toxicological risks related to manufacture of AFA sorbent

In order to determine potential toxicological effects of the AFA sorbent and its manufacture, an Occupational Health Scientist working with Aspen to refine the Safety Data Sheet for the AFA sorbent. A brief review of the scientific literature has found that there are many studies on similar classes of materials (amorphous silica combined with an organo-amine polymer phase), although nothing was found concerning toxicological risks related to manufacturing these materials. It is likely that the nanoporous network structure of the AFA sorbent is unlikely to produce any new findings for risk significantly different than those for amorphous fumed silica doped with polyamine polymers as the active sorbent material. Aspen has obtained a toxicological risk assessment of our industrial products and it states that we have no toxicology issues related to the silica aerogel materials with respect to crystalline silica content or any concerns regarding nanoparticles potentially being released during handling. The materials do not contain or release any crystalline silica (or other toxic materials) and do not shed nanoparticles upon handling. The main concern with handling is exposure to amorphous silica dust and making sure that exposure levels remain below required thresholds.

3.7.3 Assessment of physical and equipment risks by handling the AFA sorbent

The combustibility and explosivity of the aerogel solids are relevant quantities to measure as the materials produced are hydrophobic, and therefore contain a small amount of organic functionality, which can act as fuel. The content is low and the combustibility is generally class A (via ASTM E84). Samples were tested for corrosion testing on steel (ASTM C871 and C1617) and explosibility screening. The next sections summarize the test results.

3.7.3.1 AFA ignition sensitivity, explosion testing

3.7.3.1.1 Explosibility classification of AFA sorbent

The purpose of this test is to determine whether a material may present an explosion hazard when dispersed in the form of a dust cloud under ambient conditions. The Dust Explosibility Classification Test is performed using the Vertical Tube Apparatus as described by Bartknecht[14] and in accordance with ASTM E1226, the Standard Test Method for Explosibility of Dust Clouds and with ASTM E1515, the Standard Test Method for the Minimum Explosible Concentration. The initial apparatus consists of a vertically-mounted acrylic tube 32 centimeters (cm) in height and having an internal diameter of 63 millimeters (mm). At the base of the tube is a sample cup connected to a compressed air dispersion system. The total volume of the tube and sample cup is 1.2 liters (L). Two brass electrodes are mounted on opposing sides of the tube at a height of 10 cm above the base and extend into the tube. The electrodes are connected to a high-voltage transformer, which is used to create a continuous arc discharge between them. The effective energy of the continuous arc is approximately 10 Joules (J) and represents a reasonable worst-case ignition source.

The sample is classified as "explosible" if a flame is observed to propagate away and separate from the continuous arc during tests in the vertical tube apparatus. If determined to be "explosible" using the Dust Explosibility Classification Test, it is prudent to further evaluate a material in terms of ignition sensitivity and explosion severity. The AFA sorbent is classified “explosible” as shown in the test results (Figure 66), therefore further evaluation was done as specified in the sections below.

EXPLOSIBILITY CLASSIFICATION
VERTICAL TUBE APPARATUS

Powder Information

Company Name	:	**ASPEN AEROGELS INC.**
Test Powder	:	**AMINE SILICA AEROGEL**
Ref. No.	:	N/A
Origin of the Sample	:	N/A
Size Information	:	Sample tested as received, 100%<75µm
Moisture Content	:	7.8%
Comment	:	Fine, white powder

Test Information

Test Purpose	:	To determine the explosibility of a dust sample.
Apparatus	:	Acrylic vertical tube with continuous arc ignition source.
Date of Test	:	04.29.16
Operator	:	S. Ahmed

Results

Sample classified as : **Go (Explosible)**

Dispersed Powder Weight (g)	Sieve Fraction (µm)	Trials	Ignition	Flame Size	Pressure
0.25	100%<75µm	1	Yes	Large	High
0.50	100%<75µm	1	Yes	Large	High

Figure 66. Explosibility classification of AFA sorbent.

3.7.3.1.1.1 Explosion severity, max. explosion pressure, and Kst value of AFA sorbent.

The deflagration index, Kst, is used to estimate the relative explosion severity of the dust being examined. To determine Kst, dust samples of known particle size, moisture content, and concentration are ignited in a standard 20-liter test apparatus. The test chamber pressure as a function of time is recorded for successively increasing sample concentrations. The value of Kst is calculated using the equation:

$$Kst = (dP/dt)max \times [\text{Test chamber volume}]^{1/3}$$

Pmax: The maximum explosion pressure
(dP/dt)max: The maximum rate of pressure rise
Kst: The K_{st} values equivalent to maximum rate of pressure rise in a $1m^3$ vessel

The higher the value of Kst, the more potentially energetic a dust explosion. The test results are shown in Figure 67 and Figure 68.

EXPLOSION PRESSURE TEST RESULTS ACCORDING TO
ASTM Standard E 1226, ISO 6184/1 – 1995 AND BS 6713: PART 1: 1996

Powder Information

Company Name	:	**ASPEN AEROGELS INC.**
Test Powder	:	**AMINE SILICA AEROGEL**
Ref. No.	:	N/A
Origin of the Sample	:	N/A
Size Information	:	Sample tested as received, 100%<75µm
Moisture Content	:	7.8% as received, 3.4% after drying (dried for 16 hours at 50°C in oven), tested after drying
Comment	:	Fine, white powder

Test information

Test Purpose	:	To determine Kst class & maximum rate of pressure rise and maximum explosion pressure.
Apparatus Type	:	20 liter sphere explosion chamber.
Ignition Source	:	2x5000J chemical igniters.
Date of Test	:	04.30.16
Operator	:	S. Ahmed

Results

Maximum Explosion Pressure (P_{max})	:	**7.3 bar**
Max. Rate of Pressure Rise $(dP/dt)_{max}$	:	**462 bar/s**
Kst Value	:	**125 bar.m/s**

Figure 67. Explosion test results.

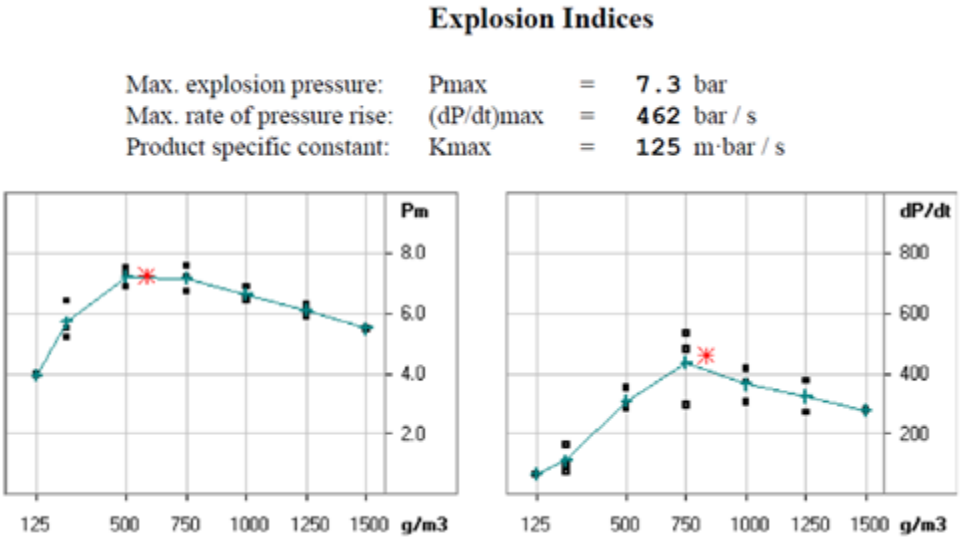

Figure 68. Explosion indices.

The relationship between the Kst value and the physical severity of the dust explosion is given in Table 25 from OSHA Directive Number CPL-03-00-008. Therefore, the AFA sorbent exhibits a weak explosion under certain conditions. As shown in Figure 69, the Kst of the AFA sorbent can be compared to other "common" materials, showing that the AFA sorbent has a lower Kst than materials such as sugar.

Table 25. Kst value and the physical severity of the dust explosion.

Dust Explosion Class	Kst (bar.m/s)	Characteristics
St 0	0	No explosion
St 1	>0 and <=200	Weak explosion
St 2	>200 and <=300	Strong explosion
St 3	> 300	Very strong explosion

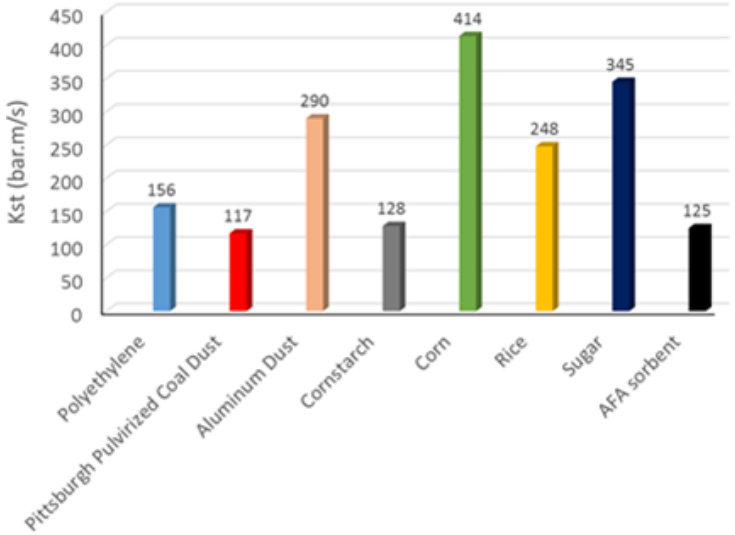

Figure 69. Kst of different materials including AFA sorbent.

3.7.3.1.1.2 Minimum Explosion Concentration (MEC) testing

Minimum explosible concentration (MEC) is the smallest concentration of material in air that can give rise to flame propagation upon ignition when in the form of a dust cloud. The test involves dispersing powder or dust samples in a vessel and attempting to ignite the resulting dust cloud with a highly energetic ignition source. Trials are repeated for decreasing sample sizes until the MEC is determined. MEC provides a relative measure of the minimum concentration of a dust cloud necessary for an explosion. As shown in Figure 70, the MEC of AFA sorbent dust is an order of magnitude higher than several common combustible dusts. These common dusts are also many times denser than AFA dust.

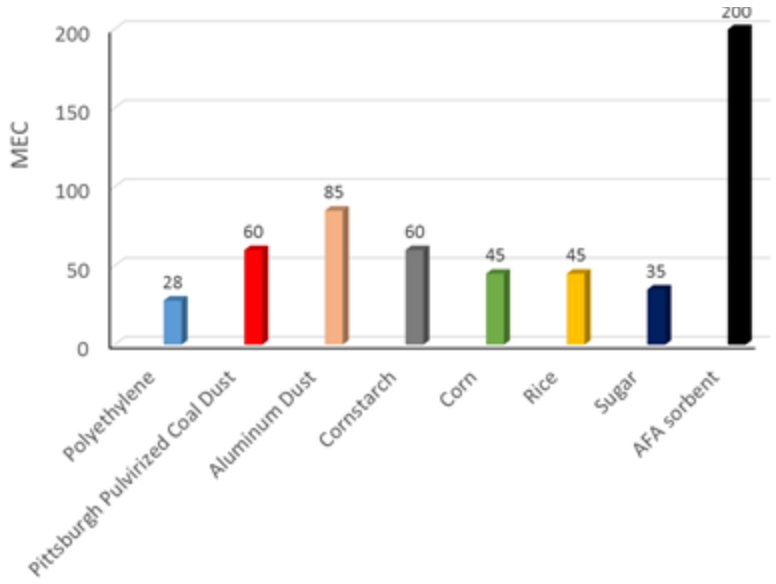

Figure 70. MEC of common materials in comparison to the AFA sorbent.

3.7.3.2 AFA corrosion testing on steel (ASTM C871 and C1617).

The AFA sorbent was extracted for chemical analysis in accord with ASTM C871 Chemical Tests (Standard Test Method for Chemical Analysis of Thermal Insulation Materials for Leachable Chloride, Fluoride, Silicate, and Sodium Ions) and the extraction solutions were then used for individual ASTM C1617 Corrosion Tests (Standard Practice for the Quantitative Accelerated Laboratory Evaluation of Extraction Solutions Containing Ions Leached from Thermal Insulation on Aqueous Corrosion of Metals).

The Accelerated Corrosion Test was run in accord with ASTM C1617, using carbon steel coupons. The material test solutions were prepared by filtering the chemical extraction solutions through a 0.45 micron filter paper and then diluting 375 ml with de-ionized water to a total volume of 3000 ml. The standard solutions used were 0 chloride (de-ionized water); 1 ppm chloride and 5 ppm chloride. Three coupon cells for each solution were tested for 96 hours. The flow rate was set for a continuous even delivery of 250 ml/day into each test cell. The hot plate temperature was controlled at 230 °F.

The calculated results, expressed in mils per year (mpy), are based on the weight loss of the steel and the full potential exposure area of the cell. The actual corrosion was more localized, occurring

in the center of the cells. The individual coupon test results for the test set is provided in the Table 26. The AFA sorbent solution produced corrosion rates below the 0 ppm chloride-de-ionized water reference standard.

Table 26. Corrosion test results.

Solution	Mass loss	MPY	Average	STD
0	0.0038	2.42		
0	0.0094	6.00		
0	0.0103	6.57	5.00	1.83
1	0.0500	31.90		
1	0.0504	32.15		
1	0.0559	35.66	33.24	1.72
5	0.1074	68.51		
5	0.0940	59.97		
5	0.1549	99.82	75.76	16.67
AFA solution	0.0029	1.85		
AFA solution	0.0029	1.85		
AFA solution	0.0038	2.42	2.04	0.27

Standards: 0 ppm Cl = 5 mpy; 1 ppm Cl = 33 mpy; 5 ppm Cl = 76 mpy

3.7.4 The compliance and regulatory implications of the technology

The regulations (State and Federal) governing the manufacturing of silica aerogel insulation are being evaluated since an ethanol-water-carbon dioxide solvent and ethoxysilane based process will be used to manufacture the AFA sorbent with the additional ethoxysilane component containing the active sorbent moiety in regards to Environmental Health and Safety.

3.7.5 Safe handling and safe storage of AFA sorbent

Aspen has provided all the physical and health hazard test results to Industrial Health & Safety Consultants, Inc. A SDS (Safety Data Sheets) for Aspen's optimized AFA sorbent will be established describing the proper and safe handling and storage of the AFA sorbent.

3.7.6 Integration of new chemicals to identify safer alternatives for AFA production.

The replacement or reduction of hazardous substances in AFA process production by less hazardous or non-hazardous substances or by achieving an equivalent functionality via technological or organizational measures has been Aspen' focus during the last budget period. The terrain for designing and selecting safer alternatives is wide and varied. Aspen recognizes the importance of integrating environmental health and safety concerns with performance, and economics. Aspen keeps focused on these broader issues as it works to target methods for designing and selecting alternative, safer chemicals and processes, and products.

In the AFA fabrication process, two amino-alkoxysilanes (BAS-1 and AS-1) precursors are used. The sol-gel procedure requires the use of organic solvent, ethanol in this case, and water to promote hydrolysis and co-gelation of the two precursors. Later, the gel is converted into an aerogel by

supercritical drying, using CO_2 as the solvent. Table 27 groups the human health effects of the different compounds used in the AFA production.

Table 27. AFA raw materials on human health effects.

	CAS Number	flammability	Acute toxicity	Carcinogenicity	corrosion	Skin Irritation	Respiratory Irritation	Eye Irritation
BAS-1	82985-35-1	L	NC	No	H	H	M	VH
AS-1	919-30-2	L	Yes	No	H	VH	M	VH
Ethanol	64-17-5	H	Yes	No	L	M	M	VH
CO2	124-38-9	L	No	No	VL	M	M	L

L: Low, M: Medium, H: High, VH: Very High, NC: Not Classified

The primary hazard identified is flammability of large quantities of organic solvents used. Reducing the use of flammable solvents, and reducing organic vapor emissions are the primary drivers that challenge Aspen to seek other potential alternatives that could mitigate hazardous concerns. A few potential alternatives and their assessment based on preliminary screenings are given in the next section.

3.7.6.1 Identify potential alternatives and initial screening

An extensive list of potential alternatives can be developed for AFA production. Aspen has focused on a few potential alternatives that could be implemented in the short term that could considerably decrease hazard concerns. Aspen has considered the following two systems:

- colloidal silica/water/amino-silane with (and without) PEI
- Methylsiliconate precursor/Methylsiliconate salt/water/PEI

The chemical alternatives to be evaluated in the assessment are:

- Colloidal silica (CS)(ex. LUDOX TM-40, 40% solution)
- Amino-silane (AS-1)
- Polyethyleneimine/water solution (PEI)
- Methylsiliconate precursor (MSP)
- Methylsiliconate salt (MS)

Table 28 and Table 29 group the potential alternative systems for AFA production and list the physical and health hazards of the different compounds considered, respectively.

Table 28. Potential chemical alternatives for AFA production.

Alternative Chemical Systems	Comments	Alternative to be assessed
CS/water/AS-1	Water based (non-flammable) Might be difficult to incorporate the amino-silane into the colloidal silica Requires a step to exchange water with ethanol, prior to (or during) supercritical drying with CO_2	Yes
CS/water/AS-1 (+ PEI)	Same comments as above.	Yes

	PEI will provide more amine sites to the porous colloidal silica matrix, thus improving CO_2 capture capacity. Solvent exchange with ethanol could extract amine if not well impregnated into colloidal silica. Consider ambient drying process to minimize amine loss and use of alcohol and CO_2 solvents.	
MSP/MS/water/PEI	High water content sol-gel system Methylsiliconate salt provides a very good combination with PEI for high quality hydrophobic gel formation with methylsiliconate sol. This route (without PEI) has shown VERY promising quality aerogel and process improvement using water as the sole solvent.	Yes*

* sorbents have been made and will be tested soon.

Table 29. Physical and health hazard properties of alternative chemicals for AFA production.

	CAS Number	flammability	Acute toxicity	Carcinogenicity	corrosion	Skin Irritation	Respiratory Irritation	Eye Irritation
CS	**7631-86-9**	**VL**	**NC**	**No**	**VL**	**L**	**M**	**L**
AS-1	**919-30-2**	**L**	**Yes**	**No**	**H**	**VH**	**M**	**VH**
MSP	**2031-67-6**	**VH**	**Yes**	**No**	**L**	**L**	**L**	**L**
MS	**16589-43-8**	**VL**	**NC**	**No**	**H**	**H**	**M**	**VH**
PEI	**9002-98-6**	**VL**	**Yes**	**No**	**H**	**L**	**L**	**L**

L: Low, M: Medium, H: High, VL: Very Low, VH: Very High, and NC: Not Classified
CS: Colloidal Silica (ex. LUDOX TM-40, 40% solution)
AS-1: Amino-propyltriethoxysilane
MSP: Methylsiliconate precursor
MS: Methylsiliconate salt (methylsiliconate sodium or potassium)
PEI: Polyethyleneimine (50% in water, MW 1,200)

Aspen recognizes that there are varying levels of confidence in the different end point categorizations (L, M, H, VH, VL), and Aspen, also, understands that measured data won't be necessarily higher confidence than the assessment. However the company has sufficient expertise to differentiate the confidence levels, and therefore will assume approximately equal confidence levels for the categorizations of end points for the purpose of this assessment. Table 30 reviews the hazard summary for the alternative and current AFA sorbents. Aspen finds that the alternative AFA chemicals show improvements over the current process where most of the ingredients used are very flammable.

Table 30. Hazard summary for alternatives and actual AFA sorbents.

	Process safety	Materials Health hazards	Materials physical hazard	Sorbent explosivity	Sorbent corrosion	Remarks
AFA current	**High**	**High**	**Flammable**	**None**	**None**	**High level safety precautions implemented at Aspen's manufacturing plant. Sorbent suitable for pilot scale up production**
AFA Alternatives	**Low**	**Low**	**Non-flammable**	**None**	**None**	**Very attractive, and safe route for AFA production Cost effective**

4 CONCLUSIONS

Using its expertise in aerogel science, Aspen Aerogels has developed and tested, at bench scale, Amine Functionalized Aerogels (AFAs) for post-combustion CO_2 capture processes based on temperature-swing adsorption, fluidized-bed process. The project team (Aspen Aerogels, Inc., The University of Akron, ADA-ES, and Longtail Consulting) has carried out numerous testing and optimization studies to demonstrate the CO_2 capture performance of novel AFA sorbents in 3 product forms: powder, pellet, and bead. For AFA performance optimization, the top two formulations developed during this project were selected to establish a plan to improve the performance of the sorbents in pellet and bead forms. These two AFA sorbents called type #1 and type #2 differ by their sol-gel chemistry and performance, but both are good candidates for CO_2 capture. Their CO_2 adsorption capacities were measured, using TGA, under different conditions of temperature and 100% CO_2 flue gas (to mimic the conditions of CO_2 adsorption/desorption used for the ADAsorb process). Both sorbents showed a good total CO_2 capacity and working capacity (14 - 20 wt.% total, and 6.6 – 7.0 wt.% working) with targets of > 12 wt. % and > 6 wt. % working, at a delta T of 60 °C (40 °C adsorption and 100 °C desorption). The heat of reaction with CO_2 for AFA sorbents is lower than other proprietary sorbent materials previously tested by ADA-ES. The tested AFA sorbents have a heat of reaction in the range of 50-60 kJ/mole CO_2. Monoethanolamine (MEA), a standard sorbent for CO_2 absorption, has a heat of reaction of 84 kJ/mole CO_2. Therefore, utilizing the AFA sorbent should reduce the energy consumption for the CO_2 capture process, in comparison to other known sorbents. The University of Akron developed an efficient low-cost coating technology that is compatible with Aspen's AFA sorbents (powder and bead forms) and has shown to provide a good resistance of the AFA pellet (and coated beads) performance to CO_2 capture degradation in the presence of SO_2. The most promising AFA sorbent was selected for scale up production and bench-scale testing in a pelletized form.

At bench scale testing, a hydrodynamic assessment of the pelletized AFA sorbent in a cold-flow fluidized bed demonstrated that good fluidization could be attained at a bed velocity of 1.5 ft/s, with a pellet density of 1150 kg/m^3. A techno-economic analysis showed that Aspen's pelletized AFA sorbent has promise for CO_2 capture applications, but also could benefit from further refinement and improvement to allow the material to be competitive with a solvent CO_2 capture system. For example, the gross power output for AFA sorbent capture is higher than the baseline MEA case. One significant issue is the compression of the flue gas to overcome the pressure drop in the adsorber bed. This is the single largest electrical energy auxiliary for this process. There are several areas for potential improvement. The optimized pelletized sorbent provided for fluidization testing and particle characterization had an unusually high apparent particle density. As noted above, this density was measured at 1150 kg/m^3, which is extremely dense for an aerogel

type material. The expected density, based on previous samples produced at Aspen, was approximately half of this value. Also, testing was delayed due to challenges in producing the pellets at the appropriate scale for the fluidization testing. These challenges lead to a greater use of binding agent than initially anticipated, causing the high sorbent density and corresponding pressure drop. If the AFA sorbent density had been in a range expected for the sorbent, and pressure drop, then the capital costs associated with the solid sorbent system would be approximately $2/MWhr lower than the NETL MEA case 12B[2]. Second, the sorbent must be tested under a practical environment to determine how many cycles the material can withstand. Attrition results were promising, but the sorbent has also not been exposed to 10,000 cycles of adsorption and desorption. Proving a greater lifespan of the sorbent or reducing the costs of the sorbent will have the greatest impact on reducing the cost of electricity and should be the focus of further investigation. There may be opportunity for significant improvement with Aspen's AFA sorbent in terms of advancing the production process, by:

1. Reducing the mass of binder, the mass loading of CO_2 would be increased as well as reducing the density of the sorbent. And this can be accomplished by using lightweight aerogel beads instead of pellets (AFA bead needs minimal "binder" as coating for SO_2 resistance, as compared to pellets). Optimized low density AFA beads could potentially reduce the pressure drop by up to 50%.
2. Lowering the density of AFA and opting for the bead form would combine to reduce capital costs and sorbent circulation rate, which is directly tied to sorbent costs due to attrition reflected in the variable operating costs.
3. Integrating an alternative route for AFA production could potentially produce AFA bead sorbent at a lower cost, further reducing the variable operating costs. The results from this project suggest that solid sorbent CO_2 capture will continue to see performance gains and lower system costs as further sorbent improvements are realized.

As part of the Environmental Health and Safety Evaluation studies, several ASTM tests were performed on the AFA powder. AFA powder showed no corrosion on steel. The AFA sorbent showed weak explosivity under specific conditions (Kst = 125 m.bar/s, max. explosion pressure = 7.3 bars, and max. rate of pressure rise = 462 bar/s). This is comparable to the Kst of other amine functionalized sorbents.

5 REFERENCES

1. Ramezan M., Skone T.J., Nsakala N., Liljedahl G.N., "Carbon Dioxide Capture from Existing Coal-Fired Power Plants", Final Report DOE/NETL-401/110907, December, 2007.
2. Fout, T., Zoelle, A., Keairns, D., Turner, M., Woods, M., Kuehn, N., . . . Pinkerton, L. (2015). *Cost and Performance Baseline for Fossil Energy Plants Volume 1a: Bituminous Coal (PC) and Natural Gas to Electricity Revision 3.* U.S. Department of Energy, Office of Fossil Energy. National Energy Technology Laboratory.
3. SBIR Phase II Project, "Superhydrophobic Aerogel as Sorbent Material for CO_2 Capture, Award Number: DE-SC0004289, Period: 08/2011 – 11/2013

4. Ramezan M., Skone T.J., Nsakala N., Liljedahl G.N., "Carbon Dioxide Capture from Existing Coal-Fired Power Plants", Final Report DOE/NETL-401/110907, December, 2007.
5. http://www.netl.doe.gov/File%20Library/Research/Coal/ewr/co2/5309-Air-Products-oxy-combustion-GHGT-8-paper.pdf)
6 . Enwald, H., Peirano, E., & Almstedt, A. (1996). Eulerian two-phase flow theory applied to fluidization. *Internaitonal Journal of Multiphase Flow*(22), 21-66.
7 . Morton, K., & Mayers, D. (1994). *Numerical solution of partial differential equations.* Cambridge University Press.
8. Kunii, D., & Levenspiel, O. (1991). *Fluidization Engineering.* Boston: Butterworth-Heinemann.
9. Begag, R., Krutka, H., Dong, W., Mihalcik, D., Rhine, W., Gould, G., Nahass, P. (2013). Superhydrophobic amine funcitonalized aerogels as sorbents for CO2 capture. *Greenhouse Gas Science Technology*(3), 30-39.
10. Molerus, O., & Wirth, K. (1997). *Heat transfer in fluidized beds.* Chapman and Hall.
11. Breault, R. (2006). A review of gas-solid dispersion and mass transfer coefficient correlations in circulating fluidized beds. *Powder Technology*(163), 9-17.
12. Wei, F., Wan, X., Hu, Y., Wang, Z., Yang, Y., & Jin, Y. (2001). A pilot plant study of 2-D dispersion-reactor model for a high-density riser reactor. *Chemical Engineering Science*(56), 613-620.
13. Sjostrom, S. (2016). *Evaluation of Solid Sorbents as a Retrofit Technology for CO2 Capture.* ADA-ES, Inc. U.S. Department of Energy.
14. Bartknecht, W. 1989. Dust Explosions: Course, Prevention, Protection. Berlin, Germany. Springer-Verlag.

6 BIBLIOGRAPHY

6.1 Redouane Begag, Principal Investigator – Aspen Aerogels, Inc.

Education and Training

Ph.D. Inorganic Chemistry, University of Lyon, 1996, France
Master of Advanced Studies (MAS) Inorganic Chemistry, University of Lyon, 1993, France
Master's Degree in Chemistry Engineering, USTHB, 1992, Algeria

Research and professional Experience:

2001 – Current - Aspen Aerogels, Inc., Scientist

- Led development teams on multiple government funded research efforts in excess of $7.0M as Principal Investigator
- Supported scale up of Aspen Aerogels manufacturing process to industrial level by optimizing the process and chemistries of fabrications
- Authored three major patents central to Aspen Aerogels intellectual property portfolio
- Developed lightweight and high strength carbon aerogels for Thermal Protection Systems (Air Force)
- Developed light weight LOX compatible aerogel materials for cryogenic applications (NASA)

- Developed glass like transparent aerogel material for Cherenkov detector application (DOE)
- Developed novel liquid natural gas (LNG) compatible aerogels (NSF)

1998 – 2001, Aspen Systems, Inc, Senior Chemist

- Developed carbide aerogel for TPS applications (NASA)
- Developed glass like transparent aerogel material for Cherenkov detector application (DOE)
- Patented "Rapid Aerogel Production Process" and "Aerogel Composite with Fibrous Batting" that enabled Aspen, in 2001, to make the breakthrough in aerogel science: Large scale up aerogel manufacturing.

1996 – 1998, University of Lyon, France, Post-Doctoral Researcher

- Performed research on various aerogels including aerogel for use in Cherenkov detectors using a fluorescence-doped aerogel under Professor Pajonk
- Participated in industrial project with ELF ATOCHEM (France) to develop a scaled fabrication for super thermal insulator silica aerogels to be used as thermal insulation material for pipelines in oil extraction.

Awards & Honors:

1. Awarded certificate of recognition from NASA JSC for the creative development of technical innovation on NASA Contract No. NAS9-00029.
2. Winning the prize for best presentation at the Carbon Capture, Use and Storage (CCUS) conference, May, 2012 in Pittsburgh

Relevant Publications:

1. G.M. Pajonk, R. Begag, et al, "Comparison of some physical properties of silica aerogel monoliths synthesized by different precursors", ISA (International Symposium of Aerogels, Montpellier, France 8-10/09/1997)

2. G.M. Pajonk, R. Begag, et al, "Florescent dye doped aerogels for the enhancement of Cherenkov light detection," *Journal of Non-crystalline Solids*, **186**, 388, (1995)

3. G.M. Pajonk, R. Begag, et al, "Optical transmission properties of silica aerogels prepared from polyethoxydisiloxanes," *J. of Non-crystalline Solids*, **210**, 224 (1997)

4. R. Begag, G.M. Pajonk, et al, "Synthesis and properties of some monolithic silica carbogels produced from polyethoxydisiloxanes dissolved in ETAC and acid catalysts," *Materials Chemistry and Physics*, **58**, .256-263 (1999).

5. P.B. Wagh, R. Begag, G.M. Pajonk, A.V. Rao, D. Haranath, D.**,** *Materials Chemistry and Physics*, **57**, 214-218 (1999)

6. W.E. Rhine, D. Ou, J.H. Sonn, R. Begag, "Transparent Ormosil Aerogels for Highly Energy Efficient Windows," 2005 Fall MRS Meeting, Boston, MA

7. A. Pierre.; R. Begag and G. Pajonk, "Structure and texture of alumina aerogel monoliths made by complexation with ethyl acetoacetate" *J. Mater. Sci.* 1999, 34, 4937

8. R. Begag, J.E. Fesmire, J.H. Sonn, " Nonflammable, Hydrophobic Aerogel Composites for Cryogenic Applications", Thermal Conductivity 29/Thermal Expansion 17 Proceedings of the 29th International Thermal Conductivity Conference and the 17th International Thermal Expansion Symposium, June 24-27, 2007, Birmingham, Alabama, USA

9. Redouane Begag, Je Kyun Lee, Danny Ou, Liya Liu, Jong Ho Sonn, George Gould, and Wendell Rhine, "Affordable Window Insulation with R-10/inch Rating," Final Report for Contract DE-FC26-00NT40998

Patents:

1. G.M. Pajonk, R. Begag, et al, Manufacturing of Monolithic Silica Aerogels, US Patent 5,795,557.
2. "Rapid Aerogel Production Process", Kang P. Lee, Redouane Begag and Zlatko Altiparmakov, US Patent 6,670,402.
3. "Aerogel Composite with Fibrous Batting", C. J. Stepanian, R. Begag and G. L. Gould, US Patent, 7,078,359.
4. "Polyimide aerogels, carbon aerogels, and metal carbide aerogels and method of making same", W. Rhine, R. Begag and Jing Wang, US Patent 7,074,880.
5. "Gel Production Via-Multi-Stream Mixing", R. Begag and Sonn, Jong Ho, US Patent Application 2007015236.
6. Aerogel metallic compositions, Wendell Rhine · Jing Wang · Redouane Begag, US patent 7071287.
7. Mitigation of hydrogen cyanide in aerogels, George Gould · Wendell Rhine · Redouane Begag, Xiangjun Hu, Patent application number: US11384035.

6.2 Shannon White, Sr. Program Manager - Aspen Aerogels, Inc.

Education and Training

Ph. D., Organometallic Chemistry, University of Wyoming, Laramie, WY, 2000
Bachelor of Arts, Chemistry, College of Wooster, Wooster, OH, 1993

Research and Professional Experience

2004-Present - Aspen Aerogels, Inc. - Senior Program Manager

Leader in commercial sales of aerogel blanket thermal insulation for a wide range of applications. Research and development of novel aerogel-based technologies.

Key Accomplishments:

- Effective management of multiple government programs simultaneously (up to 10 at one time).
- Directed preparation/submission of technical proposals (>60) for advances in aerogel technology with a high win rate (38%, more than double the national average for small businesses).
- Successful conversion of government programs (14 out of 17) into large size follow-on efforts bringing in additional research and development revenue.
- Developed procedures/strategies for management of commercial contracts with multi-national oil and gas partners such as ExxonMobil and Total. Provided work direction to all departments in Aspen's commercial business (manufacturing, quality, technical services, finance, supply chain).
- Worked with technical teams to advance key aerogel technologies in the following areas:

  Thermal Insulation

  - Satellite thermal control and hypersonic flight vehicle thermal protection for the U.S. Air Force; Thermal Batteries for the Department of Defense, Multiple NASA applications (cryogenic fluid storage, Space Shuttle and International

Space Station thermal control); Energy savings for the Department of Energy and Navy (superconducting cables, windows)

Non-thermal Applications

- Water purification; Chemical/biological protection for the U.S. Army; Electronic applications for the military (low dielectric material); Carbon capture

2001-2004 - Biotage - Chemical Safety Officer and Lab Manager

A global supplier of scientific instrumentation and associated consumable products for medicinal chemistry research.

- Pioneered research and development in organic chemical synthesis using advanced microwave technology.
- Provided technical seminars, demonstrations, and training sessions for chemists at top-level pharmaceutical companies in the area of microwave-assisted organic synthesis.
    - Developed and implemented safe laboratory practices in wet lab.

Awards / Honors

University of Wyoming top Ph. D. award for dissertation research in 1999

Relevant Publications

1. White, S.; Begag, R.; Mihalcik, D.; Fesmire, J.E.; Kerce, J.L.; Mills, G.; Buchanan, L.; Buerger, S., "Multi-Layer Aerogel Insulation for Cryogenic Applications", Cryogenics Engineering Conference, June, 2015.
2. Rhine, W.E.; Begag, R.; Dong, W.; Zafiropoulos, N.; Melnikova, I.; White, S.; Dominick, T.; Porter, M.; Naramore, A.; Schoonover, K. "Carbon Aerogels for Structural Insulation in DACS" Proceedings of the 33rd International Conference on Advanced Ceramics and Composites, Advances in Porous Ceramics and Bioceramics II, January 2015, Cocoa Beach, FL.
3. Begag, R.; White, S.; Fesmire, J.E.; Kerce, J.L. "Thin, Lightweight Aerogel Thermal Insulation Systems for Cryogenic Applications" Cryogenics Engineering Conference, June, 2013.
4. White, S.; Demko, J.; Tomich, A. "Flexible Aerogel as a Superior Thermal Insulation for High Temperature Superconductor Cable Applications", Cryogenics Engineering Conference, July 2009.
5. Coffman, B.E.; Fesmire, J.E.; White, S.; Gould, G.; Augustynowicz, S. "Aerogel Blanket Insulation Materials for Cryogenic Applications", Cryogenics Engineering Conference, July 2009.
6. Meador, M. B.; Weber, A.; Hindi, A.; Vivod, S. L.; Deshpande, K.; White, S. and Gould, G. "Adapting Cross-linking of Silica Based Aerogels to a Safer, Industry-Friendly Process," presented at the American Chemical Society Annual Meeting August, 2008.

Patents

1. White, S.; Begag, R.; Mihalcik, D., "Multilayer Insulation Systems", Provisional Patent Application 1102-01b.
2. Zafiropoulos, N.A.; Evans, O.; Rhine, W.; White, S.; Dong, W., "Thin Aerogel Material", Provisional Patent Application, 1085-01.
3. Zafiropoulos, N.A.; White, S.; Clark, J.L. "Aerogel Insulation Panels and Manufacturing Thereof" US Patent Application (US 14/202,873).
4. Zafiropoulos, N.A.; Nahass, P.; Trifu R.; Begag, R.; Rhine, W.E.; Dong W.; White, S.; Gould, G.L.; Naiman, A.; Sinta, R. "Electronic Device Manufacture Using Low-k Dielectric Materials" US 8,945,677 (application number 13/358,462).

5. Clark , J.L.; Doan, M.; Krone-Schmidt, W.; Lakomski, D.M.; Schroth, A.E.; Shaffer, C.; Smith, S. and White, S. "Encapsulated and Vented Particulate Insulation", US 8,453,393 B2. Joint patent with Raytheon Corporation; El Segundo, CA.
6. Ou, D.L.; White, S. "Aerogel Composites with Complex Geometries" WO2007011988A3 (application number 11/458,357).

6.3 Steven S. C. Chuang, Department of Chemical and Biomolecular Engineering The University of Akron

Education and Training:

Ph.D., Chemical Engineering, University of Pittsburgh, 1985.
M.S., Chemical Engineering, New Jersey Institute of Technology, 1982.
Diploma, Chemical Engineering, National Taipei Institute of Technology, 1977

Research and Professional Experience:

- 2005 – Date: Professor of Chemical and Biomolecular Engineering, The University of Akron. *Research work:* CO2 Capture, Solid Oxide Fuel Cell; Photocatalytic Synthesis of Hydrocarbons from CO2 and H2O.
- 1997- 2005: Chair of Chemical Engineering, the University of Akron.
- 1997-1997: Acting Chair of Chemical Engineering, the University of Akron.
- 1996-1997: Professor of Chemical Engineering, the University of Akron. *Research work:* Catalytic NO Decomposition, Ethylene Hydroformylation, Polypropylene decomposition.
- 1991-1996: Associate Professor of Chemical Engineering, the University of Akron. *Research work:* CO Hydrogenation, Conversion of Syngas to Higher Oxygenated Fuel.
- 1986-1991: Assistant Professor of Chemical Engineering, the University of Akron. *Research work:* Fischer-Tropsch Syntehsis, CO Hydrogenation.
- 1979-1980: Assistant Engineer of Process Design, Fu-Tai Engineering Co. (formerly, Asia Fluor Co.), Taipei, Taiwan.
- 1977-1979: Second Lieutenant in Signal Corp., Military Service in Taiwan.

Selected Publications (Over 95 referred papers):

1. "Effect of gas flow rates and Boudouard reactions on the performance of Ni/YSZ anode supported solid oxide fuel cells," A. Chien and S. S. C. Chuang. 196, 4719-4723, 2011.
2. "Tracing the Reaction Steps Involving Oxygen and IR Observable Species in Ethanol Photocatalytic Oxidation on TiO2," F. Guzman and S. S. C. Chuang, J. Am. Chem. Soc., 132, 1502-1503, 2010.
3. "Performance and Byproduct Analysis of Coal Gas Solid Oxide Fuel Cell," R. Singh, F. Guzman, R. Khatri, and S. S. C. Chuang, Energy Fuels,: 24, 1176-1183, 2010.
4. "In Situ Infrared Study of the Role of PEG in Stabilizing Silica-supported Amine for CO2 Capture" J. Tanthana and S.S.C. Chuang, ChemSusChem, 3, 957-964, 2010.
5. "Oxide-supported Tetraethylenepentamine for Carbon Dioxide Capture," J. C. Fisher II, J. Tanthana, and S. S. C. Chuang, Environmental Progress & Sust Energy, 28 (4), 589-598, 2009.
6. "Thermal and Chemical Stability of Regenerable Solid Amine Sorbent for CO2 Capture," R. Khatri, S. S. C. Chuang, M. Gray, and Y. Soong, Energy&Fuels, 20(4), 1514-1520, 2006

7. “CO2 Capture by Diamine-grafted SBA-15: A Combined FT-IR and MS Study,” R. Khatri, S. S. C. Chuang, M. Gray, and Y. Soong, Industrial Eng. Chemistry, Res, 44, 3702-3708. 2005.
8. “Improved Immobilized Carbon Dioxide Capture Sorbents,” M.L. Gray, Y. Soong, K.J. Champagne, H. Pennline, J.P. Baltrus, R.W. Stevens Jr., R. Khatri, S.S.C. Chuang, and T. Filburn, Fuel Processing Technology, 86, (14-15), 1449 – 1455, 2005.
9. “Capture of Carbon Dioxide by Solid Amine Sorbents,” M. L. Gray, Y. Soong, K. J. Champagne, H. W. Pennline, J. Baltrus, R. W. Stevens, Jr., R. Khatri, and S. S. C. Chuang, Int. J. Environmental Technology and Management, Vol. 4, 82-88, 2004.
10. “CO2 Capture by Amine-Enriched Fly Ash Carbon Sorbents” M. L. Gray, Y. Soong, K. J. Champagne, J. Baltrus, R. W. Stevens, Jr., P. Toochinda, and S. S. C. Chuang, Separation and Purification Technology, 35, 31-36, 2004.
11. “In-Situ Infrared Study of CO2 Adsorption on SBA-15 Grafted with γ-(Aminopropyl)-triethoxysilane”, A. C. C. Chang, S. S. C. Chuang, M. Gray, and Y. Soong, Energy&Fuels, 17 (2), 468 -473, 2003.

Patents, copyrights and software systems:

1. “Sulfur and Nitrogen-Compound-resistant Immobilized Amine Sorbents for CO2 Capture,” U.S. Provisional Patent Appl. US 61/285,173. Oct. 27, 2009. UA 815
2. “Metal Monolithic Immobilized Amine Absorber for Carbon Dioxide Capture,” U.S. Patent Application, Nov. 7, 2008 UA 685
3. “Coal-based Fuel Cell,” S. S. C. Chuang, PCT Int. Appl. (2006) (i.e., European Patent Application), 35 pp. CODEN: PIXXD2 WO 2006028502 A2 20060316; U.S. Patent Application; India Patent Application. UA Patent Application

Synergistic Activities and Others:

- The Editorial Board, Catalysis Communications, May, 2006 -Date
- The Editorial Board, Applied Catalysis, Jan. 2001 – Dec. 2003.

6.4 William J. Morris, Ph.D, Principal Engineer at Longtail Consulting LLC

Education and Training:

Ph.D. University of Utah Department of Chemical Engineering, December, 2011

M.S. University of Utah Department of Chemical Engineering, December, 2009

A.B. Physics and Environmental Studies with a History Minor, Bowdoin College, May, 2005

Independent Study: A Lifecycle Analysis of Alternative Vehicle Fuels

National Outdoor Leadership School Waddington Range Mountaineering, July, 2005

Research and Professional Experience:

Principal Engineer Longtail Consulting LLC. Salt Lake City, UT. Current

In 2016, Dr. Morris joined Longtail Consulting as a Principal Consulting Engineer responsible to providing detailed engineering services and analysis for clients.

Technology Manager, ADA-ES Inc. July, 2013-December, 2015.

Previous roles included Sr. Research Engineer January-June, 2013, Process Technology Development Scientist August, 2011-December, 2011. Duties include directing efforts of Research Assistants, Senior Engineers, and Field Engineers at pilot and full scale demonstrations,

DOE project management including budgets, advising senior management on technical merits of projects, working with inside legal counsel to develop invention disclosures, provisional patents, utility applications, and serving as the technology representative on the corporate safety board to develop appropriate hazard mitigation during the development process.

Analytical Chemist, Enviropro Laboratories, September, 2006-January, 2008;

Periodic consulting through July 2011. Performed EPA and NELAC certified analysis of metals, inorganic compounds, hazardous volatile organic compounds (VOCs), and gasoline and diesel range organics in a wide range of matrices such as soils, industrial wastes, water, and sludges. Developed a new analytical method to combine gasoline and VOC analysis on a gas chromatograph (GC) and mass spectrometer (MS).

Outbound Supervisor / Problem Solver, Backcountry.com, West Valley City, UT, August, 2005-October, 2006.

Increased order fulfillment by 280% per man-hour by mentoring personnel and revising fulfillment strategy while improving warehouse operations and processes. Supervised teams of up to 22 people responsible for order fulfillment.

Graduate Research Assistant

University of Utah, Salt Lake City, UT, January, 2008-August, 2011. Responsible for implementation and operation of a flue gas recycle system in order to examine the effects of flue gas contaminants on combustion characteristics and aerosol formation under practical self-sustained coal flames in an oxy-fired (O_2/CO_2) combustion environment. .

Graduate Teaching Assistant

University of Utah, Salt Lake City, UT, January, 2009-December, 2009. Provided assistance to professors instructing a course in Graduate Heat Transfer for and a course in Air Pollution Control Engineering for on campus and remote ATK students. Tutored and assisted students and lectured as required.

Bowdoin Outing Club Leader

Bowdoin College, Brunswick, ME, fall 2002-Spring 2005. Responsible for creating and executing single and multi-day outings for students and faculty while maintaining Wilderness Emergency Medical Technician licensure and risk minimization for sea kayaking, swift water, and Backcountry Mountain travel trips.

Subject Expertise:

Combustion of solid fuels, aerosol chemistry and formation mechanisms, NO_X reduction and formation mechanisms, flue gas mercury control, oxy-combustion, carbon capture and sequestration (CCS), CO_2 separation, tangential fired combustion, circulating fluidized bed (CFB) combustion and fluid mechanics, air pollution control, process engineering and development, and process as well as managerial efficiency.

Awards and Honors:

Completed the Fundamentals of Engineering (FE) exam for EIT certification. Currently pursuing Professional Engineering (PE) licensure in Utah in 2016.

John Zink Scholarship for Excellence in Combustion Research Air and Waste Management Association's Great Basin Chapter Scholarship

Golden Key Honour Society, University of Utah

Patents:

Co-inventor of patent "Process to Reduce Emissions of Nitrogen Oxides and Mercury From Coal-Fired Boilers," submitted May 13, 2012 as an extension to U.S. Provisional Application Serial No. 61/486,217, filed May 13, 2011, and Serial No. 61/543,196, filed October 4, 2011.
Co-inventor of 5 additional U.S. and international emissions control and combustion patents pending in fields related to NO_X, mercury, or CO_2 emissions reductions.

***Publications*:**

Numerous publications published. And conferences attended.

6.5 William H. Nesse, Assistant professor lecturer, University of Utah

Education and Training:

PhD, University of Utah, Mathematics, May 2008
B.S., Boise State University, Psychology major, Mathematics minor, May 2002

Research and Professional Experience

Assistant professor Lecturer, University of Utah, May 2012 - present

- Owner at Longtail Consulting LLC, January 2012 – present
- Visiting assistant professor, University of Utah, September 2011 - May 2012
- Postdoctoral research fellow, University of Ottawa, fall 2008 - August 2011.
    - Co-Principle Investigators: Distinguished Professor Leonard Maler (Cellular and Molecular Medicine) and Professor Andre Longtin (Physics)
    - Instructor, University of Utah, summer term 2011

Technical expertise:

Probabilistic modeling, machine learning, neural networks, frequentist and Bayesian statistics, operations research, cost modeling under uncertainty, statistical decision-support, stochastic dynamical systems, information theory, scientific computation, assessment, biophysics, and neuroscience.

Other technical expertise:

Proficient MATLAB, adequate Perl, MySQL, and limited Java, and C++ coding skills; sharp-electrode electrophysiology recording techniques on invertebrate animal subjects.

Private sector experience:

Data science and statistical consulting under the auspices of Longtail Consulting LLC. Clients include:
backcountry.com: two-distribution-center inventory allocation tool, and one-deal-at- a-time site sales velocity estimator.
campusbookrentals.com: statistical analysis of price-setting tools and price elasticity estimation

Teaching and Education Experience:

Lecturer, engineering mathematics coordinator at the University of Utah, teaching ordinary- and partial differential equations, complex analysis, calculus, and linear algebra. I maintain a Youtube channel of 100's of lecture videos. I co-chair the University of Utah committee on learning outcomes assessment, and am actively involved in data-driven assessment of academic programs.

***Awards and Honors*:**

U of Ottawa Faculty of Medicine 2010 Award of Excellence for Postdoctoral Studies.
One of three $1,000 grants awarded yearly in the academic division.

Invited Talks:

Information representation in temporally correlated spike trains. Max Planck Institute for the Physics of Complex Systems: (October 2010).
Information representation in correlated spike trains. SIAM Life Sciences meeting (July 2010).

Publications:

1. Nesse WH, Marsat G, Maler L, Longtin A. (in prep) Spike patterns shaped by temporal correlations contain useful information beyond the _ring rate for weak stimulus detection.
2. Marcoux CM, Clarke SE, Nesse WH, Longtin A, Maler L. (in press) Balanced ionotropic receptor dynamics support signal estimation via voltage-dependent membrane noise. Journal of Neurophysiology.
3. Nesse WH, Maler L, Longtin A (2010) Biophysical information representation in temporally correlated spike trains. Proceedings of the National Academy of Sciences of the United States of America, 107(51): 21973-21978.
4. Khanbabaie R, Nesse WH, Longtin A, Maler L (2010) The kinetics of fast short-term depression are matched to spike train statistics to reduce noise. Journal of Neurophysiology, 103(6): 3337.
5. Nesse WH, Clark GA (2010) Relative spike timing in stochastic oscillator networks of the Hermissenda eye. Biological Cybernetics, 102(5):389-412.
6. Nesse WH, Del Negro CA, Bressloff PC (2008) Oscillation regularity in noise-driven excitable systems with multi-time-scale adaptation. Physical Review Letters, 101: 088101.
7. Nesse WH, Borisyuk A, Bresslo_ PC (2008) Fluctuation-driven rhythmogenesis in anexcitatory neuronal network with slow adaptation. Journal of Computational Neuro-science, 25: 317-333.
8. Nesse WH, Clark GA, and Bresslo_ PC (2007) Spike patterning of a stochastic phase model neuron given periodic inhibition. Physical Review E 75, 031912.
9. Rohn TT, Head E, Nesse WH, Cotman CW, Cribbs DH (2001) Activation of caspase-8 in the alzheimers disease brain. Neurobiology of Disease, 8: 1006-1016.

Journals refereed:

Physical Review Letters, Physical Review E, Frontiers of Computational Neuroscience, Journal of Physiology Paris.

7 LIST OF ACRONYMS AND ABBREVIATIONS

AFA	Amine Functionalized Aerogel
UA	University of Akron
ADA-ES	ADA-Environmental Solutions
DOE	Department of Energy
NETL	National Energy Technology Laboratory
PSRI	Particulate Solid Research, Inc.
SwRI	Southwest Research Institute
°C	Degree Celsius
CO_2	Carbon Dioxide
g	gram
H_2O	Water
min	Minute
mL	Milliliter
MS	Mass Spectrometer

NDIR	Nondispersive Infrared Sensor
sccm	Standard Cubic Centimeters per Minute
SO_2	Sulfur Dioxide
T	Temperature
TGA	Thermogravimetric Analyzer
FT-IR	Fourier Transform InfraRed spectroscopy
Vol	Volume
TSA	Temperature-Swing Adsorption
MEA	monoethanolamine
TEA	Techno Economic Assessment
EH&S	Environmental Health and Safety Evaluation
cc	Cubic centimeter
PEI	polyethelenimine
N_2	Nitrogen gaz
DSC	Differential Scanning Calorimetry
P_{CO2}	CO_2 partial pressure
vol %	Volumic percent
H_2O	Water
mg	Milligram
PLC	Programmable Logic Controller
NDIR	Non-Dispersive Infra-Red
Ft	Feet
Sec.	Second
ASTM	American Society for Testing and Materials (ASTM) - GSA
T Adsp.	Temperature of adsorption
T desop.	Temperature of desorption
mol%	Mole percent
DRIFTS	Diffuse Reflectance Infrared Fourier transform spectroscopy)
Ar	Argon
TPD	Temperature Programmed Desorption
kW	Kilo-watt
µm	Micron
L	Liter
LPM	Liters Per Minute
MWe	Megawatt electric
wt.%	Weight percent
nm	Nanometer
ppm	parts per million
lb	Pound
Btu	British thermal unit (unit of heat)
MMBtu	Million British thermal unit (unit of heat)
ppmv	parts per million by volume
FGD	Flue Gas Desulphurization
EOR	Enhanced Oil Recovery
ADAsorb™	ADA –ES's CO_2 Capture Process
AI	Attrition Index

Lbf	Pound-force
Hg	Mercury
Kg	Kilogram
Psi	pound-force per square inch
˚F	Degree Fahrenheit
kJ	Kilo-Joule
mmol	Milli-mole
K	Degree Kelvin
kWe	Kilowatt electric
lbm	Pound (mass)
kWh	Kilowatt-hour
kPa	Kilo-Pascal
m^3	Cubic meter
gpm	Gallons per minute
TOC	Total Overnight Costs
TASC	Total As Spent Costs
MW	Megawatt
MWh	Megawatt-hour
OSHA	Occupational Safety and Health Administration
PEL	Permissible Exposure Limit

8 APPENDICES

APPENDIX 1

Solid sorbent capital cost estimate breakdown

Case:		B12B - Supercritical PC w/ CO2 Capture Sorbent					Estimate Type:			Conceptual	
Plant Size (MW, net):		550					Cost Base:			Jun-11	
Item No.	Description	Equipment Cost	Material Cost	Labor		Bare Erected Cost	Eng'g CM H.O. & Fee	Contingencies		Total Plant Cost	
				Direct	Indirect			Process	Project	$/1,000	$/kW
	1	**Coal & Sorbent Handling**									
1.1	Coal Receive & Unload	$5,093	$-	$2,295	$-	$7,388	$739	$-	$1,219	$9,346	$17
1.2	Coal Stackout & Reclaim	$6,582	$-	$1,471	$-	$8,053	$805	$-	$1,328	$10,187	$19
1.3	Coal Conveyors	$6,120	$-	$1,456	$-	$7,576	$758	$-	$1,250	$9,584	$17
1.4	Other Coal Handling	$1,601	$-	$337	$-	$1,937	$194	$-	$320	$2,451	$4
1.5	Sorbent Receive and Unload	$204	$-	$61	$-	$265	$27	$-	$43	$335	$1
1.6	Sorbent Stackout and Reclaim	$3,305	$-	$598	$-	$3,903	$390	$-	$644	$4,937	$9
1.7	Sorbent Conveyors	$1,179	$257	$285	$-	$1,721	$172	$-	$284	$2,178	$4
1.8	Other Sorbent Handling	$712	$168	$369	$-	$1,248	$125	$-	$205	$1,579	$3
1.9	Coal & Sorbent Hnd. Foundations	$-	$5,923	$7,809	$-	$13,732	$1,373	$-	$2,266	$17,370	$32
Subtotal		**$24,797**	**$6,347**	**$14,680**	**$-**	**$45,824**	**$4,582**	**$-**	**$7,560**	**$57,966**	**$105**
	2	**Coal & Sorbent Prep & Feed**									
2.1	Coal Crushing and Drying	$2,959	$-	$568	$-	$3,528	$353	$-	$582	$4,462	$8
2.2	Coal Conveyor to Storage	$7,576	$-	$1,631	$-	$9,207	$921	$-	$1,519	$11,647	$21
2.5	Sorbent Prep Equipment	$5,641	$244	$1,155	$-	$7,041	$704	$-	$1,162	$8,907	$16
2.6	Sorbent Storage and Feed	$680	$-	$256	$-	$936	$94	$-	$155	$1,184	$2
2.9	Coal and Sorbent Feed Foundation	$-	$687	$603	$-	$1,290	$129	$-	$212	$1,632	$3
Subtotal		**$16,856**	**$932**	**$4,214**	**$-**	**$22,002**	**$2,200**	**$-**	**$3,630**	**$27,832**	**$51**

Case:		B12B - Supercritical PC w/ CO2 Capture Sorbent					Estimate Type:			Conceptual	
Plant Size (MW, net):		550					Cost Base:			Jun-11	
Item No.	Description	Equipment Cost	Material Cost	Labor		Bare Erected Cost	Eng'g CM H.O. & Fee	Contingencies		Total Plant Cost	
				Direct	Indirect			Process	Project	$/1,000	$/kW
	3	**Feedwater & Miscellaneous BOP Systems**									
3.1	Feedwater System	$27,945	$-	$9,011	$-	$36,956	$3,696	$-	$6,097	$46,749	$85
3.2	Water Makeup and Pretreating	$7,939	$-	$2,511	$-	$10,450	$1,045	$-	$2,299	$13,793	$25
3.3	Other Feedwater Subsystems	$8,791	$-	$3,609	$-	$12,400	$1,240	$-	$2,046	$15,686	$29
3.4	Service Water Systems	$1,590	$-	$832	$-	$2,423	$242	$-	$533	$3,198	$6
3.5	Other Boiler Plant Systems	$11,027	$-	$10,425	$-	$21,451	$2,145	$-	$3,539	$27,136	$49
3.6	FO Supply Sys and Nat Gas	$361	$-	$421	$-	$782	$78	$-	$129	$989	$2
3.7	Waste Treatment Equipment	$5,208	$-	$3,015	$-	$8,223	$822	$-	$1,809	$10,855	$20
3.8	Misc. Equip	$3,532	$-	$1,092	$-	$4,624	$462	$-	$1,018	$6,104	$11
Subtotal		**$66,392**	**$-**	**$30,916**	**$-**	**$97,309**	**$9,731**	**$-**	**$17,469**	**$124,509**	**$226**
	4	**Boiler and Accessories**									
4.1	PC Boiler and Accessories	$236,271	$-	$134,626	$-	$370,897	$37,090	$-	$40,799	$448,786	$816
4.2	SCR	w/4.1	$-	w/4.1	$-	$-	$-	$-	$-	$-	$-
4.5	Primary Air System	w/4.1	$-	w/4.1	$-	$-	$-	$-	$-	$-	$-
4.6	Secondary Air System	w/4.1	$-	w/4.1	$-	$-	$-	$-	$-	$-	$-
4.8	Major Component Rigging	$-	w/4.1	w/4.1	$-	$-	$-	$-	$-	$-	$-
4.9	Boiler Foundations	$-	w/14.1	w/14.1	$-	$-	$-	$-	$-	$-	$-
Subtotal		**$236,271**	**$-**	**$134,626**	**$-**	**$370,897**	**$37,090**	**$-**	**$40,799**	**$448,786**	**$816**

Case:		B12B - Supercritical PC w/ CO2 Capture Sorbent					Estimate Type:			Conceptual	
Plant Size (MW, net):		550					Cost Base:			Jun-11	
Item No.	Description	Equipment Cost	Material Cost	Labor		Bare Erected Cost	Eng'g CM H.O. & Fee	Contingencies		Total Plant Cost	
				Direct	Indirect			Process	Project	$/1,000	$/kW
	5A	**Gas Cleanup and Piping**									
5A.1	Absorber Vessels and Accessories	$89,591	$-	$19,155	$-	$108,746	$10,875	$-	$11,962	$131,583	$239
5A.2	Other FGD	$4,675	$-	$5,261	$-	$9,937	$994	$-	$1,093	$12,024	$22
5A.3	Bag House and Accessories	$25,928	$-	$16,343	$-	$42,271	$4,227	$-	$4,650	$51,148	$93
5A.4	Other Particulate Removal System	$1,755	$-	$1,864	$-	$3,620	$362	$-	$398	$4,380	$8
5A.5	Gypsum Dewatering System	$7,040	$-	$1,187	$-	$8,227	$823	$-	$905	$9,955	$18
5A.6	Mercury Removal System	$5,171	$1,137	$5,084	$-	$11,392	$1,139	$-	$1,253	$13,784	$25
Subtotal		**$134,161**	**$1,137**	**$48,895**	**$-**	**$184,193**	**$18,419**	**$-**	**$20,261**	**$222,873**	**$405**
5B		**CO2 Removal and Compression**									
5B.1	CO2 Removal System	$146,452	$57,839	$114,809	$-	$319,100	$27,545	$95,730	$71,617	$513,992	$935
5B.2	CO2 Compression and Drying	$64,740	$9,711	$21,646	$-	$96,097	$9,610	$-	$21,142	$126,848	$231
Subtotal		**$211,192**	**$67,550**	**$136,455**	**$-**	**$415,197**	**$37,154**	**$95,730**	**$92,758**	**$640,839**	**$1,165**
	7	**HRSG, Ducting, and Stack**									
7.3	Ductwork	$11,580	$-	$7,309	$-	$18,889	$1,889	$-	$3,117	$23,894	$43
7.4	Stack	$10,082	$-	$6,834	$-	$16,916	$1,692	$-	$1,860	$20,468	$37
7.9	Duct and Stack Foundations	$-	$1,099	$1,305	$-	$2,404	$240	$-	$529	$3,173	$6
Subtotal		**$21,661**	**$1,099**	**$15,448**	**$-**	**$38,208**	**$3,821**	**$-**	**$5,506**	**$47,535**	**$86**

Case:		B12B - Supercritical PC w/ CO2 Capture Sorbent					Estimate Type:			Conceptual	
Plant Size (MW, net):		550					Cost Base:			Jun-11	
Item No.	Description	Equipment Cost	Material Cost	Labor		Bare Erected Cost	Eng'g CM H.O. & Fee	Contingencies		Total Plant Cost	
				Direct	Indirect			Process	Project	$/1,000	$/kW
	8	**Steam Turbine Generator**									
8.1	Steam TG and Accessories	$88,135	$-	$9,822	$-	$97,957	$9,796	$-	$10,776	$118,529	$216
8.2	Turbine Plant Auxiliariers	$501	$-	$1,067	$-	$1,569	$157	$-	$173	$1,898	$3
8.3	Condenser and Auxiliaries	$7,760	$-	$2,633	$-	$10,393	$1,039	$-	$1,144	$12,576	$23
8.4	Steam Piping	$33,884	$-	$13,733	$-	$47,616	$4,762	$-	$7,856	$60,235	$110
8.9	TG Foundations	$-	$1,498	$2,474	$-	$3,972	$397	$-	$874	$5,243	$10
Subtotal		**$130,281**	**$1,498**	**$29,729**	**$-**	**$161,507**	**$16,151**	**$-**	**$20,822**	**$198,480**	**$361**
	9	**Cooling Water System**									
9.1	Cooling Towers	$17,339	$-	$5,362	$-	$22,702	$2,270	$-	$2,497	$27,469	$50
9.2	Circulating Water Pumps	$3,543	$-	$260	$-	$3,803	$380	$-	$418	$4,602	$8
9.3	Circ. Water System Auxiliaries	$894	$-	$118	$-	$1,012	$101	$-	$111	$1,224	$2
9.4	Cir. Water Piping	$-	$7,529	$6,818	$-	$14,348	$1,435	$-	$2,368	$18,150	$33
9.5	Make-up Water System	$756	$-	$971	$-	$1,728	$173	$-	$285	$2,185	$4
9.6	Component Cooling Water Sys.	$729	$-	$559	$-	$1,287	$129	$-	$213	$1,629	$3
9.9	Circ. Water Foundations and Struct.	$-	$3,952	$6,561	$-	$10,513	$1,051	$-	$2,313	$13,878	$25
Subtotal		**$23,261**	**$11,481**	**$20,651**	**$-**	**$55,393**	**$5,539**	**$-**	**$8,205**	**$69,137**	**$126**

Case:		B12B - Supercritical PC w/ CO2 Capture Sorbent					Estimate Type:			Conceptual	
Plant Size (MW, net):		550					Cost Base:			Jun-11	
	10	**Ash and Spent Sorbent Handling Systems**									
10.6	Ash Storage Silos	$967	$-	$2,957	$-	$3,924	$392	$-	$432	$4,749	$9
10.7	Ash Transport and Feed Equipment	$6,419	$-	$6,364	$-	$12,783	$1,278	$-	$1,406	$15,468	$28
10.9	Ash/Spent Sorbent Foundation	$-	$218	$269	$-	$487	$49	$-	$107	$643	$1
Subtotal		**$7,386**	**$218**	**$9,590**	**$-**	**$17,194**	**$1,719**	**$-**	**$1,946**	**$20,859**	**$38**
	11	**Accessory Electric Plant**									
11.1	Generator Equipment	$2,251	$-	$359	$-	$2,610	$261	$-	$215	$3,086	$6
11.2	Station Service Equipment	$7,723	$-	$2,588	$-	$10,311	$1,031	$-	$851	$12,193	$22
11.3	Switchgear and Motor Control	$8,864	$-	$1,540	$-	$10,405	$1,040	$-	$1,145	$12,590	$23
11.4	Conduit and Cable Tray	$-	$6,079	$19,638	$-	$25,717	$2,572	$-	$4,244	$32,533	$59
11.5	Wire and Cable	$-	$11,574	$20,688	$-	$32,262	$3,226	$-	$5,322	$40,810	$74
11.6	Protective Equipment	$306	$-	$1,063	$-	$1,369	$137	$-	$151	$1,657	$3
11.7	Standby Equipment	$1,687	$-	$40	$-	$1,726	$173	$-	$190	$2,089	$4
11.8	Main Power Transformers	$15,906	$-	$238	$-	$16,144	$1,614	$-	$1,776	$19,534	$36
11.9	Electrical Foundations	$-	$428	$1,090	$-	$1,519	$152	$-	$334	$2,004	$4
Subtotal		**$36,737**	**$18,081**	**$47,245**	**$-**	**$102,063**	**$10,206**	**$-**	**$14,228**	**$126,497**	**$230**

Case:		B12B - Supercritical PC w/ CO2 Capture Sorbent					Estimate Type:			Conceptual	
Plant Size (MW, net):		550					Cost Base:			Jun-11	
Item No.	Description	Equipment Cost	Material Cost	Labor		Bare Erected Cost	Eng'g CM H.O. & Fee	Contingencies		Total Plant Cost	
				Direct	Indirect			Process	Project	$/1,000	$/kW
	12	**Instrumentation and Control**									
12.1	PC Control Equipment	w/12.7	$-	w/12.7	$-	$-	$-	$-	$-	$-	$-
12.3	Steam Turbine Control	w/8.1	$-	w/8.1	$-	$-	$-	$-	$-	$-	$-
12.5	Signal Processing Equipment	w/12.7	$-	w/12.7	$-	$-	$-	$-	$-	$-	$-
12.6	Control Boards, Panels and Racks	$685	$-	$418	$-	$1,103	$110	$55	$191	$1,459	$3
12.7	Distributed Control Sys. Equipment	$6,911	$-	$1,232	$-	$8,143	$814	$407	$936	$10,301	$19
12.8	Instrument Wiring and Tubing	$4,167	$-	$7,583	$-	$11,750	$1,175	$588	$2,027	$15,540	$28
12.9	Other I&C Equipment	$1,953	$-	$4,522	$-	$6,475	$647	$324	$744	$8,191	$15
Subtotal		**$13,717**	**$-**	**$13,755**	**$-**	**$27,471**	**$2,747**	**$1,373**	**$3,898**	**$35,490**	**$65**
	13	**Improvements to Site**									
13.1	Site Preparation	$-	$63	$1,335	$-	$1,398	$140	$-	$307	$1,845	$3
13.2	Site Improvements	$-	$2,082	$2,751	$-	$4,834	$483	$-	$1,064	$6,381	$12
13.3	Site Facilities	$3,732	$-	$3,915	$-	$7,647	$765	$-	$1,683	$10,094	$18
Subtotal		**$3,732**	**$2,145**	**$8,001**	**$-**	**$13,878**	**$1,388**	**$-**	**$3,054**	**$18,319**	**$33**

Case:		B12B - Supercritical PC w/ CO2 Capture Sorbent					Estimate Type:			Conceptual	
Plant Size (MW, net):		550					Cost Base:			Jun-11	
Item No.	Description	Equipment Cost	Material Cost	Labor		Bare Erected Cost	Eng'g CM H.O. & Fee	Contingencies		Total Plant Cost	
				Direct	Indirect			Process	Project	$/1,000	$/kW
	14	**Buildings and Structure**									
14.1	Boiler Building	$-	$10,580	$9,298	$-	$19,878	$1,988	$-	$3,280	$25,145	$46
14.2	Turbine Building	$-	$15,261	$14,214	$-	$29,475	$2,947	$-	$4,863	$37,285	$68
14.3	Administration Building	$-	$773	$817	$-	$1,590	$159	$-	$263	$2,012	$4
14.4	Circulation Water Pumphouse	$-	$211	$167	$-	$378	$38	$-	$63	$479	$1
14.5	Water Treatment Buildings	$-	$900	$819	$-	$1,719	$172	$-	$284	$2,175	$4
14.6	Machine Shop	$-	$517	$347	$-	$864	$86	$-	$143	$1,093	$2
14.7	Warehouse	$-	$351	$351	$-	$702	$70	$-	$116	$888	$2
14.8	Other Buildings and Structures	$-	$286	$243	$-	$529	$53	$-	$87	$669	$1
14.9	Waste Treating Building and Struct.	$-	$549	$1,662	$-	$2,211	$221	$-	$365	$2,797	$5
Subtotal		**$-**	**$29,427**	**$27,919**	**$-**	**$57,346**	**$5,735**	**$-**	**$9,463**	**$72,544**	**$132**
Total		**$926,443**	**$139,915**	**$542,125**	**$-**	**$1,608,483**	**$156,483**	**$97,103**	**$249,599**	**$2,111,668**	**$3,839**

APPENDIX 2

Equipment List

A major equipment list was also produced to guide the capital cost expenditures. The list is based upon the NETL case 12B list (Fout, et al., 2015). Generally, this equipment is expected to be able to withstand a 30+ year lifespan with regular maintenance and appropriate overhauls. The complete list is found in

Table **1**.

Table 1. Major equipment list for solid sorbent case.

Solid Sorbent Case – Account 1: Coal and Sorbent Handling					
Equipment No.	**Description**	**Type**	**Design Condition**	**Operating Qty.**	**Spares**
1	Bottom Trestle Dumper and Receiving Hoppers	N/A	202 tonne (224 ton)	2	0
2	Feeder	Belt	639 tonne/hr (706 tph)	2	0
3	Conveyor No. 1	Belt	1,266 tonne/hr (1,400 tph)	1	0
4	Transfer Tower No. 1	Enclosed	N/A	1	0
5	Conveyor No. 2	Belt	1,266 tonne/hr (1,400 tph)	1	0
6	As-Received Coal Sampling System	Two-stage	N/A	1	0
7	Stacker/Reclaimer	Traveling, linear	1,266 tonne/hr (1,400 tph)	1	0
8	Reclaim Hopper	N/A	56 tonne (56 ton)	2	1
9	Feeder	Vibratory	213 tonne/hr (224 tph)	2	1
10	Conveyor No. 3	Belt w/ tripper	415 tonne/hr (460 tph)	1	0
11	Crusher Tower	N/A	N/A	1	0

12	Coal Surge Bin w/ Vent Filter	Dual outlet	213 tonne (224 ton)	2	0
13	Crusher	Impactor reduction	8 cm x 0 - 3 cm x 0 (3 in x 0 - 1-1/4 in x 0)	2	0
14	As-Fired Coal Sampling System	Swing hammer	N/A	1	1
15	Conveyor No. 4	Belt w/tripper	415 tonne/hr (460 tph)	1	0
16	Transfer Tower No. 2	Enclosed	N/A	1	0
17	Conveyor No. 5	Belt w/ tripper	415 tonne/hr (460 tph)	1	0
18	Coal Silo w/ Vent Filter and Slide Gates	Field erected	919 tonne (1,009ton)	3	0
19	Activated Carbon Storage Silo and Feeder System	Shop assembled	Silo - 40 tonne (45 ton) Feeder - 157 kg/hr (359 lb/hr)	1	0
20	Hydrated Lime Storage Silo and Feeder System	Shop assembled	Silo - 269 tonne (292 ton) Feeder - 5,578 kg/hr (12,309 lb/hr)	1	0
21	Limestone Truck Unloading Hopper	N/A	34 tonne (45 ton)	1	0
22	Limestone Feeder	Belt	101 tonne/hr (112 tph)	1	0
23	Limestone Conveyor No. L1	Belt	101 tonne/hr (112 tph)	1	0
24	Limestone Reclaim Hopper	N/A	23 tonne (23 ton)	1	0
25	Limestone Reclaim Feeder	Belt	79 tonne/hr (90 tph)	1	0
26	Limestone Conveyor No. L2	Belt	79 tonne/hr (90 tph)	1	0

27	Limestone Day bin	w/actuator	325 tonne (360 ton)	2	0
Solid Sorbent – Account 2: Coal and Sorbent Preparation and Feed					
Equipment No.	Description	Type	Design Condition	Operating Quantity	Spares
1	Coal Feeder	Gravimetric	45 tonne/hr (56 tph)	6	0
2	Coal Pulverizer	Ball type or equivalent	45 tonne/hr (56 tph)	6	0
3	Limestone Weigh Feeder	Gravimetric	27 tonne/hr (31 tph)	1	1
4	Limestone Ball Mill	Rotary	27 tonne/hr (31 tph)	1	1
5	Limestone Mill Slurry Tank with Agitator	N/A	105,000 liters (28,000 gal)	1	1
6	Limestone Mill Recycle Pumps	Horizontol centrifugal	1759 lpm @ 10m H2O (460 gpm @ 40 ft H2O)	1	1
7	Hydrocolone Classifier	4 active cyclones in a 5 cyclone bank	437 lpm (112 gpm) per cyclone	1	1
8	Distribution Box	2-way	N/A	1	1
9	Limestone Slurry Storage Tank with Agitator	Field erected	592,000 liters (157,000 gal)	1	1
10	Limestone Slurry Feed Pumps	Horizontol centrifugal	1,232 lpm @ 9m H2O (325 gpm @ 30 ft H2O)	1	1
Solid Sorbent – Account 3: Feedwater and Miscellaneous Systems and Equipment					
Equipment No.	Description	Type	Design Condition	Operating Qty.	Spares
1	Demineralized Water Storage Tank	Vertical, cylindrical, outdoor	297,000 liters (79,000 gal)	2	0
2	Condensate Pumps	Vertical canned	19,400 lpm @ 200 m H2O (5,152 gpm @ 600 ft H2O)	1	1
3		Horizontal spray type		1	0

	Deaerator and Storage Tank		2,473,000 kg/hr (5,453,000 lb/hr), 5 min. tank		
4	Boiler Feed Pump/Turbine	Barrel type, multi-stage, centrifugal	42,000 lpm @ 3,500 m H2O (11,000 gpm @ 11,400 ft H2O)	1	1
5	Startup Boiler Feed Pump, Electric Motor Driven	Barrel type, multi-stage, centrifugal	12,300 lpm @ 3,500 m H2O (3,250 gpm @ 11,400 ft H2O)	1	0
6	LP Feedwater Heater 1A/1B	Horizontal U-tube	571,000 kg/hr (1,266,000 lb/hr)	2	0
7	LP Feedwater Heater 2A/2B	Horizontal U-tube	571,000 kg/hr (1,266,000 lb/hr)	2	0
8	LP Feedwater Heater 3A/3B	Horizontal U-tube	571,000 kg/hr (1,266,000 lb/hr)	2	0
9	LP Feedwater Heater 4A/4B	Horizontal U-tube	571,000 kg/hr (1,266,000 lb/hr)	2	0
10	HP Feedwater Heater 6	Horizontal U-tube	2,500,000 kg/hr (5,450,000 lb/hr)	1	0
11	HP Feedwater Heater 7	Horizontal U-tube	2,500,000 kg/hr (5,450,000 lb/hr)	1	0
12	HP Feedwater heater 8	Horizontal U-tube	2,500,000 kg/hr (5,450,000 lb/hr)	1	0
13	Auxiliary Boiler	Shop fabricated, water tube	22,400 kg/hr, 2.8 MPa, 343°C (45,000 lb/hr, 400 psig, 650°F)	1	0
14	Fuel Oil System	No. 2 fuel oil for light off	1,271,899 liter (336,000 gal)	1	0
15	Service Air Compressors	Flooded Screw	32 m3/min @ 0.7 MPa (1,120 scfm @ 100 psig)	2	1
16	Instrument Air Dryers	Duplex, regenerative	32 m3/min (1,120 scfm)	2	1
17	Closed Cycle Cooling Heat Exchangers	Shell and tube	53 GJ/hr (50 MMBtu/hr) each	2	0

18	Closed Cycle Cooling Water Pumps	Horizontal centrifugal	20,800 lpm @ 30 m H2O (5,500 gpm @ 100 ft H2O)	2	1
19	Engine-Driven Fire Pump	Vertical turbine, diesel engine	3,785 lpm @ 88 m H2O (1,000 gpm @ 290 ft H2O)	1	1
20	Fire Service Booster Pump	Two-stage horizontal centrifugal	2,650 lpm @ 64 m H2O (700 gpm @ 210 ft H2O)	1	1
21	Raw Water Pumps	Stainless steel, single suction	8,630 lpm @ 20 m H2O (2,280 gpm @ 60 ft H2O)	2	1
22	Ground Water Pumps	Stainless steel, single suction	3,450 lpm @ 270 m H2O (910 gpm @ 880 ft H2O)	5	1
23	Filtered Water Pumps	Stainless steel, single suction	2,080 lpm @ 50 m H2O (550 gpm @ 160 ft H2O)	2	1
24	Filtered Water Tank	Vertical, cylindrical	1,999,000 liter (528,000 gal)	1	0
25	Makeup Water Demineralizer	Multi-media filter, cartridge filter, RO membrane assembly, electrodeionization unit	360 lpm (90 gpm)	1	1
26	Liquid Waste Treatment System	-	10 years, 24 hour storm	1	0
Solid Sorbent – Account 4: Boiler and Accessories					
Equipment No.	**Description**	**Type**	**Design Condition**	**Operating Qty.**	**Spares**
1	Boiler	Supercritical, drum, wall- fired, low NOx burners, overfire air	2,500,000 kg/hr steam @ 25.5 MPa/602°C/602°C (5,444,000 lb/hr steam @ 3,700 psig/1,115°F/1,115 °F)	1	0
2	Primary Air Fan	Centrifugal	339,000 kg/hr, 4,600 m3/min @ 123 cm WG (746,000 lb/hr,	2	0

			163,100 acfm @ 48 in. WG)		
3	Forced Draft Fan	Centrifugal	1,103,000 kg/hr, 15,000 m3/min @ 47 cm WG (2,430,000 lb/hr, 531,000 acfm @ 19 in. WG)	2	0
4	Induced Draft Fan	Centrifugal	1,590,000 kg/hr, 31,600 m3/min @ 89 cm WG (3,505,000 lb/hr, 1,114,000 acfm @ 35 in. WG)	2	0
5	SCR Reactor Vessel	Space for spare layer	3,181,000 kg/hr (7,011,000 lb/hr)	2	0
6	SCR Catalyst	--	--	3	0
7	Dilution Air Blower	Centrifugal	180 m3/min @ 108 cm WG (6,300 acfm @ 42 in. WG)	2	1
8	Ammonia Storage	Horizontal tank	195,000 liter (52,000 gal)	5	0
9	Ammonia Feed Pump	Centrifugal	37 lpm @ 90 m H2O (10 gpm @ 300 ft H2O)	2	1
Solid Sorbent – Account 5A: Flue Gas Cleanup					
Equipment No.	**Description**	**Type**	**Design Condition**	**Operating Qty.**	**Spares**
1	Fabric Filter	Single stage, high-ratio with pulse-jet online cleaning system	1,590,000 kg/hr (3,500,000 lb/hr) 99.9% efficiency	2	0
2	Absorber Module	Counter-current open spray	64,000 m3/min (2,240,000 acfm)	1	0
3	Recirculation Pumps	Horizontal centrifugal	221,000 lpm @ 65 m H2O (59,000 gpm @ 210 ft H2O)	5	1
4	Bleed Pumps	Horizontal centrifugal		2	1

			5,365 lpm (1,411 gpm) at 20 wt% solids		
5	Oxidation Air Blowers	Centrifugal	112 m3/min @ 0.3 MPa (3,932 acfm @ 37 psia)	2	1
6	Agitators	Side entering	56 hp	5	1
7	Dewatering Cyclones	Radial assembly, 5 units each	1,333 lpm (359 gpm) per cyclone	2	0
8	Vacuum Filter Belt	Horizontal belt	43 tonne/hr (47 tph) of 50 wt % slurry	2	1
9	Filtrate Water Return Pumps	Horizontal centrifugal	818 lpm @ 13 m H2O (213 gpm @ 40 ft H2O)	1	1
10	Filtrate Water Return Storage Tank	Vertical, lined	538,000 lpm (146,000 gal)	1	0
11	Process Makeup Water Pumps	Horizontal centrifugal	4,279 lpm @ 21 m H2O (1,132 gpm @ 70 ft H2O)	1	1
12	Activated Carbon Injectors	---	157 kg/hr (360 lb/hr)	1	0
13	Hydrated Lime Injectors	---	5,578 kg/hr (12,310 lb/hr)	1	0
Solid Sorbent – Account 5B: Carbon Dioxide Recovery					
Equipment No.	**Description**	**Type**	**Design Condition**	**Operating Qty.**	**Spares**
1	Solid Adsorbent Capture System	Solid Adsorbent	2,043,000 kg/hr (4,500,000 lb/hr)	6	0
2	Condensate Pump	Centrifugal	6,000 lpm @ 1 m H2O (150 gpm @ 4 ft H2O)	1	1
3	BP Turbine	Steam turbine	22 MW (73.5-29 psia)	1	1
4	CO2 Dryer	Triethylene glycol	Inlet: 143 m3/min (4,469 acfm) @ 3.0	1	0

			MPa (439 psia) Outlet: 2.9 MPa (419 psia)		
5	CO2 Compressor	Integrally geared, multi-stage centrifugal	273,000 kg/hr @ 15.3 MPa (600,000 lb/hr @ 2,215 psia)	2	0
Solid Sorbent – Account 7: Ducting and Stack					
Equipment No.	**Description**	**Type**	**Design Condition**	**Operating Qty.**	**Spares**
1	Stack	Reinforced concrete with FRP liner	152 m (500 ft) high x 5.5 m (18 ft) diameter	1	0
Solid Sorbent – Account 8: Steam Turbine Generator and Auxiliaries					
Equipment No.	**Description**	**Type**	**Design Condition**	**Operating Qty.**	**Spares**
1	Steam Turbine	Commercially available advanced steam turbine	725 MW 24.1 MPa/593°C/593°C (3500 psig/ 1100°F/1100°F)	1	0
2	Steam Turbine Generator	Hydrogen cooled, static excitation	750 MVA @ 0.9 p.f., 24 kV, 60 Hz, 3-phase	1	0
3	Surface Condenser	Single pass, divided waterbox including vacuum pumps	2,300 GJ/hr (2,184 MMBtu/hr), Inlet water temperature 16°C (60°F), Water temperature rise 11°C (20°F)	1	0
Solid Sorbent – Account 9: Cooling Water System					
Equipment No.	**Description**	**Type**	**Design Condition**	**Operating Qty.**	**Spares**
1	Circulating Water Pumps	Vertical, wet pit	871,000 lpm @ 30 m (231,000 gpm @ 100 ft)	2	1
2	Cooling Tower	Evaporative, mechanical draft, multi-cell	11°C (51.5°F) wet bulb / 16°C (60°F) CWT / 27°C (80°F) HWT / 4340 GJ/hr	1	0

			(4110 MMBtu/hr) heat duty		
Solid Sorbent – Account 10: Ash and Spent Sorbent Recovery and Handling					
Equipment No.	**Description**	**Type**	**Design Condition**	**Operating Qty.**	**Spares**
1	Economizer Hopper (part of boiler scope of supply)	--	--	4	0
2	Bottom Ash Hopper (part of boiler scope of supply)	--	--	2	0
3	Clinker Grinder	--	5.4 tonne/hr (6 tph)	1	1
4	Pyrites Hopper (part of pulverizer scope of supply included with boiler)	--	--	6	0
5	Hydroejectors	--	--	12	
6	Economizer /Pyrites Transfer Tank	--	--	1	0
7	Ash Sluice Pumps	Vertical, wet pit	213 lpm @ 17 m H2O (56 gpm @ 56 ft H2O)	1	1
8	Ash Seal Water Pumps	Vertical, wet pit	8,500 lpm @ 9 m H2O (2,240 gpm @ 28 ft H2O)	1	1
9	Hydrobins	--	213 lpm (56 gpm)	1	1
10	Baghouse Hopper (part of baghouse scope of supply)	--	--	24	0
11	Air Heater Hopper (part of	--	--	10	0

	boiler scope of supply)				
12	Air Blower	--	23 m3/min @ 0.2 MPa (885 scfm @ 24 psi)	1	1
13	Fly Ash Silo	Reinforce d concrete	1,680 tonne (1,800 ton)	2	0
14	Slide Gate Valves	--	--	2	0
15	Unloader	--	--	1	0
16	Telescoping Unloading Chute	--	157 tonne/hr (168 tph)	1	0
Solid Sorbent – Account 11: Accessory Electric Plant					
Equipment No.	**Description**	**Type**	**Design Condition**	**Operating Qty.**	**Spares**
1	STG Transformer	Oil-filled	24 kV/345 kV, 650 MVA, 3-ph, 60 Hz	1	0
2	High Voltage Transformer	Oil-filled	345 kV/13.8 kV, 20 MVA, 3-ph, 60 Hz	2	0
3	Medium Voltage Transformer	Oil-filled	24 kV/4.16 kV, 99 MVA, 3-ph, 60 Hz	1	1
4	Low Voltage Transformer	Dry ventilated	4.16 kV/480 V, 15 MVA, 3-ph, 60 Hz	1	1
5	STG Isolated Phase Bus Duct and Tap Bus	Aluminum, self-cooled	24 kV, 3-ph, 60 Hz	1	0
6	Medium Voltage Switchgear	Metal clad	4.16 kV, 3-ph, 60 Hz	1	1
7	Low Voltage Switchgear	Metal enclosed	480 V, 3-ph, 60 Hz	1	1
8	Emergency Diesel Generator	Sized for emergency shutdown	750 kW, 480 V, 3-ph, 60 Hz	1	0

Solid Sorbent – Account 12: Instrumentation and Control					
Equipment No.	**Description**	**Type**	**Design Condition**	**Operating Qty.**	**Spares**
1	DCS - Main Control	Monitor/keyboard; Operator printer (laser color); Engineering printer (laser B&W)	Operator stations/printers and engineering stations/printers	1	0
2	DCS - Processor	Microprocessor with redundant input/output	N/A	1	0
3	DCS - Data Highway	Fiber optic	Fully redundant, 25% spare	1	0